Dissipative mechanisms during the debonding of high performance foam pressure sensitive adhesives for automotive

Antoine Fleury

PSL★
UNIVERSITÉ PARIS

THÈSE DE DOCTORAT
DE L'UNIVERSITÉ PSL

Préparée à l'ESPCI Paris

Mécanismes dissipatifs lors du décollement d'adhésifs sensibles à la pression haute performance (foam PSA) dans l'automobile.

Dissipative mechanisms during the debonding of high performance foam pressure sensitive adhesives for automotive

Soutenue par
Antoine FLEURY
Le 04 septembre 2019

Ecole doctorale n° 397
Physique et chimie des matériaux

Spécialité
Physico-chimie

Composition du jury :

Véronique, LAZARUS Professeur, ENSTA ParisTech	*Présidente*
Valérie, NASSIET Professeur, ENI Tarbes	*Rapportrice*
Christophe, DERAIL Professeur Des Université, Université de Pau et des Pays de l'Adour	*Rapporteur*
Cyprien, GAY Chargé de Recherche, Université Paris-Diderot CNRS	*Examinateur*
Matteo, CICCOTTI Professeur, ESPCI Paris	*Directeur de Thèse*
Etienne, BARTHEL Directeur de Recherche, ESPCI Paris	*Co-directeur*
Pauline, d'Herlincourt Ingénieur, Renault	*Invitée*

ESPCI PARIS
EDUCATION SCIENCE INNOVATION

Les plus grands produits de l'architecture sont moins des Ïuvres individu-
elles que des Ïuvres sociales, plutôt l'enfantement des peuples en travail que
le jet des hommes de génie.

Victor HUGO

Contents

vi

List of Figures

List of Abbreviations

PSA	Pressure Sensitive Adhesives
SIMM	Sciences et Ingenierie de la Matiere Molle
SBR	Styrene Butadiene Rubber
AB	Acid-Base
d	dispersive
p	polar
PTFE	Poly Tetra Fluor Ethylene
PMMA	Poly Methyl Meth Acrylate
LEFM	Linear Elastic Fracture Mechanics
NLFM	Non Linear Fracture Mechanics
SVD	Single Value Decomposition
SSY	Small Scale Yield
FEM	Finite Element Modeling
SEM	Scanning Electron Microscopy
EDX	Energy Dispersive X-ray
WLF	William Landel Ferry
EFM	Equivalent Fibril Model
FEG	Field Emission Gun
IPA	Iso Prop Anol
TTS	Time Temperature Superposition

List of Symbols

$E_{surface}$	surface energy	$J.m^{-2}$
S	entropy	J/m^2
γ	surface free energy	$J.m^{-2}$
θ	angle	rad
W_{adh}	work of adhesion	$J.m^{-2}$
Tg	glass transition temperature	K
T	temperature	K
μ', μ'' (resp. G', G'')	shear moduli	Pa
w	Dupré fracture energy	$J.m^{-2}$
U_w	strain energy	J
U_{el}	elastic energy	J
G	strain energy release rate	$J.m^{-2}$
σ	stress	Pa
r	typical distance to the crack tip	m
E	Young modulus	Pa
Γ	fracture energy	$J.m^{-2}$
v	crack propagation velocity	m/s
ϕ	viscoelastic function	-
L_{EA}	elasto-adhesive length	m
ρ^*	radius of curvature of the crack tip	m
λ_α, λ_β	Kaelble lengths	m
h_b	backing thickness	m
a, a_0	adhesive intial thickness	m
Y	Kaelble strands Young modulus	Pa
b	width of peel samples	m
ν	Poisson ratio	-
a_T	TTS shift parameter	-
$\dot{\epsilon}$	strain rate	s^{-1}
ω	frequency	Hz
t	time	s
ϵ	strain	-
F, F_{peel}	peel force	N
V_{peel}, $V_{peeling}$	peeling velocity	$m.s^{-1}$
L_{dr}, l	debonding region length	m
r_c, R	radius of curvature of the backing	m
I	quadratic moment	m^4
M	bending moment	N.m
T	tangential force	N
s	curvilinear abscissa	-

q	lineic force	$N.m^{-1}$
P	Laplace pressure	Pa
ϵ_{max}	maximal fibril deformation	-
σ_0	stress in the debonding region	Pa

0.1 Introduction

Currently the even more competitive car making field is at a watershed in its history. Whether it is with the new kind of powertrains (full electric, hybrid...) or with the use of new materials, innovation and development sound as it is necessary for a car builder to stay on track. In this framework, bonding used as an assembly technology has been more and more present in the automotive world. More specifically, car manufacturers such as Renault, have been advised to use Pressure Sensitive Adhesives (PSA) designed for automotive application. In general, one can find them in domains going from microelectronics to biomedical as they represent an adhesive solventless solution. However, introducing such complex materials in a mass production-oriented system is not the easiest task to achieve. That is why the company offered to finance a doctorate research program based on this topic. Hence, the work described in the following thesis was initially motivated by one purpose: gaining qualitative and quantitative knowledge around the foam PSA behavior. In order to address such a generic industrial objective, we organized the study around the triptych product-process-material. This approach enabled us to dive quickly into a more fundamental research on the PSA behavior itself but keeping in mind the industrial application.

The first chapter consists of contextualizing the usage of PSA in the automotive industry. In spite of its small size compared to the rest of the car, we observe that PSA materials are one of the cornerstones of the future high tech automotive world. In the same chapter, we review the latest scientific breakthroughs regarding application process and classic PSA. Thus we can build a strong and relevant problematic for the doctorate thesis.

The second chapter is entirely dedicated to the characterization of the PSA for high bonding applications. At the beginning of this study, the partner company gave us a totally unknown material subjected to trade secret protection. That is why the research starts by developing and adapting measurement techniques to define the internal structure and the main behavior of the material of interest. The results are even more attractive since they supplement researches on materials for deep water equipment.

The third chapter focuses on dissipative mechanisms identification. Then we build a phenomelogical model to describe the performance of an adhesive joint made with the foam PSA. The model is called Equivalent Fibril Model. We apply it to 90°-peel test. We then explain quantitatively our model using non linear rheology. A second model, called Transposition Model, links results from different loading conditions (peel test and flat ended probe tack test). That is the first time that such models are presented for the very specific foam PSA.

The fourth chapter exhibits the link existing between adherence performances and foam PSA debonding region shape. The morphology of the foam

PSA during the debonding and the adherence energy level associated collapse on a master curve (morphology vs adherence). The results are found in triggering the peeling velocity, the interfacial adhesion between adhesives and substrates and the damage of the foam PSA.

The last chapter sums up the scientific conclusions of the study and gathers the takeaway messages. It also provides the reader with perspectives and supplementary works which should be done to enrich the research on this topic.

Chapter 1

Foam Pressure Sensitive Adhesives in the automotive field

1.1 Why mastering PSA use in the automotive industry?

Mastering PSA use in the automotive industry can seem a bit out of the scope of an automobile manufacturer top one priority. We could think that such a question should remain in the tape supplier perimeter and that only its specifications should interest the car builder. Nothing is less fair and we describe why.

1.1.1 Economic and strategic interests

Renault Group is part of one of the largest world car manufacturer, the Renault Nissan Mitsubishi Alliance. Thanks to their factories across the world, from Tanger in Morocco to Moscow in Russia, the Alliance produces more than 10.6 million vehicles per year (2017 figures)[42]. In order to reach such a number at the lowest cost, all the production lines in factories are organized around the same systematic organization.

On the schematic of the figure 1.1, we observe that the car is assembled following a defined sequence which decreases as much as possible timeouts. Firstly, the body of the car is fabricated, chemically treated and painted. The surface treatment is called cataphoresis. It consists of depositing a layer to protect the body of the car from corrosion. The painting protocol is organized in three steps. The surface of the body of the car, initially chemically treated, is covered by a layer of paint primer. The vehicle is then baked and another layer is deposited, that is the base coat containing the pigments giving the color. This base coat is then reinforced by a top coat which is designed to protect the base coat. It is also worth noticing that this top coat is more and more designed to exhibit the lowest surface tension possible to prevent dust and dirt from attaching to the car. The final structure of the surface of the car is described on the graph of the figure 1.15. After its construction and painting, the body of the car is blended with the powertrain (assembled on
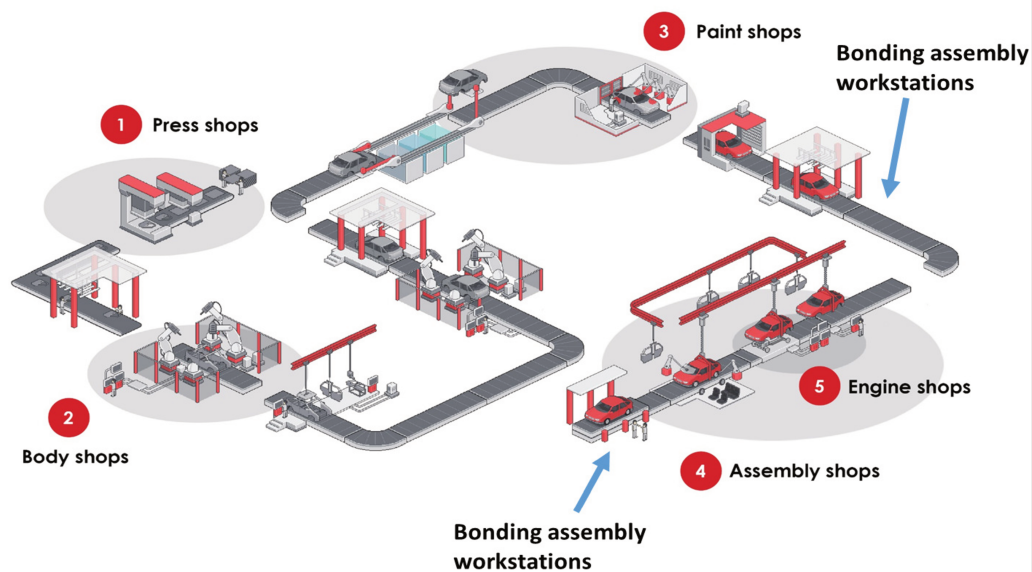
FIGURE 1.1: Location of bonding assembly workstations in an
automotive production line

another production line). The almost car is then enriched with all the accessories and devices needed. PSA are essentially used during this final stage but some parts are bonded just after the painting stage.

Such a technique is mandatory to keep a sustainable production system

The main interest for using PSA in the automotive industry is to save production time. Production time is very costly in a mass production system (more than 10.6 million vehicles produced each year). If a car manufacturer uses traditional assembly tools such as clips to attach an antenna to a car, it must first drill holes for the clips before doing the cataphoresis treatment and the painting (see figure 1.1). It must then check that the holes have not been filled by chemical treatments or painting stages. If so, new holes need to be drilled and the car needs to be repainted before moving forward. Eventually the antenna is attached to the body of the car in the final stage of the production line (see figure 1.1). In the case where the car manufacturer uses PSA, the antenna is directly bonded to the car in the final stage of the production line (see figure 1.1). The economic interest is colossal based on the large number of vehicles produced.

From a marketing point-of-view, PSA also seem to be a panacea. As said in the introduction, the automotive field has never been so competitive. To keep the lead in a domain like this one, an automaker must relentlessly offer new services to customers. In the pursuit of this goal, a phenomenon

is gaining momentum: customization. According to the *English Oxford Living Dictionaries*, customization is the action of modifying something to suit a particular individual or task. When customers buy a new car, they want it to be unique. To be able to deliver a unique vehicle to a single customer over millions, car manufacturers have integrated customization in their car fabrication processes. Thanks to the use of PSA, they can attach small parts as aesthetics beams or emblems on a car without troubling all the production line. The system is very straightforward and reasonably time consuming. On a normal workstation, there is a box with optional parts that operators can bond or not depending on the car customer will. On a production line, each operator has a certain amount of time dedicated to operations so car manufacturer has to plan bonding operations which match with the initial task timing. PSA allow them to do so. Thus, there is no delay in the production between two different cars. Thanks to these small aesthetics items, differences between vehicles can seem minor regarding the complexity of a modern car but putting an emblem or a chromed beam can change all the aesthetics and convinces the customer to buy a vehicle. Hence, customization is essential for the sales strategy of the car manufacturer. Thanks to PSA solutions, the cost of such a marketing differentiation remains well controlled.

Another meaningful advantage of using PSA is to contribute to the weight reduction of a new car. The fact of subsidizing the classic assembly tools as clips, screws etc... allows manufacturers to get rid of heavy elements compared to PSA. "When bonding solutions will be generalized on all structural and non-structural parts of a vehicle, kilos will be saved", Renault production expert said. With such a weight decrease, it is obvious that car fuel or electric energy consumption will also greatly decrease. From this point of view, it turns out that PSA make the car greener which is of prime interest for both economic and strategic automakers interests.

Even if PSA are relevant solutions to address many challenges of the modern automotive world, it remains some factors to consider, especially in the framework of a doctoral research. They are all due to the fact that the topic regards mass production in workshop environment. It means that production imperatives will be likely to alter the performance of PSA. More precisely, the industrial process is driven by the production line which can cause default in the bonding formation, the atmosphere can be polluted by dust and/or wax which can contaminate the substrate onto which a PSA is supposed to adhere. In addition, the shape of substrate is induced by aesthetics rules which can differ from scientific requirements to get optimal bonding performances. These materials have obviously been designed in labs and have been tested to meet industrial specifications. The goal of the research is then neither to question the chemical formulation of the PSA nor to contest their structure. The objective is to understand how the PSA work and how industrial imperatives can influence their behavior.

FIGURE 1.2: Letters debonding on the trunk of a car

1.1.2   Industrial need in such a PhD research

The interests for the car manufacturer of using PSA is now clear. Diving deeper into the study, one question pops up: what happens during PSA failure? In other terms, can we understand PSA failure? More than being selective when choosing PSA commercial references, giving comprehensive answers to those questions would lead to the Grail for industrial companies. Indeed, industrialists would like to predict PSA failure. Prediction is a very tough and intriguing point when talking about adhesives. There are a large number of critical factors driving PSA performance. According to an automaker point of view, PSA failure must be understood for two reasons: brand identity conservation and safety. The latter regards PSA use in the framework of autonomous vehicles.

Brand identity protection

In appendix A, we observe that PSA are widely used to assembly letters and company emblems on cars. Even though not vital for vehicles well functioning, these small parts must stay in place for all the service life. They account for the identity of the car. A debonding can lead to a catastrophic appeal decrease for a car brand. It suffers from a low quality image which affects irretrievably the future sales.

On the figure 1.2, the initial name of the car was "SCENIC". This loss generates a bad image for the brand Renault which is the car producer. If the debonding occurs in the guarantee period, the debonding of one single letter will doubly impact the automaker since it will have to pay to recall the vehicle and fix it. More importantly, if a default of bonding process is highlighted when a single car is recalled, then the company has to recall all the

vehicles produced by the same production line. Such a situation can quickly cost millions of euros. Whether it is for protecting the brand image or saving millions in recalls, PSA failure must be understood by car manufacturers to prevent them from occurring.

Safety

With the increase in automation in cars due to the growing popularity of autonomous vehicles, more and more sensors and cameras are being used in cars. Most of them are carried by parts which themselves are attached to the body of the car or on bumpers. For the reasons mentioned above, car makers make such demanding assemblies using PSA. It is easy to understand that sensors must remain correctly attached to the car. A loss of one of them would result in a catastrophic accident, potentially causing death. Without sensors or cameras the autonomous car would be blind, with no driver inboard. That is why PSA failure must be vitally understood to be able to, once again, reduce the risk of debonding. In this case, it is no longer only commercial or financial issues car makers can face but major safety threat for customers.

1.2 When industrial interests meet academic research: state of the art of the research on PSA

When talking about PSA, one can often confuse them with glues. However, as we will detailed in this section, PSA and glues are fundamentally different. Firstly, in the bonding process, glues establish strong chemical bonds with the substrate whereas PSA substrates interfacial adhesion levels are most time driven by molecular adhesion. Secondly, the performance of glues mainly comes from the strength of the chemical bonds they establish with substrates. In the case of PSA, performance comes from their ability to dissipate energy. These differences make glues and PSA two distinctive classes of materials.

Inside the PSA family, it is now of interest to differentiate classic PSA which do not require external treatments other than an applicative pressure and the so called hotmelt PSA. The latter require curing process when bonded to a substrate. This curing is needed to remove solvent, favor cross linking... PSA studied in the framework of this PhD thesis are solventless, classic PSA. Here, we focus on the most widely used PSA adhesives which are acrylics polymer based PSA [9]. Their high resistance to oxidation, and therefore aging, undoubtedly justifies such popularity [85]. Foam PSA, although very thick (∼mm thickness size), are included in this denomination. For this reason, we reviewed in the following subsections the relevant part of the literature regarding classic PSA. We first look at the bonding formation and then, focus on the debonding process. In the whole thesis, we call *foam PSA* or *automotive PSA* or *automotive foam PSA* the thick tape given by

the company (similar to commercial reference GT6012 from 3M). We call *thin PSA* or *thin films PSA* the classic office tapes commonly assimilated to PSA denomination.

1.2.1   The bonding formation

The key point to study adhesion phenomena is the notion of length scales. Generally, one can distinguish three domains: the nano-world where everything sticks naturally and spontaneously, the transition scale ($\sim \mu$m) where no obvious adhesion or detachment occur, and the macroscopic engineering world where spontaneous adhesion is not common to encounter ($\sim$mm). In that case, the use of bonding solutions like PSA is required. For those materials, the objective of the contact formation stage is to come very close to the substrate surface (less than 5nm [57]) to establish interactions. Between PSA and substrates, the early stages of the interfacial strength is driven by molecular adhesion (van der Waals forces) [17]. In the long term, interfacial adhesion increases which is due to the dynamic and uncross linked nature of PSA [1]. For example, the adhesion for a polar PSA increases according to the dynamic of the polar groups in the material bulk which have to reach the interface to establish polar interactions (see next subsection). In a nutshell, whether it is in the short or the long term, PSA interfacial adhesion is firstly piloted at the molecular scale.

Molecular adhesion occurs at a very small range (less than 5nm [57], smaller than the classic short range interactions such as electrostatic forces. Hence, an intimate contact between PSA surface and substrate is of prime interest to establish good interfacial interactions and favor bonding strength.

However with PSA, it is also possible to engender stronger interactions between the PSA and the substrate by depositing an adhesion promoter. Adhesion promoter is designed to chemically react with the substrate by forming chemical bonds with it. In that case, we are no longer in the case of molecular adhesion but strong chemical interactions. Excepted for some extreme cases (see Chapter 3 and Chapter 4), we will mostly not use adhesion promoter in the frame work of this research.

According to the literature [18, 37, 4, 5, 38], the question of the bonding formation for a PSA can be seen as a coupling of two parameters: one is extrinsic, the substrate surface state and the other is intrinsic, the rheology of the PSA.

Where does molecular adhesion come from?

When talking about PSA adhesion, we know that a close and intimate contact between the adhesive and the substrate, around 5nm is sufficient to establish adhesion [57]. However, to go further in the study, it is worth understanding whence this interfacial adhesion comes from.

Whether it is in the bonding process (see fig 1.4) or during the debonding (see fig 1.7), the interface plays a major role. The interfacial adhesion is regarded as the core of many models of debonding energy description [60, 30]. As previously said, the interactions implied in PSA adhesion are mostly weak. When talking about weak adhesion, one can quote the Keesom interaction (between molecules with permanent dipole), the Debye interaction (between a molecule with a permanent dipole and a molecule with an induced dipole), the London or dispersive interaction (between molecules which together induce a dipole) and the donor-acceptor interaction [32] also called acid-base interaction (takes place when hydrogen atom is shared between two molecules which creates a hydrogen bond).

Theoretically, one should be able to evaluate the ability of an adhesive to establish these kind of weak bonds by studying surface free energies of the substrate AND the adhesive [61, 60]. At the first order, a contact between a PSA and a surface is established if the interfacial surface free energy is lower than the surface free energies of the PSA and the substrate taken separetely. In condensed matter (solid or liquid), the atoms and molecules in the bulk remain together because of strong bonds existing among them. However, at the extreme surface, the atoms of the final layer have less neighbors so that they have an excess of energy (bonding energy being negative). This energy excess is called surface energy. This surface energy corresponds to the total amount of energy, $E^0_{surface}$, (or enthalpy) consumed by the creation of a new surface. Rigorously, it differs from the surface free energy, γ (or free enthalpy) which describes the amount of the energy available to react within a potential interface [15]. The link between the surface energy and the surface free energy is made with the energy used in the disorder of the elements of the material, $S_{surface}$ – called entropy – which can be written as the following relationship:

$$\gamma^0 = E^0_{surface} - T.S^0_{surface} \tag{1.1}$$

or

$$\gamma = E^0_{surface} - T.\frac{d\gamma}{dT} \tag{1.2}$$

According to the equation above, the surface energy and the surface free energy are only equal at the absolute zero [15]. The difference between surface energy and surface free energy is often neglected by industrialists which prefer to talk about surface free energy using the name surface energy even if it is, theoretically, nonsense according to the explanation above.

As mentioned earlier, this surface free energy has to be taken account

when one wants to study adhesion problems. Many researchers have been focused on its measurement. For the liquids, works during the 70's and 80's [48] led to efficient methods: Du Nouy setup, Wilhemy setup [2] or the well-known in industry, the pendant drop method [3]. Nonetheless, it is necessary to keep in mind the fact that in PSA adhesion problems there is no liquid. An easy way to measure this free energy would be to use the melt solid (so a liquid) [29] and extrapolate the results using relevant parameters. Harding [45] did the calculations with silica at 25°C. This protocol is difficult to use with foam PSA because of their complex chemistry.

Like for the liquids with the surface tension measurements and calculations, many methods have been developed to determine the surface free energy of a solid. However, on the contrary to the liquids, results obtained for the solids are strongly dependent of the method used [15]. For example, according to the literature, the polyethylene has a surface free energy between 24mJ.m^{-2} [76] and 55mJ.m^{-2} [67], the PTFE has a surface free energy between 18mJ.m^{-2} [86] and 34 mJ.m^{-2} [67]. And within the same method, Carré [11] showed that the value was likely to vary, between 41 and 49mJ.m^{-2} with PMMA for instance. For these reasons, one must be careful with the method used when determining the surface free energy of solid. Regarding substrate, it is much easier to carry out such measurements. Pendant drop method [3] or sessile drop method are well adapted. They are used for measuring the polar and dispersive components of the surface free energy of a solid (substrate) utilizing polar and dispersive liquids. In this configuration, a single drop is deposited on the substrate and the spread of the drop is recorded to measure the angle θ (figure 1.3).
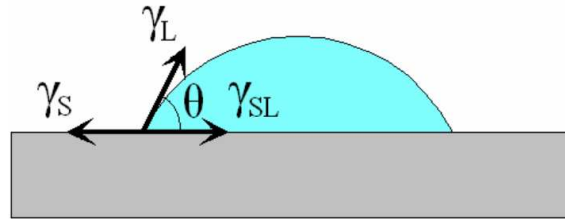
FIGURE 1.3: Young's angle

θ is not a constant angle and it is necessary for experimenters to define clearly their measurements: advancing angle, receding angle, angle after X seconds of stabilization...

These methods have been used in automotive industry. As it was likely, all top coats used exhibit a surface free energy between 40 and 45mJ.m^{-2}. In such a configuration (see figure 1.3), one can recall the Young's equation [84]:

$$\gamma_l.cos\theta = \gamma_s - \gamma sl \tag{1.3}$$

Because cos is decreasing on $[0 ; \pi/2]$, the spreading of the liquid is obtained for $\gamma_l < \gamma_s - \gamma_{sl}$ which means that the spreading coefficient $S = \gamma_s - (\gamma_{sl} + \gamma_l)$ [16] is positive. Fowkes in 1967 [33] proposed to decompose the surface free energy by a sum of energies of different origins:

$$\gamma_i^{total} = \gamma_i^d + \gamma_i^p + \gamma_i^{AB} \tag{1.4}$$

where d stands for Dispersive, p for Polar and AB for Acid-Base.

Dispersive interactions

In the cases of two non-miscible liquids or a non-polar liquid with any solid or a non-polar solid with any liquid, Fowkes [33] proposed that the influence of one phase on the other is equal to: $\gamma_1 - \sqrt{\gamma_1^d.\gamma_2^d}$ (resp. for the other phase: $\gamma_2 - \sqrt{\gamma_1^d.\gamma_2^d}$). So the interfacial energy is given by $\gamma_{12} = \gamma_1 + \gamma_2 - 2\sqrt{\gamma_1^d.\gamma_2^d}$ hence the Dupré energy [28], which describes the link between the adhesion energy and the surface free energies of the two materials assembled, is:

$$W_{adh} = \gamma_1 + \gamma_2 - \gamma_{12} = 2\sqrt{\gamma_1^d.\gamma_2^d} \tag{1.5}$$

To recall [15, 17], most of the early stage interactions occurring in the bonding process of a PSA comes from the dispersive forces. For acrylate based PSA, the long term is driven by polar interactions (presented later on) [10]. According to Benedek et al. [10], "Acrylate-based PSA are highly polar and the polar groups are initially oriented into the bulk adhesive and away from the surface because of the presence of a silicone-coated liner (highly non polar)". Hence, when that kind of PSA is deposited onto a substrate, it will first establish dispersive bonds as depicted in this part and then, as time goes by, polar group will rotate towards the interface substrate adhesive and establish polar bonds which will explain performance which is observed some time after the bonding process.

Polar interactions

One just saw that by considering only the dispersive interactions occurring within an interface, it was possible to link adhesion energy and surface free energy of the two materials. However, most adhesives have a total surface free energy larger than the only contribution of the dispersive interactions. Historically, the first guess was that excess of energy comes from a polar contribution [50]:

$$\gamma_i = \gamma_i^d + \gamma_i^p \tag{1.6}$$

Based on the equation (1.5), Owens [50] wrote this expression of the adhesion energy: $W_{adh}^p = 2\sqrt{\gamma_1^p.\gamma_2^p}$ which gives the following expression of the adhesion energy:

$$W_{adh} = W_{adh}^p + W_{adh}^d = 2\sqrt{\gamma_1^p.\gamma_2^p} + 2\sqrt{\gamma_1^d.\gamma_2^d} \tag{1.7}$$

From this expression, we define the polar and dispersive contribution. Hence, it is theoretically straightforward to determine the surface free energy of any solid. If one measures the contact angle of a purely dispersive liquid on a solid, the equation (1.4) combined with the equation (1.5) will give directly the dispersive component of the surface free energy γ^d. Then, the equation (1.7) allows to calculate the polar component γ^p, in using another polar liquid such as deionized water [50].

However, it is worth noticing that this approach does not allow to describe which kind of interactions take place behind the term "polar". For Fowkes [33], the non dispersive forces come from the acid base interactions generating hydrogen bonds. Strictly speaking, polar interactions coming from the establishment of Keesom or Debye bonds are negligible when talking about the adhesion of a polymer on another. But never in the literature, we observed a strict model or even measurements linking precisely the polar component of the surface tension and the interfacial adhesion of an acrylate based PSA. We can only quote works [8, 61, 60] who showed a link between the overall surface tension and the adhesive joint performance but never a predictive law.

AB interactions

Acid-base interactions describe mainly two mechanisms: an exchange of proton (Broensted acid) or an exchange of an electron pair (Lewis acid). In both cases the base is the same but the acid is a proton donor (Broensted) or an electron pair acceptor (Lewis). Drago [27] showed that the hydrogen bonds come from Lewis interactions. To evaluate quantitatively such a force, two approaches have been proposed: the first one by Drago [27] valid at the so-called "Drago scale" and adapted by Fowkes to the interface solid-liquid [32]; the second one by Gutmann [44]. For a purely polymeric interface, the acid base interactions will be very close to the monomers constituting the two polymers. However, in the framework of this study, we will not consider specifically the AB intercations but assume that, if such interactions take place, they are included in the polar contribution.

In a nutshell, interactions occurring at the interface when bonding a PSA onto a substrate are mostly dispersive when talking about instantaneous adhesion (tack response). In the specific case of highly polar acrylate based adhesives, dispersive interactions are gradually overcome by the polar interactions which become more and more dominant in the long term behavior. That is why, no clear evidence of a model predicting quantitatively adhesion performances thanks to substrate surface energy was found. The only information one can get from such a surface measurement is a hint on the ability of a PSA to potentially attach well on a substrate. For example, if one takes SBR (purely dispersive material with no polar group within) to attach a weakly dispersive and highly polar part, it is straightforward to predict a bad quality assembly. To conclude on this part, a reasonable hypothesis we can make is that the interfacial adhesion of foam PSA (acrylate based PSA) is mainly due to weak interfacial interactions. When talking about molecular adhesion, we are considering weak interactions (a few tens of $mJ.m^{-2}$ [57, 58]). In the frame work of this research, we use surface energy measurement to evaluate the quality of the surface treatments we use to trigger the interfacial adhesion level (see Chapter 2).

Interfacial interactions are formed during the bonding process. The latter can be described by the schematic from figure 1.4. The PSA is first pressed onto a substrate to deform it and adapt to the surface roughness (center image 1.4). This deformation induces internal stresses occurring at the neighborhood of the surface in the PSA. Elastic energy is thus stored within the bulk of the material. To prevent the material from spontaneously debonding when the pressure is removed (spontaneous debonding due to the immediate release of the elastic energy [40, 34, 73]), the pressure must be applied during a sufficient time to allow the material to reach its viscous regime. Such a condition is controlled by the tape rheological behavior depicted below. Once, most of the internal energy has been dissipated, the pressure is removed and the adhesive joint is formed (right image on fig 1.4).
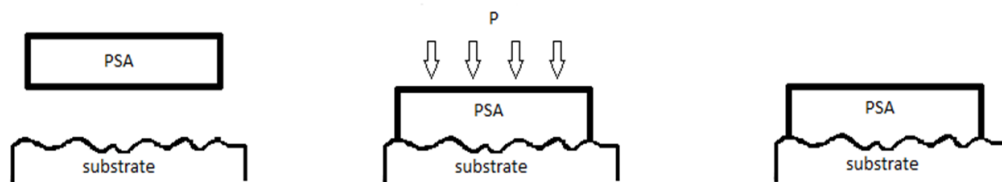
FIGURE 1.4: PSA bonding process

Role of the rheology in the contact formation

The rheology is often the hard point when studying PSA. For long times, researches on PSA in the automotive field where led by mechanical engineers who were not familiar with the science of rheology. In the contact formation perspective, rheology refers to the stage abusively called in the industry

wetting of the adhesive. Works [18, 10] carried out until recently unveiled the fundamental influence of the rheology on the PSA ability to bond onto a substrate. In figure 1.4, we have seen that dissipation is crucial to allow the PSA to correctly "wet" the substrate surface. Hence, it becomes logical that glass transition temperature (Tg) is key. Tg will drive the dissipative regime and therefore the PSA applicability domains. Also, to be a good adhesive, PSA must be soft enough to adapt to substrate surface roughness (so exhibiting a low elastic modulus) but stiff enough to resist to debonding (so exhibiting a high elastic modulus). These two antagonist conditions are met thanks to the polymeric structure on fig 1.5. As a reminder "soft" means that materials have a low shear modulus relative to their bulk modulus and where elastic restoring forces are mainly of entropic origin [18].
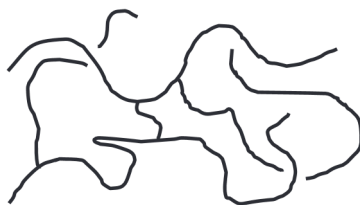
Pressure-sensitive-adhesive

FIGURE 1.5: PSA chains structure [18]. PSA polymer chains are entangled (energy dissipation) and weakly crosslinked (energy storage).

PSA materials are both entangled to dissipate energy and crosslinked to prevent flowing at the macro scale from occurring (weak crosslinking). This structure will store strain energy elastically when deforming during the pressure application time to the surface (see fig 1.4). If the material was fully elastic, this energy should not exceed the reversible Dupré work of adhesion. In this scenario, the amount of energy stored within the material would depend on the roughness of the substrate surface. To couple roughness and material behavior would therefore be of primary when wanting to predict performances of an adhesive joint. However, this coupling is very difficult and hardly takes into account all the diversity of surfaces encountered in the automotive industry [20, 34, 47, 72]. What is more, to be efficient the PSA material must not be only elastic. As seen previously, this stored energy is naturally a driving force to spontaneously debond the PSA from its substrate [40, 34, 72]. Hence, a real PSA is no longer only elastic but exhibits a high viscoelastic behavior. According to Creton et al. [18], this viscoelasticity will allow to dissipate most of the stored elastic energy. Thus, performance of the adhesive joint strongly depends on the history of the material. In other terms, the pressure applied during a specific time at a certain temperature to bond a PSA will influence the whole resistance of the adhesive joint. This energy dissipation will thus reduce the risk of spontaneous debonding by dissipating the residual energy stored because of the local deformation of the PSA to accommodate substrate roughness. Thanks to this local deformation,

the material will form an intimate contact between the adhesive and the substrate. This intimate contact (less than 5nm [57]) will engender the expected adhesion of the PSA material with the substrate.

Rheology is the key driver of a good adhesive material. The question which logically follows is: can we provide the industrialists and PSA users with quantitative criteria to guarantee a good interfacial adhesion formation? An empirical answer has been given by a scientist from 3M company called Dalhquist [21]. He presented in his article three criteria.

- Glass transition temperature well below the usage temperature (chains must be mobile)

- Low shear modulus (10 - 100kPa) when tested at a characteristic frequency of 1Hz (strain energy to conform to even rough surfaces)

- Elastic character at low frequency or long times (preventing the creep)

The big advantage of such criteria is that they are easily applied on PSA rheological data. For example, on the figure 1.6, we find two graphs presenting PSA rheometer measurements (μ' (elastic behavior) and μ'' (dissipative behavior)) for a small strain shear loading.
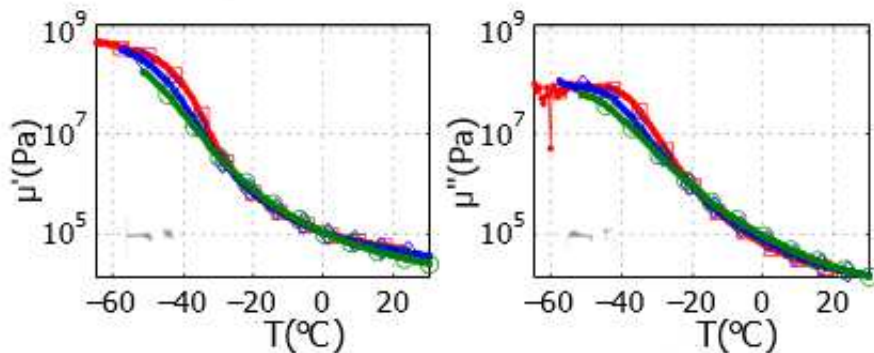
FIGURE 1.6: Rheology of the thin PSA scotch 600 3M (office tape) [78] at 1Hz

In applying the criteria, we can say here that the application temperature domain should be ideally higher than 15°C. Tg (-25°) being measured as the inflexion point of the μ' curve, 15° would allow to respect the first criterion. For this temperature domain, we verify that shear modulus meets the 10-100kPa. Eventually, at low frequency (so at high temperatures in the hypothesis of TTS) we can observe on the μ'' curve that the dissipative parameter is very low. According to Dalhquist, office tapes are supposed to adhere to most kind of substrates.

In this part, we saw that the rheology of the PSA materials plays a significant role in the contact formation. Temperature and frequency conditions

during bonding process pilot PSA surface "wettability". The latter being driven by the chemical formulation, PSA adhesive behavior can then be triggered by modifying the chemistry to cope with a dedicated system. If rheological behavior is satisfying, molecular adhesion is likely to occur which is the base for adhesive joint performance.

1.2.2   The debonding stage

Debonding a PSA can be defined by the breakage of the interface between the substrate surface and the adhesive itself. This stage is represented on figure 1.7.
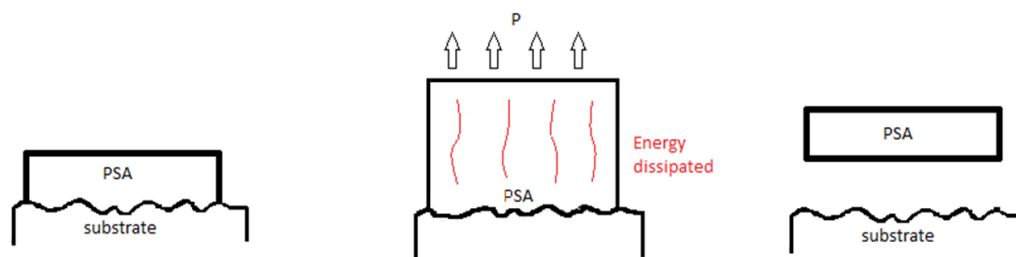
FIGURE 1.7: PSA Debonding process

One can firstly assume that the adhesive is optimally bonded to a substrate (first drawing from fig 1.7). Then, PSA material is loaded to break the interface (second image). Being soft (see the definition above [18]), the PSA material deforms a lot. During the deformation, PSA dissipates a lot of energy. More the PSA are loaded, more energy is dissipated. This amount of dissipated energy cannot then reach the interface to break it. As a result, one has to provide more and more energy to debond the tape from the substrate which increases adherence level. At some point the energy provided is so large that even with strong deformation the adhesive can no longer dissipate energy and so the interface breaks (called "adhesive failure case", in the third image). The failure can also occur in the bulk (called "cohesive failure case") if the material internal bonds are not strong enough to undergo bulk stresses.

Paradoxical performances of the PSA

The previous explanation on energy dissipation associated to PSA deformation highlights one specificity of the PSA. Adhesive performance of such a material are paradoxical. Indeed, as mentioned in the graph of Kendal [57] (see figure 1.8), we see that if PSA adhesive performances were only due to the interfacial interactions, the overall fracture energy that a PSA could reach would be around a few tens of $mJ.m^{-2}$. This energy level corresponds to the energy needed to break weak bonds (see molecular adhesion above). However, on the figure of Kendall [57] we observe that much larger (resp. smaller) fracture energies are measured. This performance increase (resp. decrease)

is due to the fact that energy is dissipated in the bulk of the material (resp. the substrate surface is altered). That accounts for all the paradox of the PSA behavior. The interfacial <u>adhesion</u> is relatively weak but, thanks to intrinsic properties of the material, the overall <u>adherence</u> is much higher. In the same way, when substrate surface is altered, the interfacial adhesion cannot set properly and the bulk dissipative mechanisms cannot be activated so the overall adherence is even lower than the theoretical adhesion [10]. When using PSA, the most important thing is to ensure that the conditions for activating the internal dissipative mechanisms are met. This is one of the main objectives of this PhD: to understand how dissipative mechanisms act in foam PSA to promote their appearance.
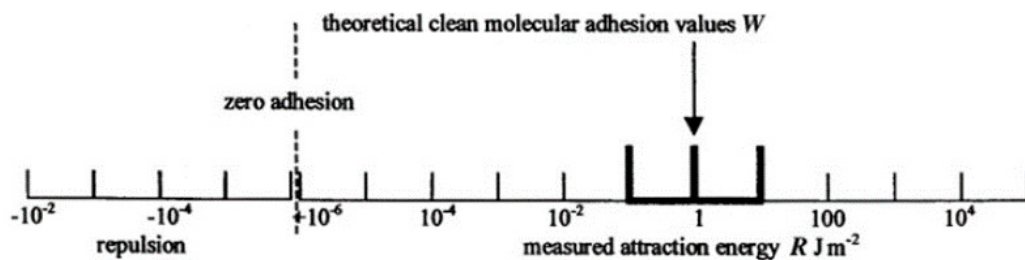
FIGURE 1.8: Adherence length scales: beyond molecular adhesion [57]

As we can imagine, the interest of car makers is primarily in better knowing how to enhance energy dissipation through dissipative mechanisms activation. In the trade literature, we did not find any previous works which were done on these mechanisms in foam PSA. The only ones which have been extensively studied concerned thin and confined PSA materials (thin PSA).

The other case, when PSA adhesive performances are limitied by a substrate surface alteration, is also of interest, especially in order to understand the activation criteria of enhancing phenomena. This point is critical for the car manufacturers which have to design relevant assembly processes to prevent such catastrophic situations from happening. Laying the foundations for such a relevant assembly process is another objective of the PhD program.

Enhancing adhesive performances: how PSA dissipate energy?

When PSA are well bonded to a substrate, when the contact formation is made according to the specifications detailed in part 1.2.1, the adhesion reaches an optimum. That is the necessary condition for the internal dissipative mechanisms to activate and to grow. Without a good adhesion, without a good contact formation, one cannot expect the PSA to be efficient [18, 15, 10, 59]. As previously said, we observed that PSA dissipative mechanisms have been extremely well studied in the literature for the thin PSA (around 100 μm-thick) [51, 38, 10, 18]. Globally, researchers have divided the study into

two stages. First, the initiation of the debonding (initiation of the crack) and then, the debonding front propagation (propagation of the crack).

Initiation of the debonding

Interfacial rupture is the easiest to understand when evoking the initiation of the adhesive debonding. This is the rupture which takes place between the adhesive and the substrate. When an adhesive is bonded to a surface, the contact at the interface is never perfect. Some air bubbles are confined between asperities or other flaws [18].

To quantify them, non-destructive tests are proposed in the literature [68, 69, 63]. The main interest for those tests is that they are applicable in an industrial mass production system. One technology is particularly interesting to describe the interface: multi-emitters multi-receptors tests. They are based on the SVD (Single Value Decomposition) method [68]. Another interesting way to do so is the method presented by Lefebvre et al. [63]. Although interesting, those techniques are not a panacea and the interface characterization remains still today a hot topic for researchers.

Because of the imperfect interface, when the polymer is submitted to a loading as tension, this condition generates a negative hydrostatic stress on those bubbles [36, 17]. The hydrostatic pressure value is strongly dependent on the confinement. The latter is especially high when the adhesive is geometrically confined between two rigid subtrates. As a reminder, we consider geometrical confinement when sample lateral dimensions are not at least ten times higher than the material thickness. In such conditions, these air bubbles tend to grow as cavities. Once a cavity is generated at the interface between the adhesive and the substrate, it grows and develops as presented in figure 1.9 [39]. On this schematic 1.9, one can see that cavities have a common origin, but the development can take two paths. When interfacial adhesion is not very high, debonding can be described by the lateral growth of cavities which progressively leads to a global debonding of the polymer (upper case). In case of high adhesion and high material toughness, cavities will tend to grow vertically. The walls between cavities become thinner and thinner until the creation of elongated polymer parts which are called fibrils (fibrillation or fingering process) [62]. The overall work of debonding can thus become very high. Polymeric PSA being highly viscoelastic, energy dissipated in the fibrils depends on their strain rate and the material temperature [13, 7]. In the relevant regime, adherence energy can easily reach some thousands of kJ.m^{-2}.
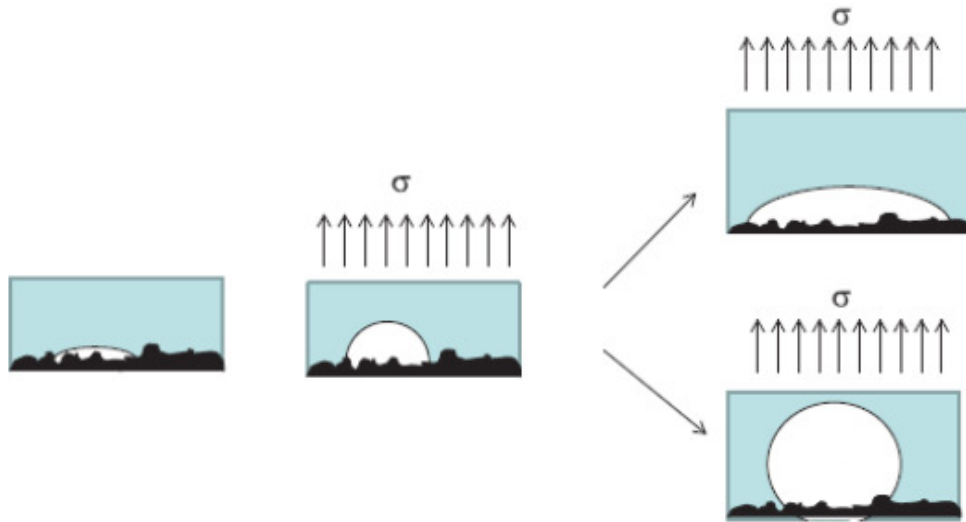
FIGURE 1.9: Cavity growth under uniaxial tension conditions
[18]

These specific configurations can be recreated in lab using the flat ended probe tack test (further details are provided in Chapter 2). The flat ended probe tack test, as depicted in figure 2.15, allows to obtain the curve from the figure 1.10. On this curve, we distinguish direct views of the debonding interface between the adhesive and the substrate.
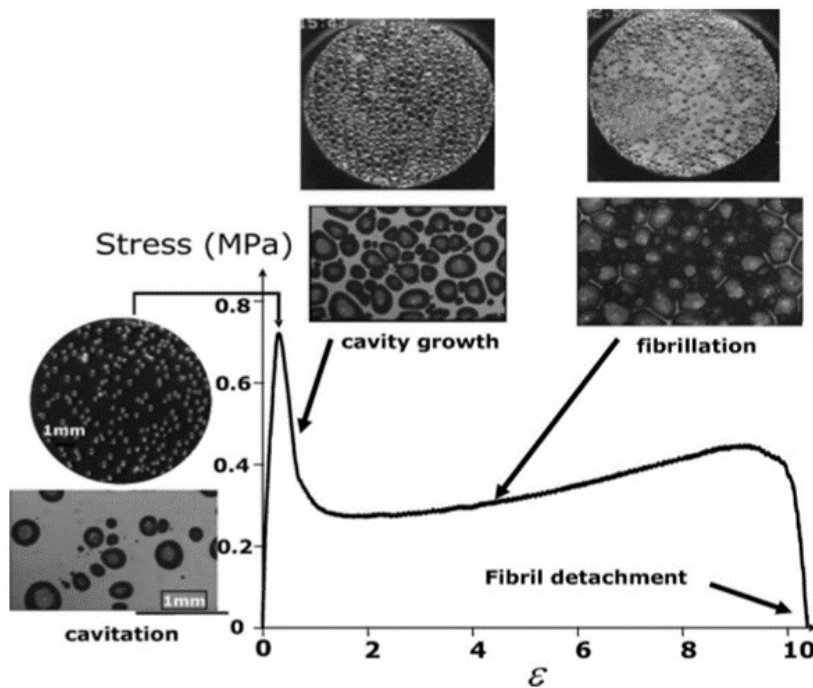
FIGURE 1.10: Tack results for thin PSA using the instrumented flat ended probe tack setup from the SIMM lab [18]

The curve shows clearly the different stages of the debonding crack initiation. Firstly, there is the cavitation phenomenon which appears according to figure 1.10. Then, there is the cavities growth leading to fibrillation process. The thin PSA is then totally fribrillated and the debonding occurs when the single and independent fibrils detach from the substrate. The overall interface rupture is often brutal (end of the curve on the figure 1.10).

Propagation of the debonding front

Once the debonding is initiated, the crack front has to propagate. During this stage the evolution of the debonding is easier studied regarding a steady state regime. A relevant solicitation in this case is the peel test. As presented in the Chapter 2, peeling can engender both cohesive or adhesive failures. The latter has been mostly encountered when studying the debonding propagation of thin PSA [15, 78, 77, 54, 55].

Peeling can be realized at different peeling velocities and from different angles. The PSA being soft materials, it is required to use a backing. The choice of the backing is of first interest. It must be stiff to prevent the debonded part of the adhesive from deforming in tension. But, it must also be elastic enough to bend without plasticizing excessively. By nature, the backing layer confines the adhesive from a fracture mechanics point of view (detail in the fracture mechanics subsection). The idea to keep in mind is that the adherence energy depends on the choice of the backing.
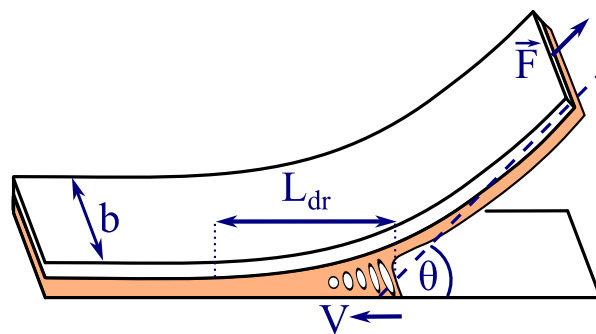
FIGURE 1.11: Peel test modeling [78]

From peel tests, extended researches were carried out regarding the bulk fibrillation process [78, 77, 8, 13]. When flat ended probe tack test points out the creation of the fibrils from cavities nucleation, peeling focuses on mechanisms development. Thanks to instrumented peel test setups like the one presented in Chapter 2, phenomenological models have been enriched by in situ measurements [78, 77]. Recently, such tests have even provided quantitative non linear rheological explanations of those models [13].

Fracture mechanics

In terms of fracture mechanics theories, classic LEFM and NLFM theories still remain feasible under one condition: the substrate must be considered as

infinitely stiffer than the adhesive tape. A good approximation is to consider $E_{substrate} > 100 E_{adhesive}$ [18].

In the interfacial case, reversible Dupré interfacial work of adhesion [28] is written as:

$$w = \gamma_{adhesive} + \gamma_{substrate} - \gamma_{interface} \tag{1.8}$$

It defines the lowest thermodynamic fracture energy an interface can exhibit. This approach is purely elastic. If the PSA were fully elastic materials, adherence would be then equal to w.

Pioneering the domain of fracture mechanics, Griffith [41] associated the creation of a new crack to the conversion of mechanical energy into the purely elastic Dupré work of adhesion [18]. Hence, he introduced the strain energy release rate where:

$$G = \frac{\partial U_w}{\partial A} - \frac{\partial U_{el}}{\partial A} \tag{1.9}$$

This formulation set the bases for the first approach of fracture mechanics: the singularity based model. This model is developed under LEFM conditions. It stands that all the non linear mechanisms happen in a very small region at the vicinity of the crack whereas all the material bulk remains linear elastic (SSY condition). In such configuration, singularity induces a singular stress field diverging with the inverse square root of the distance r from the crack tip:

$$\sigma(r) \sim \frac{K}{\sqrt{r}} \tag{1.10}$$

where K depends on the sample loading ($K \sim \sqrt{EG}$).

Here, the crack propagation (so the debonding for adhesive material cases) is driven by the stress intensity factor which is a material property ($K_c \sim \sqrt{E\Gamma}$ with Γ the adherence energy). If $K > K_c$, there is propagation. At the equilibrium, $G = \Gamma$.

As mentioned above, the performances are paradoxical [57]. Taking into account these dissipative mechanisms, the closest model developed was the one of Maugis et al. [65]. The amount of dissipated energy is there represented by an intrinsic function ϕ so that no other energy losses occur outside ϕ. In those conditions, G becomes:

$$G = w(1 + \phi(a_t.v)) \tag{1.11}$$

where a_t is a temperature parameter and v the limit propagation velocity.

This relationship remains valid if the elastically deformed volume in the bulk can be clearly separated from the length scales of the dissipative processes. However, in most modern PSA, energy is dissipated by mechanisms

appearing in small regions BUT developed in PSA bulk [78]. In that case, Maugis et al. [65] approach is not the most relevant.

In order to couple these bulk dissipative phenomena with fracture mechanics theories detailed above, Creton et al. [18] proposed a multiscale approach represented on figure 1.12.
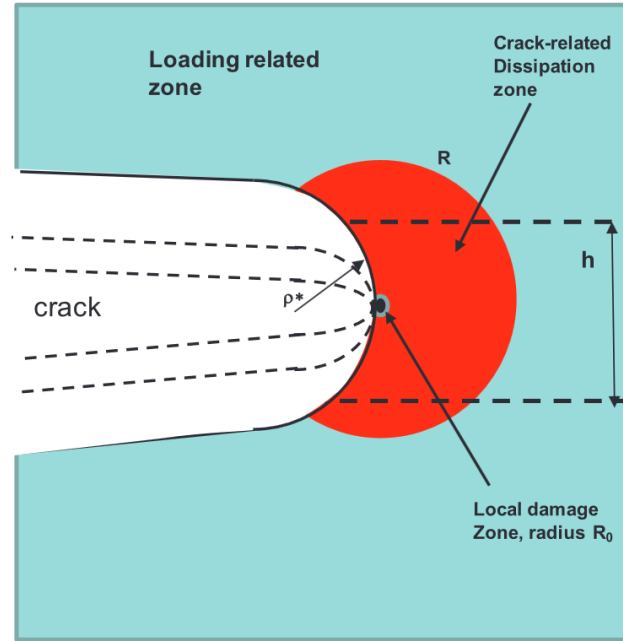
FIGURE 1.12: Schematic of a propagating crack in a soft material [18]

The bulk dissipative mechanisms such as fibrillation are now seen through the bulk dissipated energy Γ and the non linear interfacial phenomena are seen through a Γ_{local}. The transition between these two zones remains poorly explained [18, 22]. In this approach the physical value which drives the crack propagation is the elasto adhesive length, $L_{EA} = \frac{\Gamma}{E}$. When ρ^*, the radius of curvature of the crack tip, reaches L_{EA} value, the crack (debonding front for adherence) propagates. It is worth noting that L_{EA} is an intrinsic parameter. The schematic of the figure 1.12 highlights also a relevant point. Developing dissipative mechanisms in the bulk, PSA can have a theoretical dissipation region size (in red on figure 1.12) larger than the sample thickness. In such situation, the material cannot dissipate as much energy as it could theoretically do. The material is "mechanically confined". Taking into account such bulk dissipation region, peeling models have been based on phenomenological approaches. The first one has been proposed by Kaelble [51, 52, 56, 53, 54]. It assumes that the interface of bonding can be divided in regions of equal size which have the same linear elastic behavior (see figure 1.13). The confinement effect is neglected as well as cavitation. This is a purely elastic model. This has been then improved by using non linear elastic springs.
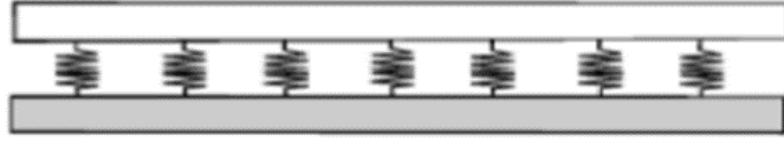
FIGURE 1.13: First Kaelble model

This first approach has been the groundwork for its adaptation to viscoelastic materials taking into account for the first time the tape rheological behavior [37] in the 70's. All the description and the length scales remained the same. Moving further, an extended model was recently provided by Villey [78, 77] where, more than the only rheology, actual physical dissipative mechanisms are taken into account.
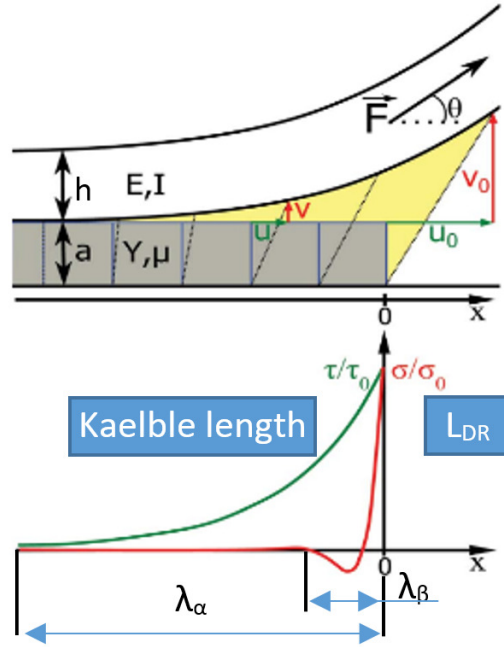
FIGURE 1.14: Kaelble's length scales [51, 52]

In this configuration, some assumptions have been made. The debonding region is defined by the Kaelble zone. In a peel test, the latter defines the region where the stretch energy and the bending energy of the backing is progressively transferred to the adhesive tape. According to Kaelble's model [51, 52], two characteristic lengths can be extracted. The first one is λ_α. It determines the length of the first zone where the stretch energy of the backing induces a shear of the adhesive tape. Calculations based on loading energies give:

$$\lambda_\alpha \sim \sqrt{\frac{Eah_b}{\mu}} \tag{1.12}$$

The second characteristic length λ_β describes the length of the zone where the bending of the backing loads the adhesive tape with a progressive cleavage loading. It is worth noticing that the following pattern accounts for a peeling at any angle (not too small [51, 52]). As well as for λ_α, calculations based on loading energies result in:

$$\lambda_\beta \sim \sqrt[4]{\frac{EIa}{Yb_{backing}}} \tag{1.13}$$

However, the definitions of Kaelble zone are questionable when it comes to describing the behavior of a material with high cavitation and fibrillation processes. In such conditions, Kaelble zone is extended thanks to the L_{dr}, the length of the dissipative region (or debonding region). The comprehension of those geometrical lengths is given by the schematic of figure 1.11.

We saw in this part how PSA can dissipate energy. With a sufficient interfacial adhesion coming from molecular adhesion (see 1.2.1), the PSA highly deforms when loaded during the debonding stage. This load engenders the creation of cavities, cavitation process. They occur mostly at the interface with the substrate. Because materials depicted in the literature are thin (around 100 μm thick) only very few cases of bulk origins cavitation were reported. Those cavities, if the material is tough enough, form fibrils, also called fibrillation process. These fibrils, single and independent, are then loaded in uniaxial tension where their ability to dissipate energy is driven by the viscoelastic behavior of the polymer they are made of.

To visualize the importance of dissipative mechanisms, we can recall the example of chewing gum. Chewing gum adheres easily even if its bonds are weak. Its strong adhesion comes from its high viscous behaviour which can dissipate most of the energy given by the plastic deformation due to the attempted removal. In this case, the molecular adhesion is not huge but the macroscopic dissipation mechanisms amplify it enormously.

Many attempts to model the behavior of thin PSA in peeling conditions were reported and the most relevant seem to be the ones derived from the foundation-based approach of Kaelble. The lattest version described by Villey et al. [78] gives a relevant starting point to study the behavior of the foam PSA.

The limits of PSA usage: when the substrate surface is altered

On the contrary to the previous situation, we saw that the PSA overall adherence can also be lower than the theoretical interfacial bonding performances one can expect from molecular adhesion. This situation is encountered when this molecular adhesion does not take place between the adhesive and the

substrate surface. According to the trade literature, there are mainly two factors which can lead to that kind of poor interfacial adhesion [59, 15]: **surface contamination** and **surface geometry**.

In the first case, contamination affects dramatically the molecular adhesion in reducing it. If the molecular affinity of the surface is important, contamination can cause repulsion of the molecules likely to lead to a "weak" failure of the adhesive joint. Contamination is defined by the second law of the theory of adhesion proposed by Kendall [57]: "Contaminants can be either solid particles or fluids (water, grease, air...)." They have three origins:

1) Environment during bonding of the adhesive (workshop atmospheres with dusts, grease, human perspiration, air...). In the automotive industry it is mostly the presence of dust and wax clouds which can be troublesome.

2) Primary preparation of surfaces of the substrate (paintings, varnish, demolding agents...) [46]. The composition of the substrate surface of a painted car is multilayered (see the figure 1.15).
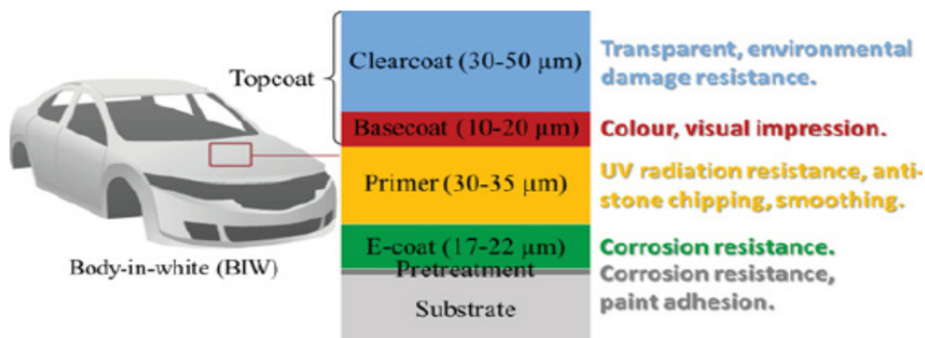
FIGURE 1.15: Painting layers in automotive field [81]

The final varnish is tailored to exhibit a low surface tension (around 45-50dyn.cm^{-1}) to avoid dust and mud aggregates to stick to the car. For the same purpose the polar contribution of the varnishes is thus reduced. The affinity to acrylate based PSA is then reduced.

3) Secondary preparation substrates surfaces (solvents...). In the automotive domain, in order to remove potential contaminants from the substrate, car makers use solvent-soaked wipers. In his PhD, Horgnies [46] showed that the choice of the cleaning solvent is critical for the adhesive joint performances.

Contamination reported before consists of the settlement of molecular layers of contaminants disturbing the establishment of the intermolecular interactions (schematic a) or even causing breakage of the chemical bonds (schematic b).
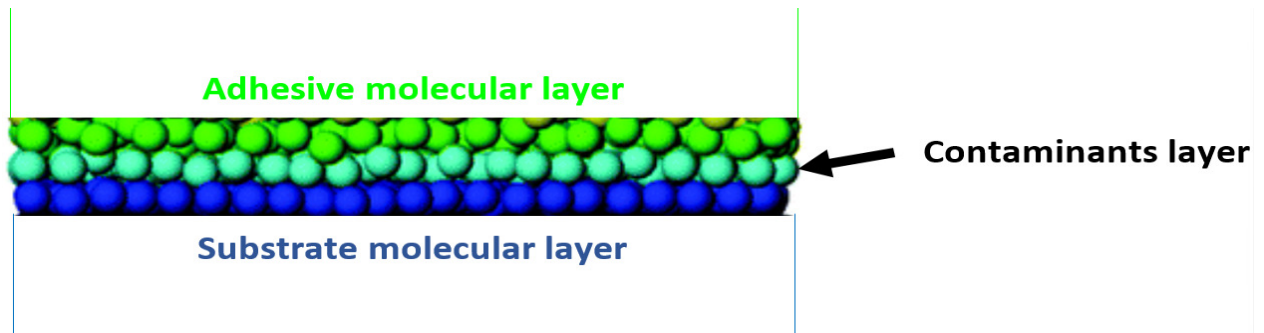
FIGURE 1.16: Screening effect of contaminants

In the second case, substrate surface geometry can decrease the molecular adhesion in two situations. First of all, because of the local roughness of the substrate. Roughness is one of the most influential parameter acting on the molecular adhesion energy. It can be useful for both improving and reducing the adhesion. Under this angle it appears to be paradoxical. In fact, in order to understand the roughness-related mechanisms, one must take into account the stiffness of the adhesive plus the actual roughness of the substrate surface [57]. If roughness is high, the adhesive has to be soft enough to accommodate and spread the most on the contact zone. On the contrary, if the surface is relatively smooth, the adhesive must be stiffer. These results have been established by Fuller and Tabor in 1975 [34]. The difficulty to take into account roughness when studying adhesion problems is its randomness. Johnson [49] proposed a statistical method to model all the asperities. Implementing this computer model, Fuller and Tabor found out that roughness and elastic modulus (i.e. stiffness) evolutions are equivalent [34]. Physically, roughness can be defined by being an obstacle for the wetting of the adhesive to the substrate surface in the case of elastic material. However, when the adhesive material is highly viscoelastic, this roughness can enhance interfacial adhesion by maximizing the surface contact. Adhesion enhancement and decrease are then piloted by the couple material viscoelasticity and substrate roughness.

Another situation where substrate surface geometry can decrease interfacial adhesion is encountered when substrate and bonded part have a different curvature. Such a difference leads to increase residual stresses within the PSA. On the figure 1.17, we can observe the problem more clearly.

On the photograph, we see that the difference of curvatures of the two materials (beam and body of the car) loads the PSA on the edges (in blue circles). Hence the latter is bonded while being mechanically loaded. Even if the contact is correctly made, locally the material undergoes mechanical stresses and is likely to debond after the application pressure removal.

Since the 60's with Kaelble [51], PSA materials have never stopped being an intriguing topic for researchers. Most researches have been carried
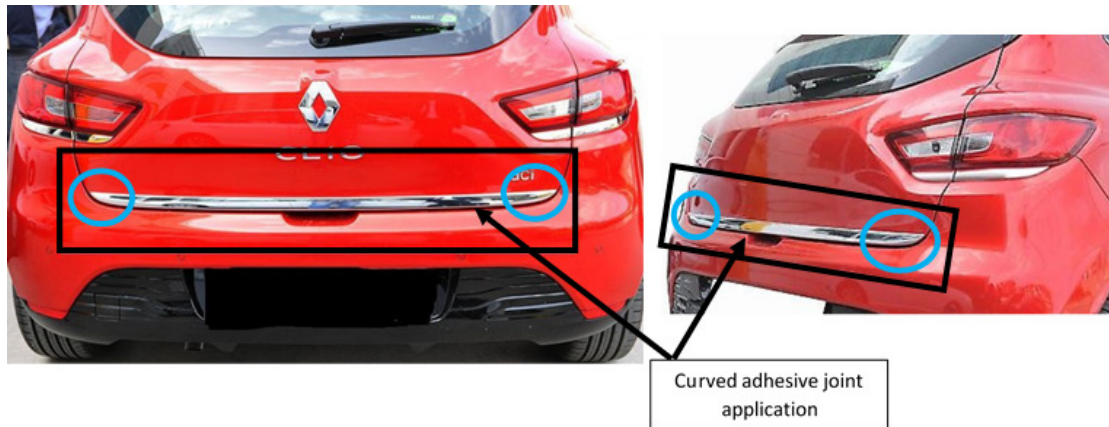
FIGURE 1.17: Curved adhesive joint application

out focusing on the thin and confined PSA. For such materials, the literature provides us with qualitative and quantitative tools to understand their behavior. The main idea to keep in mind is that adherence problems are multi scales. For the bonding stage, one highlighted the role of the rheology on the contact formation. That allows the material to create an intimate and stress-less contact with a substrate. Such a close contact is a prerequisite for the establishment of molecular adhesion which is the keystone of the adhesive performance. Regarding the PSA debonding, researchers understood that thanks to energy dissipative mechanisms such as cavitation or fibrillation, it is possible to enhance PSA adhesive joint performances. Researchers built models to explain the material behavior. These models come from two different ways. The first ones derive from the "foundation-based approach". They seem to take well into account the dissipative mechanisms, essential for the foam PSA. The second ones derive from the "singularity-based approach" but they do not seem to be so relevant when large strain fibrillation occurs. The last point evoked in the literature brings to light PSA usage limits. Although it improves adhesion, the surface chemistry of the substrate can also significantly reduce the performance of adhesive joints. To explain this, surface contamination and mechanisms related to geometry were mentioned.

1.3 PhD problematic definition

Besides the scientific research objective, the doctorate program presented in this thesis has another challenge. It must also address industrial questions. The first question that both industrial and lab have is to characterize the material itself. What is the structure of such a material? As we said previously, the material studied here is a commercial product so with an unknown characterization. What is more, its characterization is not trivial. It is a soft, thick, and sticky material. Dedicated methods and tools have to be designed.

Regarding the literature, the second question which pops up concerns the rheological behavior of the foam PSA we study. From a scientific point

of view, carrying out rheological tests is interesting for both experimental protocol design and measurements. Does the particular material structure impact the rheological behavior in small strain regime? From an industrialist point of view, carrying out such tests could allow them to approach their bonding process from a rheological point of view. This was never done in most automotive companies.

The third point emphasizes the debonding stage. For a scientific purpose, it is very exciting to unveil the physics behind the energy dissipation. How energy is dissipated in the foam PSA? Do the dissipative mechanisms follow the same rules as for thin PSA? Previous researches never looked at the impact of bulk structure in the dissipative phenomena appearance. How do they affect the material behavior and especially, adhesive joint performance? Is adherence energy still enhanced in the same proportion by dissipative mechanisms? Does the substrate surface state impact mechanisms activation? For the car maker involved in this doctorate program, the goal of this third point is to open the black box of foam PSA debonding. Before this work, a bonded assembly failure was explained by the simple sentence: "The assembly breaks.". It is obvious that such an accident report is not sufficient to implement sustainable solutions to prevent deficiency from occurring again, especially in systematic processes. Thus, in the following thesis we explain in a mass production oriented language what happens when the PSA debonds. We offer solutions to rethink the way bonding is made in factories, the way assemblies are designed.

The last question regards modeling. In the literature, we found numerous descriptions of the main mechanisms implied in the energy dissipation. Could they be applied to foam PSA? From a mechanical point of view, performing fracture mechanics in such a material is a real challenge. Moving from crack tip singularity to large strain dissipative models, the foam PSA debonding behavior is a perfect system to find links between those two approaches. Hence, one the PhD objective will be to formulate phenomenological models coping with the foam PSA particularities? As we saw in the above contextualization, this research aims at becoming more quantitative regarding the design of PSA bonded assemblies. Thanks to the work which is presented in the following thesis, the ultimate goal is to lay the foundations to move to a more predictive approach of adherence.

The latter points highlight the strong industrial need for developing knowledge around foam PSA. The literature review pointed out the missing elements in the scientific community. According to what has been said before, the key problem concerns the way foam PSA dissipate energy. That is based on this point that new phenomenological models will be built. Hence, the common goal of predicting bonding failure shared between researchers and industrialists would be fulfilled. To open the black box of the foam PSA, we then focus on the following problematic: *Dissipative mechanisms during the debonding of high performance foam pressure sensitive adhesives for automotive.*

Chapter 2

Foam PSA for high bonding performance

PSA for high bonding performance are a very exclusive class of adhesives. They mainly differ from the others by their large thickness (around 1 to 3 millimeter-thick). At the beginning of the doctoral research, the PhD partner company came with a roll of this specific tape adhesive. The first question we asked ourselves was: what is inside this material? Hence, the PhD research starts by developing a strategy to characterize the material itself. As we further describe such material has a very unpredictable and intriguing architecture when thinking about an adhesive. Once we identify the material structure, we establish a strategy based on the dedicated literature to study all the debonding stages, from crack initiation and propagation to final detachment.

2.1 Material characterization

In order to characterize the material, we first unveil the material structure thanks to optical microscopy, SEM and microtomography X. Then, we focus on the rheological behavior of the tape. Beyond knowing the foam PSA rheology, the goal is also to compare foam PSA with thin PSA (both with a similar chemical composition) extensively studied in the literature [24, 10, 83]. Eventually, we concentrate on the large strain behavior of the tape. This characterization is relevant because the foam PSA is supposed to deform a lot during the debonding. Such large deformation sollicitates non linear rheology which pilots energy dissipation and so adherence energy [13]. Thanks to the results of this characterization we then provide the main features to implement in potential FEM calculations.

All the experiments presented afterwards are carried out either in the Soft Matter Sciences and Engineering Lab, SIMM of ESPCI school in Paris or in the Renault Technocenter in Guyancourt.

2.1.1 Structure identification

Optical Microscopy

The first characterization experiment is a straightforward optical observation. We observed PSA morphology from its surface. With a magnification x200, we can see the presence of many spherical bubbles (fig 2.2). The maximal size is around 100 micrometers diameter. Although the PSA is made of acrylate monomers, the color is grey. After making a short benchmark, we found out that PSA colors are purely for aesthetics (colors of the external parts of the car) and marketing (brand differentiation among suppliers). Color is given to the material thanks to the presence of black carbon particles (less than 10% volumic) and Titanium Dioxide TiO_2 (less than 10% volumic). It is worth noticing that such low concentrations, less than 10%, should not affect the mechanical behavior of the tape [26].
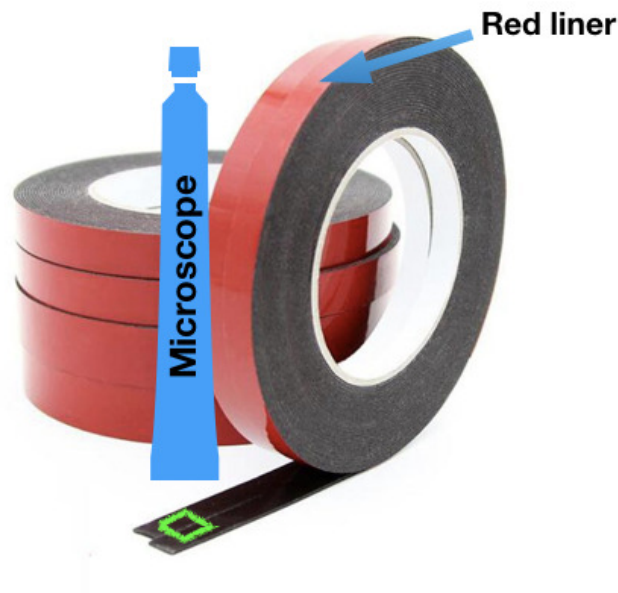
FIGURE 2.1: Microscopic observations of the foam PSA surface (area in green). The unstretched tape (a on fig 2.2) is observed with the red liner to prevent potential damages due to liner debonding from occurring. The stretched sample (b on fig 2.2) is observed without the red liner to be easily deformed.

Scanning Electron Microscopy

In order to confirm the nature of the "bubbles" observed with the limited range optical devices, we use for more accuracy the FEG SEM technology. The machine is the Magellan FEI Thermofisher with a vacuum chamber of 10^{-5}mbars, a voltage in the range of 0 - 30kV.
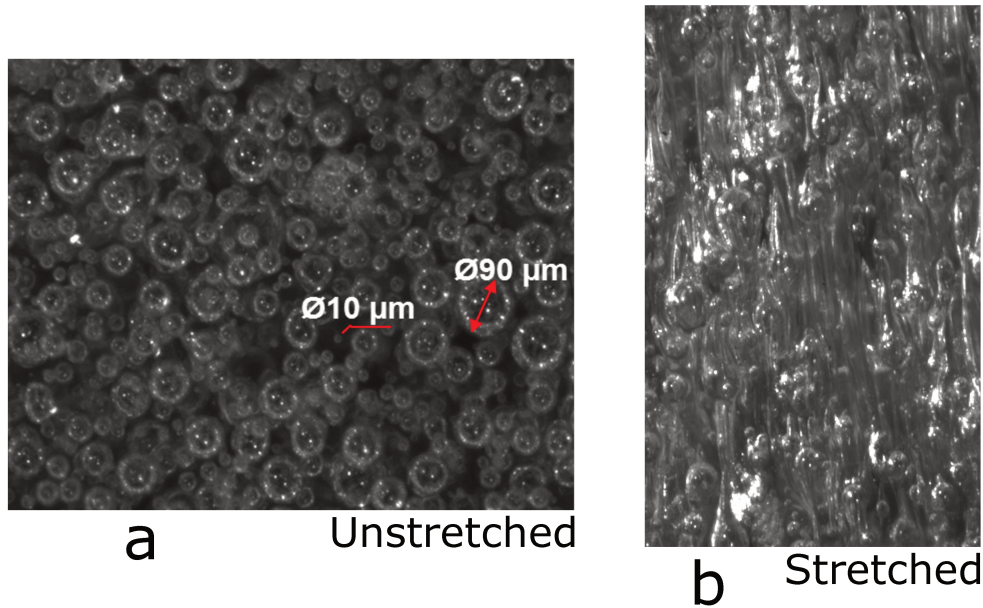
FIGURE 2.2: Microscopic observations of foam PSA surface. a image refers to unstressed sample and b image refers to sample stretched at around 400%

For the first experimental round, we metalized all the samples. For an unknown material it is the simplest manner to get accurate pieces of information. We start by recording images from the surface of the underformed sample (image fig 2.3). To be able to determine the internal composition we then observe a section of the undeformed material (image fig 2.4). To get a clear and observable section, we worked on developing a method to cut the material. PSA being highly viscoelastic, cutting is very troublesome. The simplest technique we found is to drown the sample into liquid nitrogen. We notice that drowned in liquid nitrogen, samples exploded one after the others. That is another hint of potential presence of beads inside. Such beads could increase internal stresses (causing the observed explosions) when the material cools down quickly as with liquid nitrogen. Onto the broken parts, we deposited a metal layer during ten seconds and directly put them in the vacuum chamber of the microscope. According to the metalization machine, the deposited layer of gold is less than 20nm. In doing so we obtain the comprehensive images 2.3 and 2.4.

On the two images of the surface, we observe the presence of spherical shapes which are flush. It is worth noticing that the small roughness we tend to distinguish is in fact a bias due to the metal layer deposition. On the image of the section 2.4, we confirm the presence of real spherical beads drowned in the matrix. A closer look to them allows to say that there are hollow microspheres (see figure 2.4).

The measurement of shell thickness gives a value of 2 micrometers (see fig 2.5). EDX characterizations return that microspheres are made of glass.
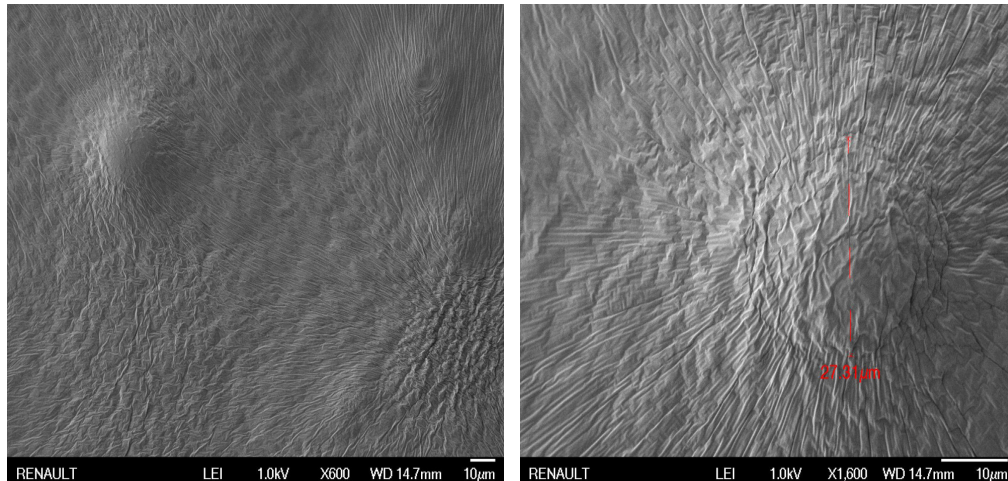
FIGURE 2.3: SEM observations of the unstressed material
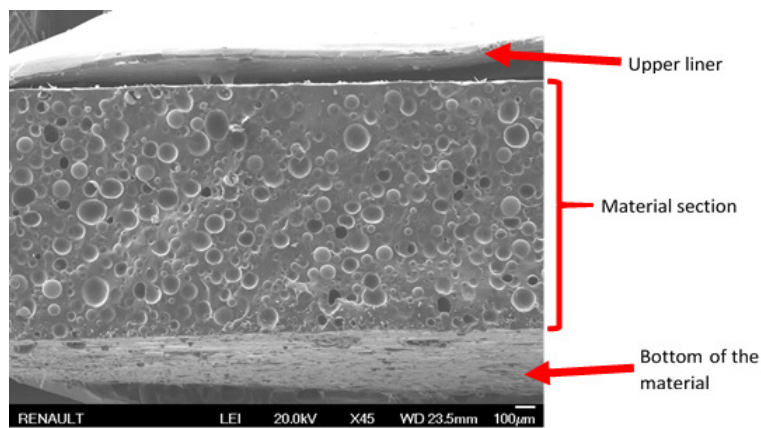
FIGURE 2.4: SEM section observations of the "liquidly nitrogenely" cut material.

Typical use of that kind of beads in other domains (bumpers forming, reinforced polymers... [6]) hinted that they could received a surface treatment during material production. With our EDX device we checked that no such treatment was made. That means also that no interfacial adhesion triggering (between spheres and matrix) is made at the scale of the beads.

Even if we performed SEM on as many sections as we could, this type of observations remains too local to generalize results. That is why we move to another characterizing technology which is the micro tomography X.

Micro Tomography

Micro tomography X is a technology where internal structure of materials can be observed in a non-destructive way. X-rays are emitted and then pass trough the sample of interest before reaching a detector. The final result is an assembly of all the images reconstructed based on this receptor while the sample is spinning. Eventually, we obtain a 3D image of the object structure we are studying. Technology principle is illustrated on fig 2.7.
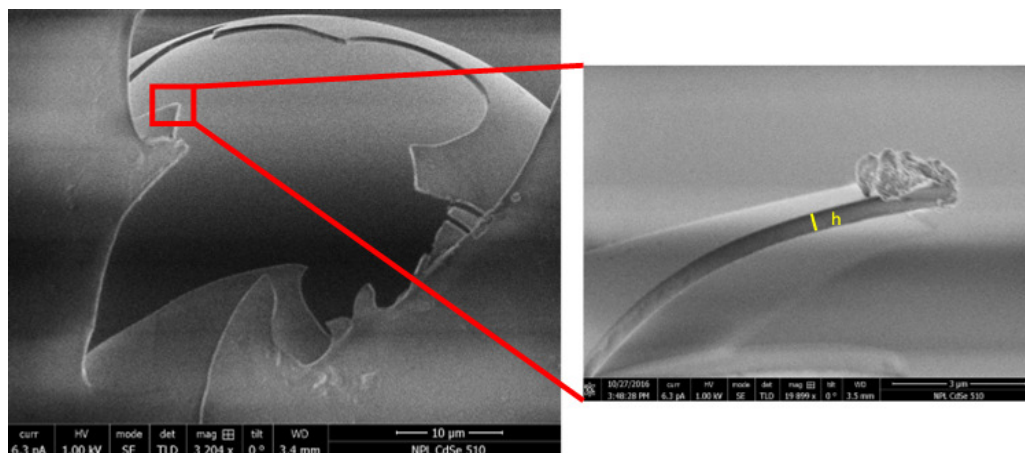
FIGURE 2.5: Microspheres wall thickness measurement
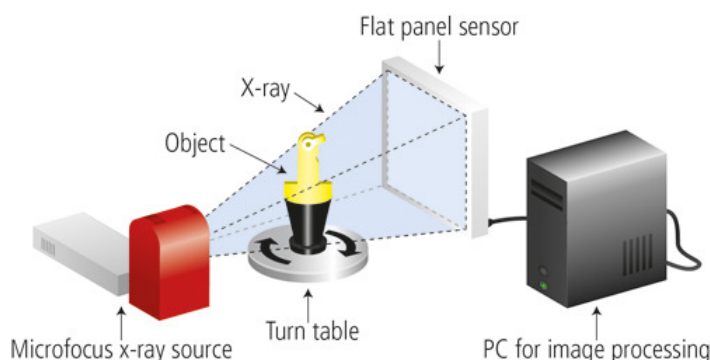
FIGURE 2.6: X ray tomography principle

The machine used in this PhD work is the microtomograph located in Renault technocentre in Guyancourt. The biggest challenge to overcome in such test is the low materials densities. The density of the hollow spheres is very close to the air as well as the polymer one. Hence, the emission parameters must be adapted to trigger the X-rays beam (*nb: it would have been much better to work on a synchroton with a phase contrast*). The image presented on figure 2.7 shows a slack taken during one emission period. From all the slacks we got we reconstructed the full structure of the sample.

Based on these measurements, we post-treat images to get a quantitative idea of the PSA structure. There is 37% percent in volume of hollow glass microspheres and their size are continuously spread over the range [10μm to 100μm]. Such glass microspheres are largely used in industries going from pharmaceutical companies to defense domain. They are most of the time filled with inert gas such as nitrogen [75].

Structure of the foam PSA

According to results obtained with these three characterizing techniques, optical microscopy, SEM and microtomography X, we can describe the structure of foam PSA as follow. It is a composite material where the matrix is
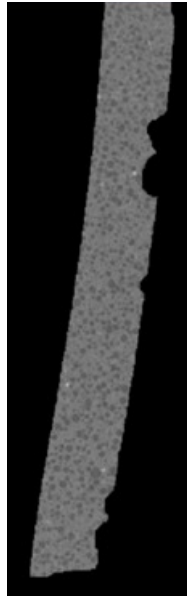
FIGURE 2.7: Slack obtain from tomographic experiment. The croped part on the right edge corresponds to image post processing correction

the acrylate-PSA itself (fully incompressible) and where there are two types of fillers. At the nanoscale, there are black carbons and TiO_2 particles which have no effect and the mechanical behavior. At the mesoscale (around μm scale), there are hollow glass microspheres. On the contrary to the previous ones, these fillers are likely to strongly affect on the tape behavior. This effect will be of major interest in the framework of this research.

Discovering such a peculiar structure made us think about the structure of another class of materials, **the syntactic foams**. An extensive review was provided by Ruckebusch [75]. He showed the relevance of using such architectures to resist to high pressure applications. Syntactic foams are indeed widely used for deep water devices where external pressure is gargantuan. The latest hollow glass microspheres can generally undergo "external pressures exceeding 2000 bars", Ruckebusch said [75]. Drown in resins or elastomers, they account for materials lightness and resistance. At this point of the structure identification, we were glad to find that such an interesting architecture was also used in other domains. However, all these syntactic foams applications motivated industrial and academic researchers to study the material in compression and not in tension which is the case when studying debonding [14].

We saw in the state of the art review (in part 1.2) that PSA polymers like acrylates are entangled and crosslinked exhibiting a "soft" behavior [10]. Such a behavior differs a lot from the mostly elastic elastomers used in classic syntactic foams [14, 43]. To check if this architecture affects the incompressibility of the matrix, we use a simplified model of automotive tape structure. From a general point of view, we evaluate the compressibility of an foam PSA

in its unstressed initial state represented in the schematic of the figure 2.8.
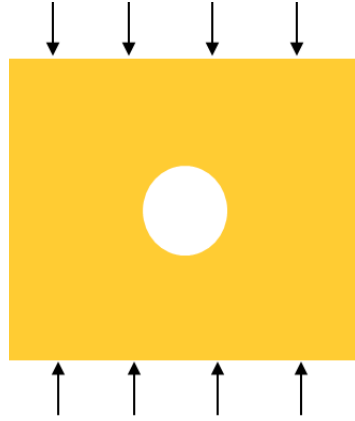
FIGURE 2.8: Simplified model of foam PSA structure

We first assume the presence of one single hollow glass microsphere having the average diameter of the spheres in the real material. We then assume the material loaded in compression. Hence, calculations give the following Poisson's ratio for the pseudo syntactic foam.

$$\nu_{foam} = \frac{1}{2} - \frac{1}{6(1 - \alpha_s)} \frac{E_{foam}}{E_{sphere}} \left[\frac{3}{2}(1 + \nu_{sphere})\alpha_s - 2(1 - 2\nu_{sphere}) \right] \qquad (2.1)$$

We consider here that α_s is the shape parameter of glass microspheres. For a_i the internal radius and b_e the external radius of the sphere in the simplified model (figure 2.8), we have: $\alpha_s = (\frac{a_i}{b_e})^3$, shape parameter with $a_i = 48 \ \mu$m and $b_e = 51 \ \mu$m (average size of the spheres).

Numerical result gives a Poisson's ratio of 0.4998 which highlights that taking unstressed foam PSA as being incompressible is a reasonable hypothesis. As it stands, the structure we have in mind to represent the foam PSA is presented in the figure 2.9.
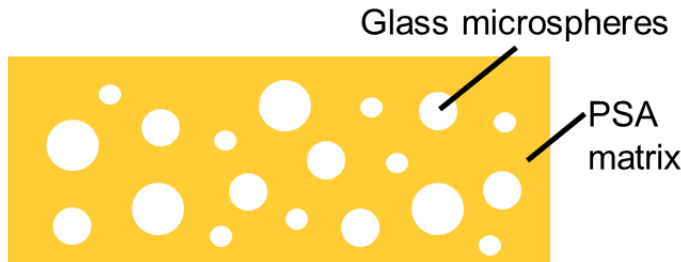
FIGURE 2.9: foam PSA architecture: syntactic foam

To sum up, we have a syntactic incompressible foam made with a acrylate based polymeric matrix and hollow glass microspheres having a size

spread continuously within the range [10μm to 100μm]. In a first approximation (justified by the following rheological characterization), we consider the acrylate based polymeric matrix very close to thin PSA presented in the bibliography (see part 1.2). Following this point, it is very interesting to carry out measurements to see how this peculiar architecture impact or not rheological behavior of the foam PSA. It is also of prime interest from an industrialist point of view to check if the Dahlquist criteria remain valid for this type of material [21].

2.1.2 Rheological characterization

To perform rheological measurements, we used the Anton Paar Rheometer Physica MCR 501. This rheometer allows measurements in small strains shear loading. The geometry chosen was a contact plan. The key with that kind of material is to take into account the high material viscoelasticity [66]. At low temperatures (around -40°C which is well below the glass transition temperature ≈ -25°C), the material behaves like a brittle material. During exploratory tests, we observed a thickness decrease of 17% corresponding to 0.2mm (as a reminder the initial thickness of the material is 1.2mm). On the contrary, for high temperatures (above 50°), the material swells significantly (0.15mm, 13% of the initial thickness). This behavior change is very troublesome because it also increases the risk of slipping of the PSA between the two contact planes. We solved this geometry change problem by applying a vertical axial force of 1.1N ($\approx$ 22Pa). This force was high enough to prevent slipping from occurring and low enough not to compress excessively the PSA.

According to this classic protocol [66], we performed rheological measurements depicted in the figure 2.10.

Based on these results, a TTS (time temperature superposition) is made by determining a_T shift parameters thanks to a WLF law. The reference temperature is 21°C. Those shift parameters will be also used in the part 3.3. To take into account classic limitations of WLF transposition, the shift is made between Tg -10° and Tg + 80°C.

Rheological results 2.10 and 2.11 highlight the large dissipative domain which is in good accordance with the bibliography on PSA [24, 10, 15, 18]. In the case of the foam PSA, the glass transition regime is very wide (width of the tanδ bell on fig 2.10. By convention, we then measure the Tg as the midpoint of this regime which corresponds to the inflexion point of the G' curve. According to the graphics presented above, Tg $\approx$ -25°C. On the temperature measurements, we observe that the optimal minimum application temperature according to Dahlquist [21] (Tg + 40°C) is 15° which is exactly the lowest application temperature in automotive factories. The second criterion for Dahlquist is that the PSA material must exhibit an elastic-like behavior for very small frequencies. This condition is required to prevent tape from
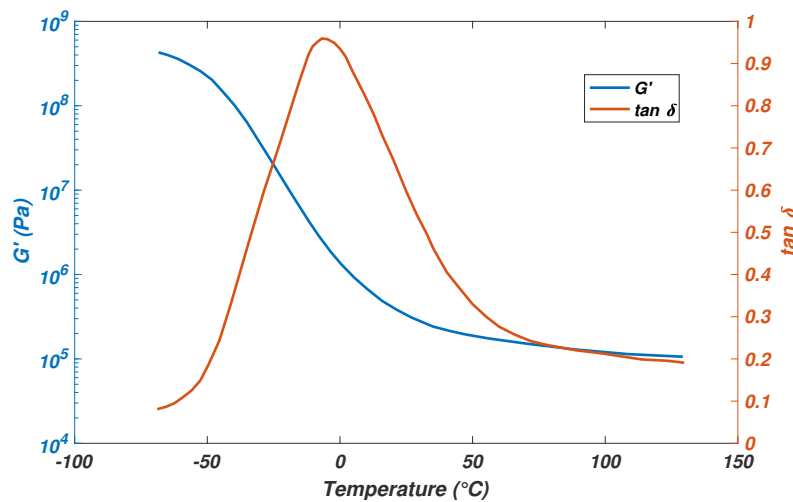
FIGURE 2.10: Foam PSA rheological behavior in small strain regime. The test is carried out by soliciting the material in shear from -60°C to +130°C. At every 3°C a frequency sweep is carried out between 10^{-1}Hz and 10^1Hz. G' and tan $\delta = \frac{G''}{G'}$ are plotted on the graph with respect to temperature.

creeping. On the fig 2.11, we observe that this condition is met. G' is clearly larger than G'' for frequencies below 1Hz. At 1Hz we also distinguish that G' is equal to 400kPa which is ~100kPa, the last Dahlquist condition. This high value, compare to thin PSA, can be explain by the high thickness of the material. To prevent a so soft material from creeping, crosslinking level might be higher which increases G'. Hence, we can say that foam PSA, even being much thicker than any other thin PSA, are likely to spontaneously bond to any substrates. It is important to note here that the high material thickness do not seem to affect the linear small strain regime studied with this test.

Moreover, it is worth noticing that the tan δ which is the ratio between the ability of the material to dissipate energy by molecular mechanisms (G'') over the ability of the material to store energy under elastic form (G') is very high (up to 0.5) in a certain frequency range [1Hz,10^3Hz]. A so large value reinforces the idea of the great ability of foam PSA to dissipate a large amount of energy. According to what we said in part 1.2. bonding effectiveness is directly related to linear rheology [21, 10, 24, 15, 18]. It is then not surprising that we observe the same rheological characteristic with foam PSA. Their high thickness (10 times thicker than classic thin PSA) and particular structure (syntactic foam) does not affect this linear small strain rheological behavior. In Chapter 3, we will go further in the study of foam PSA rheology by focusing on the relationship likely to exist between non linear rheology and adhesive performance.

In an application oriented mindset, the optimal frequency range for the contact formation is then defined by the high value of tan δ. Given by the graph from the figure 2.11, this range is [1Hz to 10^3Hz]. In small strain
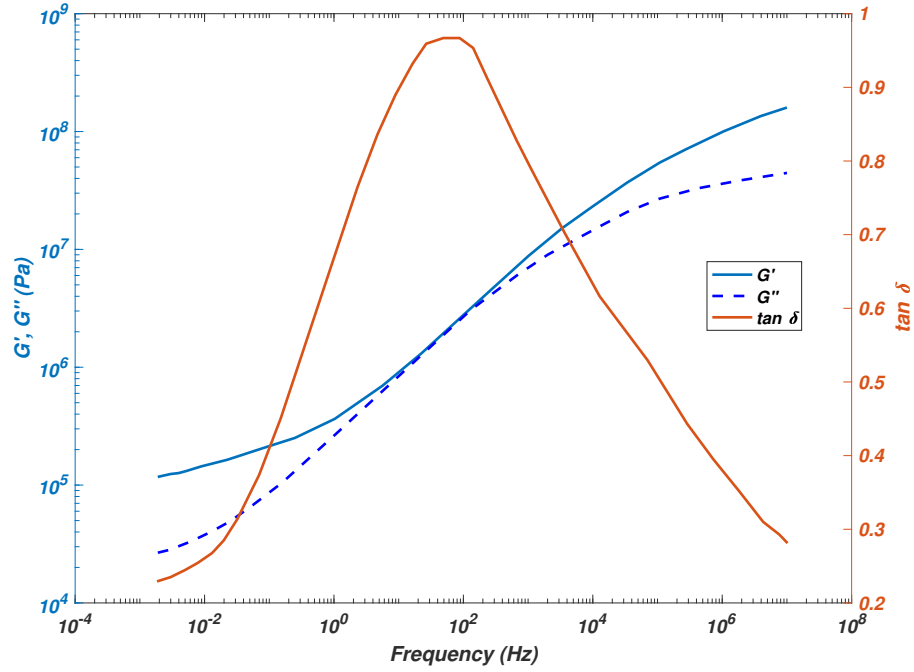
FIGURE 2.11: Foam PSA rheological behavior in low shear level regime, frequency dependency of the master curve [23]

regime corresponding to the conditions met during bonding process, if we use the Cox-Merz principle [80] ($\dot{\varepsilon} \sim \omega \sim \frac{1}{t}$), 1Hz $\sim$ 1s can be assimilated to a manual bonding process (pressure applied by the fingers of operators during approximately 1s). Following the same principle, 10^2Hz would correspond to a pressure application of 10ms which is the condition met by robotic applications of PSA. These frequencies belong directly to the optimal bonding frequency. Even more, 10^2Hz is the frequency corresponding to the maximum reached by tan δ. We can deduce that it refers to the situation where the tape is the most able to dissipate energy. Interestingly, the first remark we can make is that robotic industrial processes are then much likelier to obtain a good interfacial adhesion. Based on this conclusion it is worth noting that a short accident survey in the partner company showed that 100% of the last parts debondings happened on manual PSA applications.

These measurements show very interesting results. We first observe that foam PSA behave according to the Dalhquist criteria for spontaneous adhesion. We can thus reasonably think that bonding process and so, interfacial adhesion, is driven by the same parameters than for classic thin PSA. The particular structure of foam PSA (its high thickness and the presence of beads) does not change the linear small strain rheology of the tape compared to the one observed with classic acrylate thin samples. Like for thin PSA [35], from a rheological point of view, contact formation for foam PSA is then supposed to occur in the same manner. After the contact formation, we lay the emphasis on the first step towards the debonding process of foam PSA: studying their non linear behavior.

2.1.3 Tensile test behavior

When talking about material characterization, the most common test performed is the uniaxial tensile test. The setup used is the classic Instron 5980 placed in an oven for temperature controlled tests (see figure 2.12). This machine is equipped with an optical extensometer and tests have been carried out using sensors of 10N and 100N capacity.

FIGURE 2.12: Tensile tests setup: Instron machine ref 5980

In order to characterize the large strain behavior of the PSA material, we started by performing tensions until rupture for different strain rates at 23°C. The geometry of the testing samples is the classic "dumbbell" shape.

On the graph 2.13, we observe that strains at rupture are very high for all the strain rates. We also observe that strain rates have a major influence on the material behavior. That is in good accordance with the literature [10, 18] where we can find that such a material is likely to be highly viscoelastic in a non linear regime to dissipate energy (see PSA definition part 1.2). In addition, we distinguish hardening phenomenon which occurs at the end of the loading. This hardening is rate-dependent. Such a phenomenon has been evoked in recent articles [13, 77] to explain the fibril detachment from a substrate. We come back on this point later in the thesis.

To complement the characterization of foam tape dissipative behavior, we carry out cyclic tension tests. In order to have an idea of the maximal strain before a potential damage, we performe loading unloading cycles with an increasing maximum strain. It starts at 50% of deformation. After each cycle, the material has 15 minutes to relax before the re-loading sequence. The strain rate is arbitrary chosen at 0.05s^{-1}. This choice is motivated by a larger
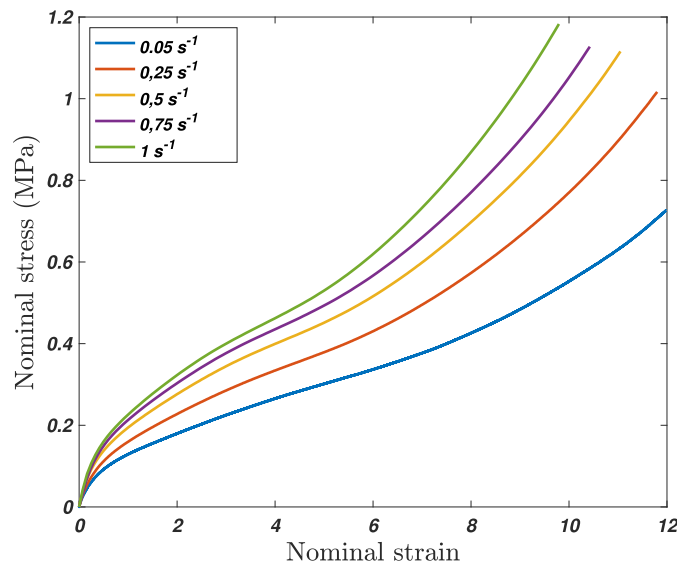
FIGURE 2.13: Tensile tests foam PSA responses

hardening effect at higher strain rates. In doing so, the objective is to reduce its influence on the tape behavior. As previously said, tension tests are widely used when taking about material characterization. The interest of this test here consists of soliciting in a large strain tension regime a syntactic foam structure. In general, the literature reports uniaxial loading quasi uniquely in compression [14]. This is motivated by the industry where most of the researches on syntactic foam are conducted for deepwater applications, oil and gas, estate building... [75]). The results obtained with such cyclic loadings are presented in the graph of the figure 2.14.

On the graph 2.14 we can see that when considering the three first cycles (in blue on the graph), loading paths are roughly the same. However, from the fourth cycle to the end (in brown on the graph) loading paths are lower and lower. This means that the material becomes softer and softer with the number of cycles increase. Such a behavior is very similar to damage observed generally with "Mullins effect". However, this explanation is quite surprising since the black carbons concentration is too low to have a significant influence on the mechanical behavior of the tape [26]. Due to the particular structure of foam PSA, we thought that the presence of hollow glass microspheres could then plays a role in this softening effect. This hypothesis will be confirmed in Chapter 3.

The experiments depicted above allow us to define clearly the architecture of the material. The foam PSA have a syntactic foam architecture composed mainly by a matrix (made of a soft acrylate polymeric material) and hollow glass microspheres (size distribution belonging to [10μm, 100μm]. In volume the percentage of those beads is of approximately 40%. In its unstressed state, a reasonable approximation is to consider the foam PSA as an
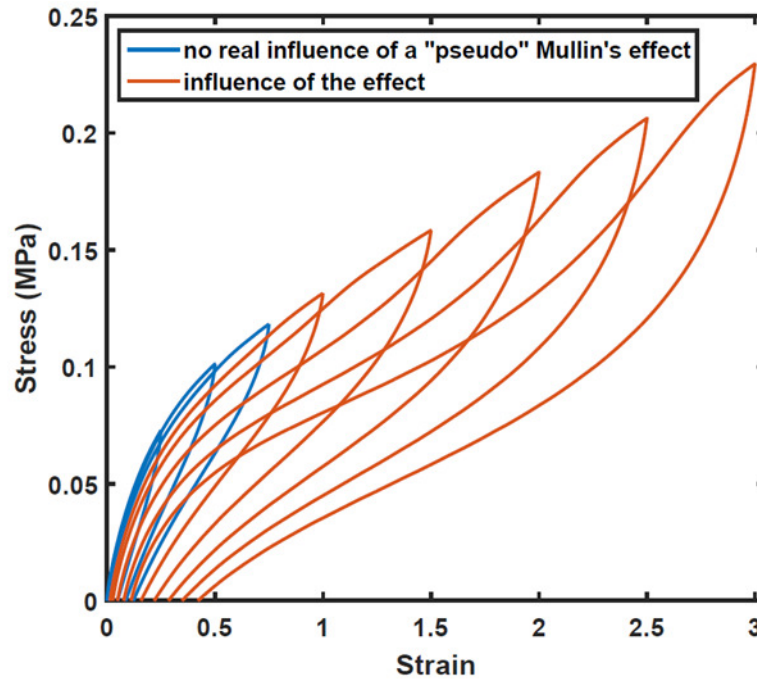
FIGURE 2.14: Cyclic tests exhibiting softening effect

incompressible material. Characterization of the tape rheology leads us to assume that the same parameters as for thin PSA (pressure, application frequency and temperature) pilot the contact formation of foam PSA. We can also assume that the particular structure of foam PSA does not influence the small strain linear rheological response of the material. When deforming in large strain regime, foam PSA behavior exhibits large strains prior rupture (up to 800% deformation). They are strongly rate dependent and a hardening phenomenon occurs at high strains (more than 600% deformation). Cyclic loading experiments revealed a softening mechanisms affecting the material behavior at around 80 to 100% deformation. This effect is likely to related to the presence of the hollow glass microsphere in the material bulk. This very general characterization allows us to formulate hypotheses which lay the foundations to the following study. We can now dive more specifically on the dissipative mechanisms characterization.

2.2 Strategy to study PSA debonding

The goal of this research is to gain a comprehensive knowledge of the dissipative mechanisms occurring during the debonding of foam PSA. To achieve that, it is of prime interest to have a relevant strategy to study the debonding itself. The two main tests we used were the flat ended probe tack test and the peel test at 90°. Firstly, the flat-ended probe tack test regards debonding from its initiation [19]. The second one is the peel test at 90° [15]. When the test is performed at a constant peeling velocity, it engenders a steady state debonding of the adhesive. The setup used for our research differs from classic ones by the addition of an instrumentation. The latter allows to record

direct optical observations of the bulk dissipative mechanisms taking place during the debonding. For this reason, in the PhD framework, instrumented peel test at 90° consists of the main test used. From an industrial point of view, this choice is even more relevant because all bonding specifications are defined according to performances that PSA reached during peeling at 90°. That is another reason which shows the relevance of understanding the mechanisms taking place within adhesives during such a test. Based on the results we obtain from these two kinds of experiments, we then describe dissipative mechanisms as activated at a very small scale ($\sim \mu$m). Hence, we present in last subsection our own particular micro scale tension setup.

2.2.1 Flat ended probe tack test

Flat ended probe tack test imposes a well-defined geometry of loading on the adhesive layer but does not provide information on steady state propagation [19]. The flat punch geometry is chosen according to Creton et al. [18]. Such geometry is the most adapted for highly viscoelastic and soft adhesive where the process zone 1.12 can be larger than the sample dimensions. Industrially, the standard closer to the protocol used is the ASTM D2979-95, pressure sensitive tack of adhesives using an inverted probe machine. The setup is illustrated in figure 2.15.
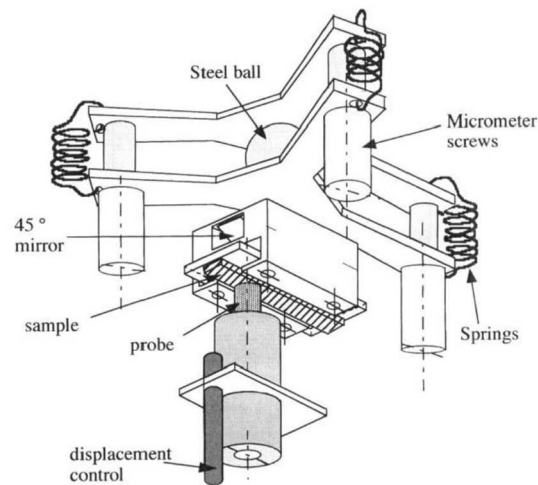
FIGURE 2.15: Instrumented flat ended probe tack test setup used in the SIMM lab.

Observations of the interface during the debonding can be made thanks to the mirror at 45° through the glass substrate. Alignment between the substrate and the adhesive sample is made thanks to the three micrometer screws. Probe velocity, application pressure and temperature are piloted which allows to fully controlled the contact formation process.

In this adhesion test, the PSA is bonded onto the probe (an 8-millimeter diameter disk is glued to the probe). The probe + adhesive is approached to a

2-millimeter thick stiff glass plate at a controlled velocity. Then, the contact is made by applying a defined pressure during a certain amount of time which allows to establish the contact (for more details see part 1.2.1). After applying the pressure, the probe is moved back without debonding to observe a dwell time in a quasi unstressed configuration. Then, the debonding occurs. The probe + adhesive goes back at a controlled velocity to detach the PSA disk from the glass substrate. The most important feature of that kind of test is repeatability. When studying adhesive resistance, so many factors can play in the debonding that having a repeatable test protocol is key. To evaluate the repeatability of our test protocol, we performed two series of tests for two different substrates. Both of the two series had the same bonding process and the same debonding velocity of $10^2 \mu m.s^{-1}$. The difference was in the interfacial adhesion level. Substrates for the first series were treated to be strongly adhesive (see part 2.3 for the substrate adhesion triggering) whereas substrates of the the second series were treated to be weakly adhesive. On the figure 2.16, we observe that in both cases the curves are superimposed. It means that our protocol has a good repeatability for two different experimental conditions (shapes of the curves are explained in detail in Chapter 3).
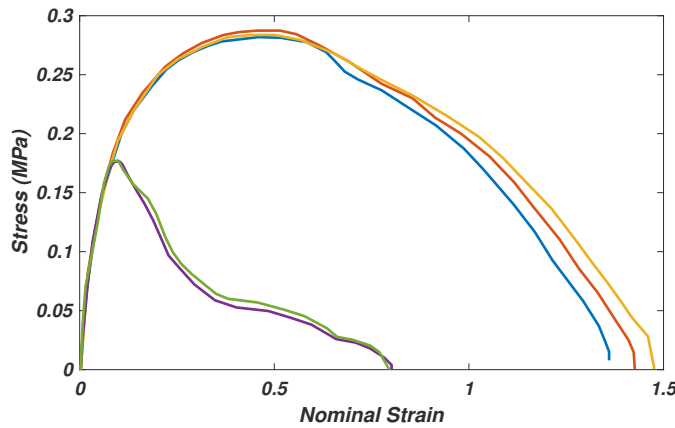
FIGURE 2.16: Probe tack test result repeatability

From the flat-ended probe tack test, the classic value extracted is the work of debonding. It corresponds to the area under the strain-stress curve multiplied by the initial thickness of the PSA disk a:

$$W_{deb} = a \int_0^{\epsilon_{max}(\dot{\epsilon})} \sigma(\epsilon)d\epsilon \tag{2.2}$$

.

We can also extract the peak stress σ_{max} which defines the maximum effort to activate the main dissipative mechanisms. The last common parameter used is the maximum fibril extension of the material prior to rupture. However, with respect to the architecture of the material of interest in this study (foam PSA), it is not likely that such a fibrillating process occurs. In Chapter 3, we will confirm that it does not.

As we saw, the instrumented flat ended probe tack test used in the SIMM lab is robust and the protocol is repeatable. Thanks to this test setup, all parameters affecting the contact formation are controlled. Hence, the adhesive behavior can be studied from the bonding process to the final detachment from the substrate. However, flat ended probe tack test is limited by the geometry of the contact plan. To get more comprehensive results regarding dissipative mechanisms it is worth moving to different debonding conditions with the peel test at 90°.

2.2.2   Instrumented peel test at 90°

Peel test is ideal for focusing on steady state debonding front propagation but it loads the adhesive in a more complex geometry [18] than the probe tack test. The pull force is applied on the backing layer and the latter loads the adhesive subsequently. The backing choice is determinant when performing a peel test. The latter must be stiff enough to prevent the part of the tape which has been debonded from the substrate from deforming. Such a deformation would affect the peel force measured. The goal of a peel test is indeed to load exclusively the dissipative region around the debonding (see the yellow square on the schematic of figure 2.17).
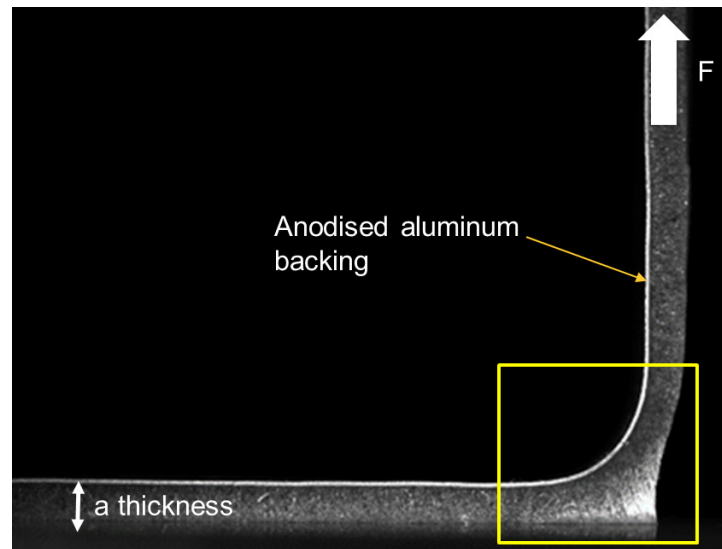
FIGURE 2.17: Foam PSA with an aluminum backing foil peeled at 90° from a glass substrate. Image recorded thanks to the instrumentation of the peel test setup 2.18.

In the frame work of this project, we chose a 127-micrometer thick anodised aluminum foil. This choice was made to stay in accordance with industrial imperative where standards are based on the use of that specific reference (*Lawrence* & *Frederick*). The backing choice influences dramatically adherence energy measured. From characterizing uniaxial tension tests, we evaluated that adhesive had a Young modulus of E= 350kPa at $0.05s^{-1}$. The backing has a Young modulus of E = 72GPa. It is then largely much stiffer

than the adhesive (around 100 times more) and thin enough to bend easily. When peel samples (adhesive + backing) are bent during peeling at 90° energy dissipation is related to the sample bending. However, due to the large thickness of the adhesive, the sample bending could be no longer driven by the bending of the backing but also being dependent on the adhesive. We have ruled out this case thanks to a bending equivalent moment determination (see B). This contribution is low enough to validate the use of this specific backing foil.

The big advantage of the setup we built in the SIMM Lab of the ESPCI is to be equipped with a camera. This camera is placed on the edge of the sample to record images of the debonding region (see the picture 2.18). In the following chapters we will observe that this tool allows to visualize directly the dissipative mechanisms occurring at the macro scale (∼mm size).
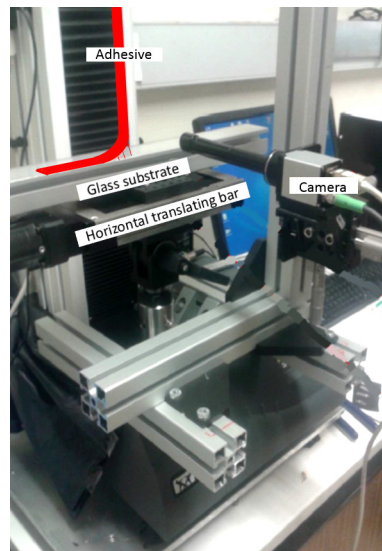
FIGURE 2.18: Instrumented peel test setup

From the peel test, the classic value measured is the force F. It corresponds to the force applied to propagate the debonding at a constant peeling velocity. In a steady state regime, this force is close to be constant (see the figure 2.19). On peel tests measurements, we visualize a plateau force from which we can calculate the fracture energy Γ which derives, for a 90° peeling, from the following relationship:

$$\Gamma = \frac{F}{b} \tag{2.3}$$

where b is the width of the adhesive sample.

As presented in part 1.2.2, like substrate (glass) is infinitely stiffer than adhesive (foam PSA), this energy can be assimilated to the adherence energy, Γ. As a reminder, we call adhesion energy the local interfacial energy

(surface) and adherence energy the resistance energy which is obtained after contribution of the bulk mechanisms (surface + bulk).
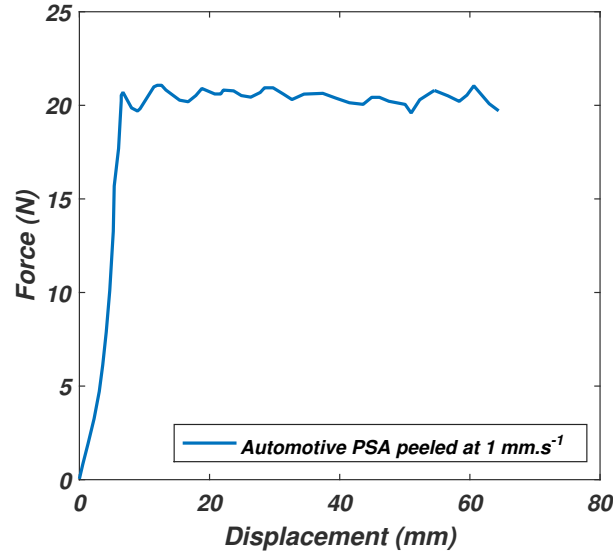
FIGURE 2.19: Example of the peel test plateau force measurement for the foam PSA peeled at 1 mm/s.

In a nutshell, the instrumented peel test setup used in the SIMM lab is a relevant tool to study the dissipative mechanisms occurring in the debonding region of foam PSA. In Chapters 3 and 4, we will focus on effects of interfacial adhesion triggering and peeling velocity change. As we said before, dissipative mechanisms study required to go at a very small scale (μm) to understand how they are activated. To do so, we designed our own test setup.

2.2.3   Tensile tests

The last test to study dissipative mechanisms occurring during debonding is the widely used tensile test. In part 1.2, we saw that adherence problems must be studied with a multi scale approach. For this purpose, we first carried out tensile tests at the macro scale ($\sim$mm) as presented in part 2.1.3. In these normal test conditions, observations are limited to the optical range. To overcome this limitation and go at a much lower scale, we designed our own in situ SEM tensile test setup. Designing such a device implies to cope with SEM vacuum chamber imperatives (high confinement, vacuum conditions 10^{-5}mbars, short range displacements control). This technical solution is presented on the two photographs of the figure 2.20.

Using a piezo actuator we managed to reduce dramatically the setup size. For example, the height of the actuator is only 15mm. As we can see on the photographs 2.20, the adhesive sample is directly pulled over a distance of 26mm under the electron beam (SEM column) of the microscope. As we will
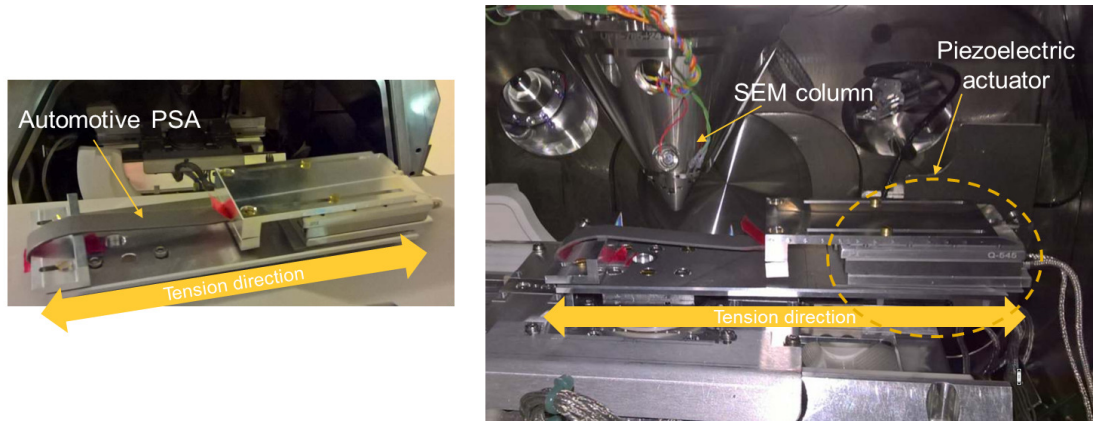
FIGURE 2.20: Micro tension test setup. The piezoelectric actuator is piloted in displacement and velocity. The connecting wires (on the right of the image) are connected to the controller through a flange adapted to SEM chamber conditions. The flange was part of the setup design.

present in Chapter 3, this setup allow us to study bulk dissipative mechanisms which had never been observed before. This tool is specifically relevant for studying multiscales materials.

2.3 Substrate surface preparation

2.3.1 Surface treatment for repeatable adhesion tests

When performing adhesion tests like probe tack or peeling, a recurring issue is the repeatability of the results. The big advantage of this doctoral project is that we use only commercial tape references. So samples behavior does not differ from each other. Hence, the key point is the substrate surface state pre preparation [74]. In the automotive industry, Horgnies et al. [46] showed that the substrate surface state is never the same. When the color of the car changes, interfacial adhesion can also change [46]. To overcome this major problem, the strategy was to use controlled substrates where the surface chemistry is fully controlled. To achieve that, we define a glass cleaning process and we then describe a simple way to trigger adhesion level.

How to make repeatable surfaces for adhesion tests?

Based on one of our research objectives on visualizing dissipative mechanisms, we decided to use glass substrates because of the possibility to visualize the tape behavior through them. The developed cleaning process is based on a slight surface abrasion. The glass slide is first wiped with a tissue presoaked with a Cerium Oxide CeO_2 solution. In the solution CeO_2 particles have the size of 200nm and a volumic concentration of 15% which allows to abrade slightly the glass surface during the wiping. This abrasion removes all the contaminants which might be attached. It also exposes all the OH sites which favors molecular adhesion with the adhesive. Then the wiped slide is

cleaned with acetone and dried with nitrogen gas flow to remove this excess of particle.

Results obtained with the peel test at 90° illustrate the robustness of this preparation protocol. The three plateaus depicted in figure 2.21 show a good repeatability of the peel test with this preparation. Such a result is very promising because peeling is a very complex loading. Between two debondings with the same experimental parameters, tape samples behavior can easily differ. In our work, we succeeded in guaranteeing a high enough control of our substrate surface chemistry to obtain such a result. The latter is even more relevant when considering the Chapter 4 where we study the morphology of the debonding region during the peel test at 90°.
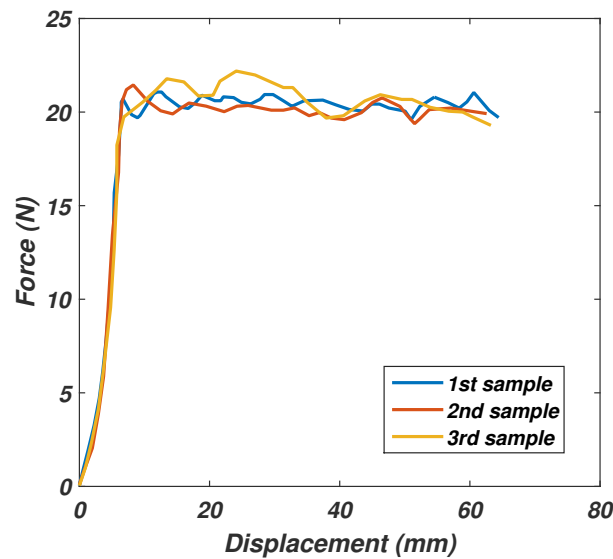
FIGURE 2.21: Peeling plateau force repeatability. The three tests are carried out for a peeling velocity of 1mm.s^{-1}

Adhesion level triggering method

Once we succeeded in having a repeatable process, we found means to trigger easily the substrate adhesion level. The most efficient way we found in the literature is silanization. For the sake of simplicity, we chose a liquid silanization process developed in the SIMM lab. The silane solution is deposited onto the substrate after the treatment presented before.

The first step of the protocol is to prepare an acidic solution to contain the silane.

$$Solution1 = IPA(130g) + H_2O(14.5g) + HCl(0.36g)_{12M} \qquad (2.4)$$

The second step deals with the mix between silane solution and solution 1. This mix is quickly made in a fume hood to prevent silane from oxidizing.
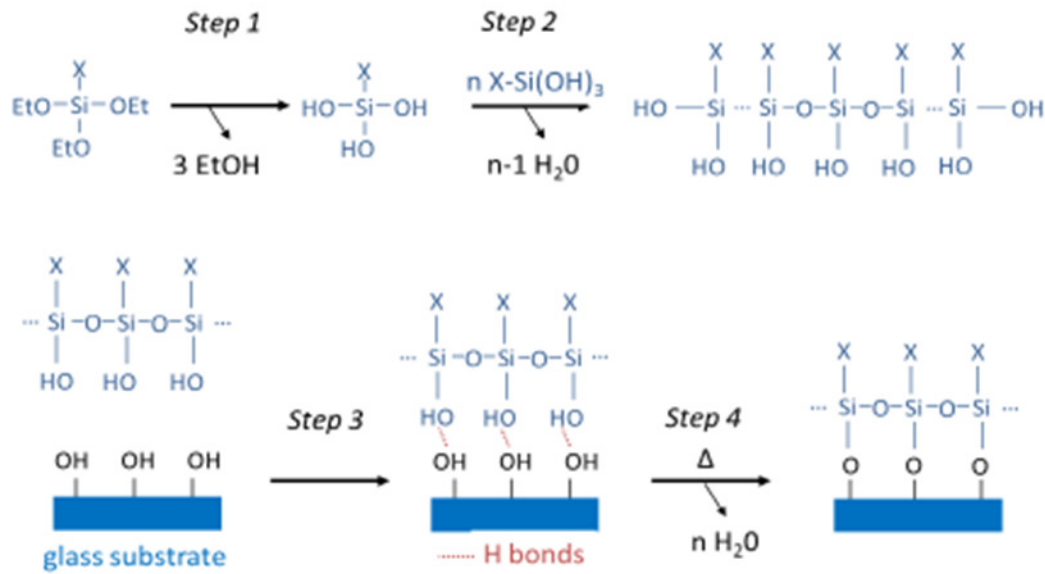
FIGURE 2.22: Silanization protocol

$$DepositingSolution = Solution1(10g) + Silane(0.33g) \qquad (2.5)$$

Once the depositing solution is homogeneous (after roughly 30 min of stirring), the solution is deposited onto the substrate surface thanks to a pre-soaked wiper. The excess of solution is removed with optical wipers preventing dust from contaminating the surface.

The final step is to heat the substrate (110°C during 30 min) to remove water from the surface.

We used three different silanes to get three different adhesion levels. Perfluorosilane for very weak adhesion, Octyltriethoxysilane for weak adhesion and (3-aminopropyl)triethoxysilane for higher adhesion. These treatments worked as well as we expected according to figure 2.23 which presents the peeling measurements made with these three samples for an arbitrary chosen debonding velocity.

Triggering molecular adhesion is a very complex task which is considerably facilitated by the use of silanes. Depositing a thin molecular layer with a controlled chemistry aiming at increasing or enhancing interfacial adhesion is achieved by using a robust protocol. The described technique in this section presents many advantages. First of all, it is applicable to glass substrate (relevant to observe phenomena). Secondly, the silane is deposited through a liquid solution which decreases largely the process complexity. Eventually, according to the silane choice, this treatment covers a wide range of adhesion (see fig 2.23).
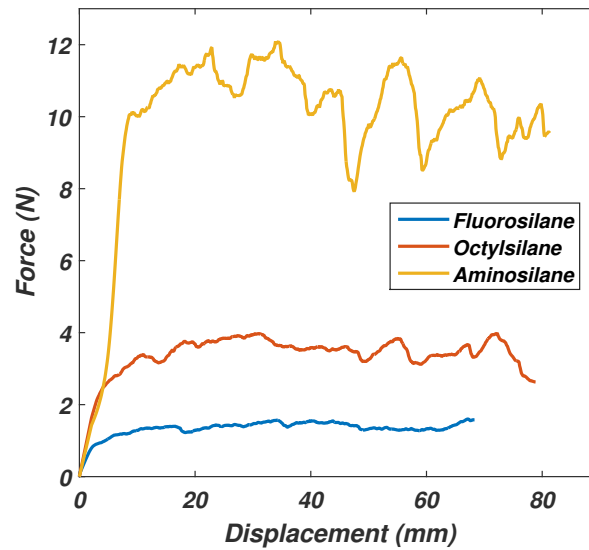
FIGURE 2.23: Silanization effect observed with peel tests. The three silanes used exhibit very different adhesion levels. On the figure, the plateau force corresponding to aminosilane shows instabilities. They are due to a bad quality of the silane. For high adhesion tests performed in Chapter 3, we used a commercial solution of aminosilane designed specifically by the tape supplier.

2.4   Conclusion

Chapter 2 lays the groundwork for identifying dissipative mechanisms occurring during the debonding of foam PSA. We started by characterizing the structure of the adhesive material. Using classic characterization techniques like optical microscopy, SEM, EDX measurements and microtomography X, we pointed out the particular structure of our samples. Foam PSA have a syntactic foam structure. They essentially consist of two components: a polymeric matrix (60% of the total volume) and hollow glass microspheres (40% of the total volume). We saw that it was reasonable to consider this structure as incompressible in the unstressed state. We continued the characterization by investigating its rheological behavior. We performed classic small strain shear cyclic loadings to determine its rheological parameters. We then comfirmed that its behavior meets the Dahlquist criteria which define the rheological properties for good adhesive performance. Results showed that it is reasonable to consider that contact formation of foam PSA and thin films PSA are driven by the same parameters. Based on the storage modulus G' and dissipative modulus G'' evolution with respect to the frequency (master curve built thanks to a TTS WLF law), a straightforward approach to point out the differences existing between a manual and a robotic tape application is highlighted. For the foam PSA of this research, we showed that robotic application is the most recommended to dope energy dissipation process during the bonding stage. When studying adherence, large strain

regime is of prime interest. To characterize foam PSA behavior in this domain, we carried out classic uniaxial tension tests. We observed that such materials exhibit large deformations prior to rupture. They are strongly rate dependent and for high strains, hardening is likely to take place. The latter is more and more significant when strain rate increases. Thanks to cyclic loading tests, we brought to light a damage effect similar to Mullin's effect. However, EDX measurements revealed that the percentage of black carbons (and other nanoparticles) is not important enough to influence the overall material behavior. For this reason the plausible cause we evoked to explain this damage effect is the presence of the hollow glass microspheres. This lead will be investigated in Chapter 3.

After characterizing our samples with classic techniques, we established our strategy to study PSA debonding. Studying adherence problems requires to take substrate as well as tape into consideration. The two chosen adherence tests are the flat ended probe tack test and the peel test. Both of the used setups are instrumented. This instrumentation differs from classic tack and peel tests where the only information provided is the needed force to detach. In the framework of this PhD, we are able, thanks to our image recording systems, to directly visualize phenomena occurring next to the debonding front. In other terms, we are able to observe dissipative mechanisms development. Such tools are critical in the pursuit of our research problematic: *Dissipative mechanisms during the debonding of high performance foam pressure sensitive adhesives for automotive*. As we will see in Chapter 3, activation and early stage development of these mechanisms take place at very small scale ($\sim \mu$m). This scale is beyond the maximum optical resolution. That is why we had to develop and build a system to go at a lower scale. To achieve to do such a challenging observation, we designed our own SEM in situ tensile setup piezoelectrically actuated. This setup differs from classic tensile tests by its vacuum chamber compatibility and its minimalist size. Eventually, we defined our surface treatment protocols to obtain repeatable substrate surface chemistry exhibiting controlled interfacial adhesion levels. Such a condition is a prerequisite to get quantitative results with adherence tests like the one presented above. Based on our material characterization and on the hypotheses formulated regarding foam PSA bonding process, we can now go further into dissipative mechanisms identification by answering the question: *How do foam PSA dissipate energy?*

Chapter 3

How do foam PSA dissipate energy?

In the pioneering works of Kaelble [56] and Gent [37], and thanks to more recent articles [25, 82] we saw that performance of an adhesive joint made with thin PSA comes from the PSA ability to deform and to dissipate energy. The objective is now to extend the research to the foam PSA. How do they dissipate energy? How is energy dissipation affected by the particular syntactic foam structure? Decreasing? Enhanced? To answer these questions, we will first carry out adherence tests using our two instrumented setups described in Chapter 2. Thanks to the instrumentation, the objective is to identify the development of dissipative mechanisms within the debonding region during debonding. Secondly, we will perform micro tensions to quantify the role of the microspheres in the overall adherence. Based on the identification of these mechanisms, we will integrate all these results in a phenomelogical model regarding the energy dissipation in the $90°$ peel test. Then, a rheological model gives a relevant explanation of how most of the energy is dissipated. Chapter 3 presents the first hints of how peeling results of the foam PSA can be transpose to the flat ended probe tack test.

3.1 Identification of the dissipative mechanisms

The identification of the dissipative mechanisms is made in two steps: firstly at the macro scale (around 1mm size objects) and secondly at the micro scale (around 1μm). The macro scale is met with the instrumented tack and peel setups whereas the micro scale is reached with the SEM in situ tensile test.

3.1.1 At the macro scale

Flat ended probe tack test

As mentioned in part 2.2.1, we start by performing this test to observe the early stage of the interfacial phenomena. Before going directly to the observation of mechanisms, we first compare foam PSA behavior with thin films PSA. For thin PSA, typical results are presented in the fig 3.1.
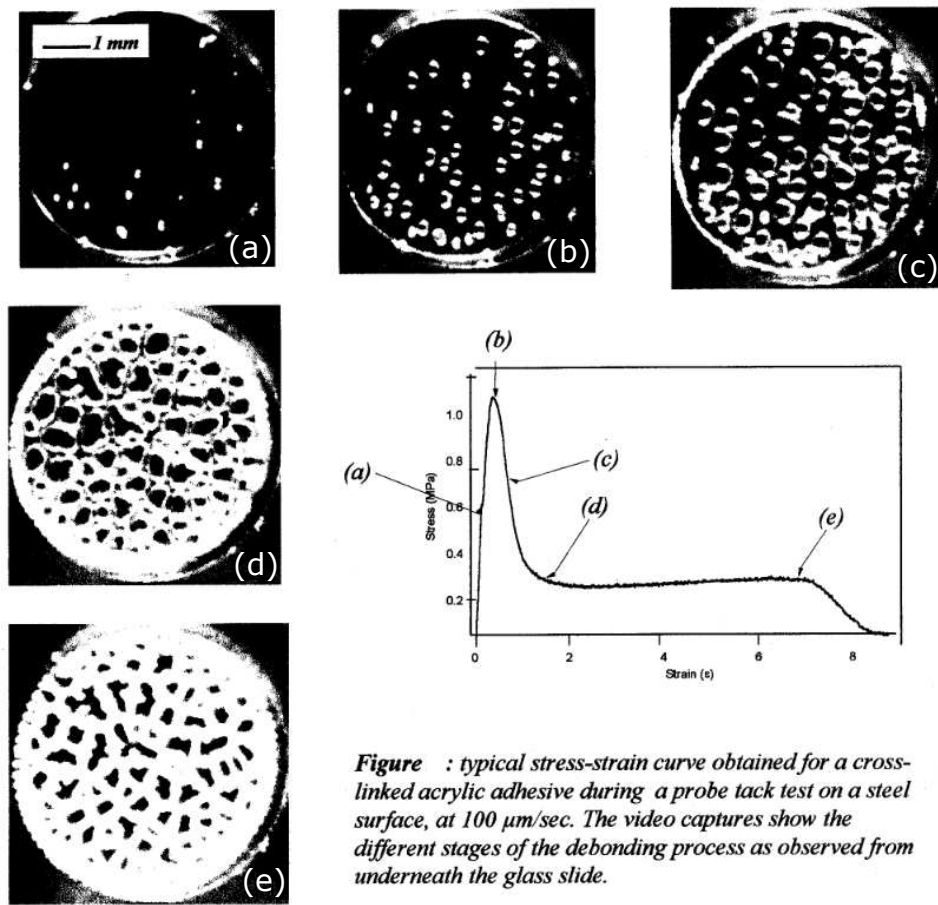
Figure : *typical stress-strain curve obtained for a cross-linked acrylic adhesive during a probe tack test on a steel surface, at 100 μm/sec. The video captures show the different stages of the debonding process as observed from underneath the glass slide.*

FIGURE 3.1: Typical probe tack results for thin PSA [64]. The figure shows the strain stress curve from the start of the debonding process to the final detachment of the thin PSA. These experiments are carried out with the same instrumented flat ended probe tack test setup. Thanks to the camera we can observe interfacial debonding reported on the images (a) to (e).

Generally speaking, for such thin PSA films, the debonding starts at the interface by the cavitation of small air bubbles trapped during the bonding process [39]. On the strain stress curve of figure 3.1, we observe the initial high increase of stress which corresponds to the cavitation process. Then, the peak stress accounts for the start of the cavities growth which leads to fibrilation process. The fibrils are then elongated in uniaxial tension (see the stress plateau of figure 3.1). It is now relevant to compare results from figure 3.1 and those obtained with foam PSA for the same protocol. Results are presented on figure 3.2.
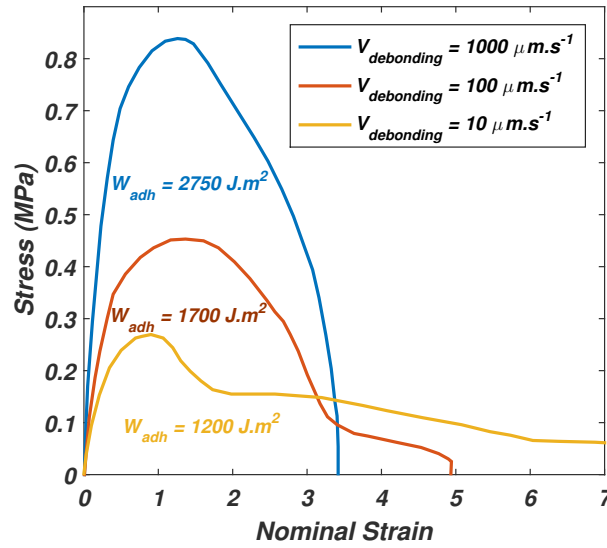
FIGURE 3.2: Flat ended probe tack results for foam PSA. Used substrates are glass slides prepared with the protocol presented in part 2.3.

On the graph 3.2, we see that the curves are totally different compared to acrylate thin PSA films. It does not necessarily mean that dissipative mechanisms are different but it shows that the increase of thickness and the addition of glass beads change the material dissipative behavior. To test separately each influence, the most relevant protocol would be to carry out tests with the matrix without the microspheres. However, because of the trade secret around the project (CIFRE contract), we were not able to obtain these samples. In the following and in Chapter 4, we will see that we can find astute alternatives to move forward.

Another element which is worth mentioning when looking at figure 3.2 is the rate dependency of the behavior. On the three curves of the figure 3.2, the effect of the velocity on the adherence is clear. For each test, interfacial adhesion is supposed to be the same (same substrate surface preparation 2.3). Hence, the adherence changes can come from two points: a rate dependent mechanisms change in the bulk or/and an dissipative mechanisms change at the interface. Concerning thin PSA, such a rate dependent behavior is also observed. It comes from fibrils which dissipate energy according to the strain rate they undergo during the debonding process. Following this analogy, we saw in part 2.2 that foam PSA exhibit in large strain regime a strong rate dependency. This rate dependency could control internal mechanisms which could trigger its bulk dissipation capability and therefore its adherence. The second plausible cause explanation could come from the interfacial PSA behavior. That is why the emphasis is now laid on the comparison between interfacial behaviors of thin PSA and foam PSA before the propagation of the debonding front.

As we saw in the presentation of the test in 2.2.1, the setup used in the

SIMM lab allows to observe optically the interface before the propagation of the debonding front. The photographs on the figure 3.3 compare the interfaces of a thin PSA and an foam PSA at the moment where interfacial cavitation reaches its peak (roughly after peak of the bell shapes on the figures 1.10 and 3.2).
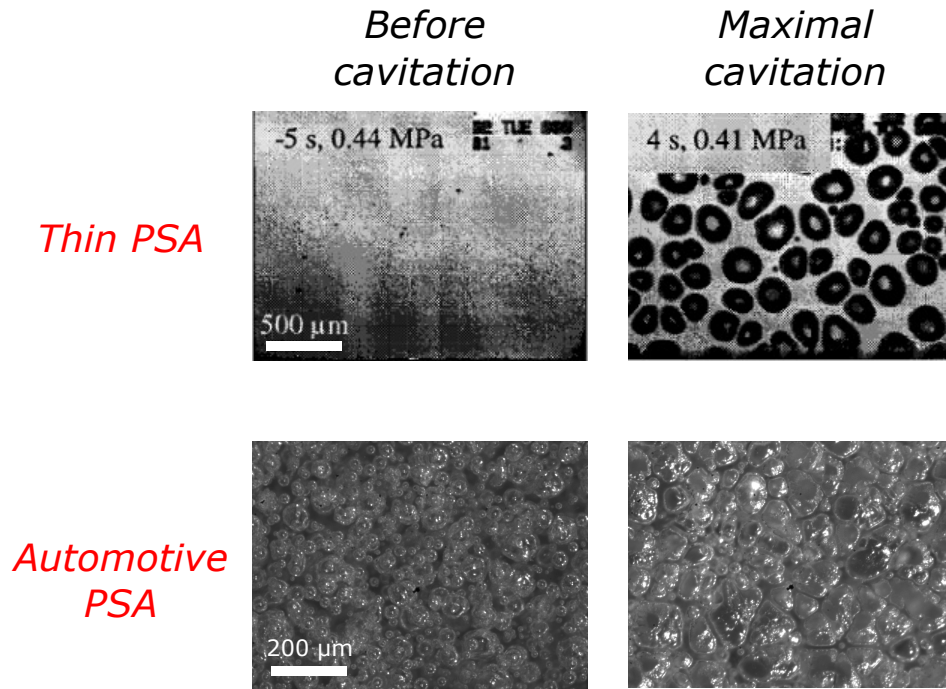
FIGURE 3.3:   Interfacial cavitation comparison between thin PSA [12] and foam PSA.

On the top of the figure 3.3, the thin PSA is entirely cavitated at the interface. These cavities lead to fibrils which strongly propagate throughout the material thickness. In comparison with the bottom image, we notice that the foam PSA is also cavitated but the video recording shows that this cavitation remains limited to the bulk. This region of cavitation is close to the interface but not at the interface. The cavitation occurs at the boundary between the hollow glass microspheres and the matrix. All the spheres seem to contribute to the overall cavitation. No interfacial cavitation has been observed during all the experiments. As with the thin PSA, the population and size of the cavities seem to depend on the interfacial adhesion level. In the thin PSA case, the size of the cavities is approximately twice bigger than the foam PSA ones. Concerning thin PSA, the size of the cavities is driven by the toughness of the material [18] whereas in the case of foam PSA, volumic distribution and diameter of the sphere initiating the cavity seems to determine its critical size. These sphere matrix decohesions in the neighboring of the interface seems to locally deconfine the material in a region close to the interface. This deconfinement can plausibly decrease the hydrostatic pressure at the interface which could explain the non occurrence of classic interfacial cavitation observed in thin PSA [39] (air bubble trapped during the

contact formation which grows with the hydrostatic pressure increase due to the debonding). From a mechanical point of view, the flat ended probe tack test accounts for a confined traction test. The presence of glass microspheres close to the interface, through nucleating cavities (thanks to sphere matrix decohesion), seems to allow the material to deconfine. This observation is in good accordance with the idea stating that the thickness of the material (the bulk) and the addition of glass beads can play a role in enhancing the dissipation process. Indeed, if a local interfacial deconfinement occurs, cavities at the interface are unlikely to appear and, consequently, unlikely to initiate a rupture. Hence, the interfacial adhesion is artificially enhanced by the presence of the hollow glass microspheres.

Beyond the only explanation that bulk mechanisms in the case of foam PSA can reduce cavitation at the interface, it is worth highlighting the significant geometrical confinement difference with the thin PSA case. For the same lateral dimensions, classic PSA are much thinner than foam PSA (around 10 times thinner). For this reason, in the probe tack test, geometrical confinement of the thin PSA samples is much larger than the foam PSA ones. This problem has been extensively studied in the literature [79]. Conclusion of those works showed that the equivalent stress can be multiply by 2 at the center of the sample. Following the example of the literature, we conducted FEM calculations to evaluate confinement effect on our sample. On the figure 3.4, we plot the equivalent stiffness when material is assumed to be incompressible ($\nu = 0.4999$) and slightly compressible ($\nu = 0.44$). To simplify the calculations, we reduce the problem to the situation prior cavitation occurrence and in the small strain regime. We define by h the sample thickness and by r the radial coordinate at the interface ($r = 1$ represents the edge of the sample).
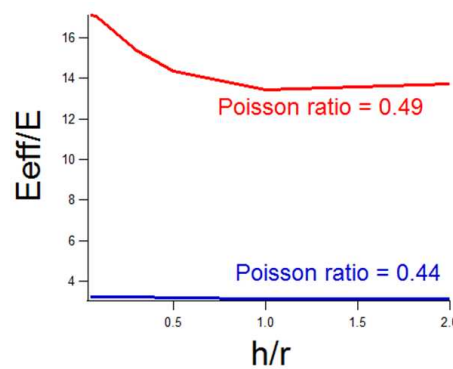
FIGURE 3.4: Confinement influence on the material stiffness.
Mean foam PSA confinement, h/r = 0.3.

On this figure 3.4, we note that confinement is large enough to have a nonnegligible effect. As we know that a high confinement increases hydostatic pressure value, it can then cause cavitation and make cavities grow. We can reasonnably think that confinement could have an impact on spheres matrix

decohesions observed near the interface in the foam PSA (see fig 3.3). Confinement can be considered as one of the activation parameters for sphere matrix decohesions.

To sum up, flat ended probe tack tests performed with the foam PSA exhibit different results than with the thin PSA. Strain stress responses differ as well as interfacial mechanisms. We observe that cavitation mechanism does not appear at the interface between the substrate and the adhesive (encountered with the thin PSA) but within the bulk of the adhesive. More specifically, cavitation appears after the decohesion of the glass microspheres from the matrix, in a bulk region close to the interface with the substrate. Following this conclusion a new question pops up: if the spheres matrix decohesions can occur in a small strain regime near the interface, how the whole syntactic foam structure behaves in a large strain regime? Such conditions are easier to study when performing the 90° peel test [54, 38, 78].

Peel test

As presented in part 2.2.2, the instrumented peel setup used in the framework of this study is the 90° peel test instrumented with a side camera to record videos from the debonding region [78]. The tests used here comply with the standards of the automotive industry [15]. As a reminder, the dissipative region is the region where one assumes that most of the energy dissipation occurs. Peeling was performed at many debonding velocities and for different controlled interfacial adhesion levels. An example of image recording is reported on figure 2.17. From the material characterization of Chapter 2, we figure out that foam PSA behavior are strongly rate dependent. This rate dependency has been observed in the flat ended probe tack test in the previous subsection. To evaluate the influence of changing peeling velocity and thus strain rate, peelings at different velocities are carried out. Results are presented in figure 3.5. Evolution of the adherence energy Γ with respect to the peeling velocity is detailed in the figure 3.6.

On the images from the fig 3.5, we see that the size of this debonding region increases with the increase of the adherence energy. Also, this adherence energy increases with the debonding velocity 3.6. That means the higher the debonding velocity, the larger the debonding region. This last observation is counter intuitive compared to office tapes (thin PSA) of Villey et al. [78, 77, 13]. He showed that it was the inverse phenomenon occurring for the thin PSA. The debonding region size (it means the fibrils length) decreases with the increase of the debonding velocity. These observations remain the same when increasing the adhesion with the substrate for the same peeling velocity (see figure 3.5). In others terms, for the foam PSA the wider the debonding region is, the more energy is dissipated. However, it is worth mentioning that with the foam PSA, we cannot distinguish a clear fibrillation process at the macro scale (∼mm) like observed during thin PSA debondings [8, 77]. Although occurring in the material bulk, energy is here dissipated
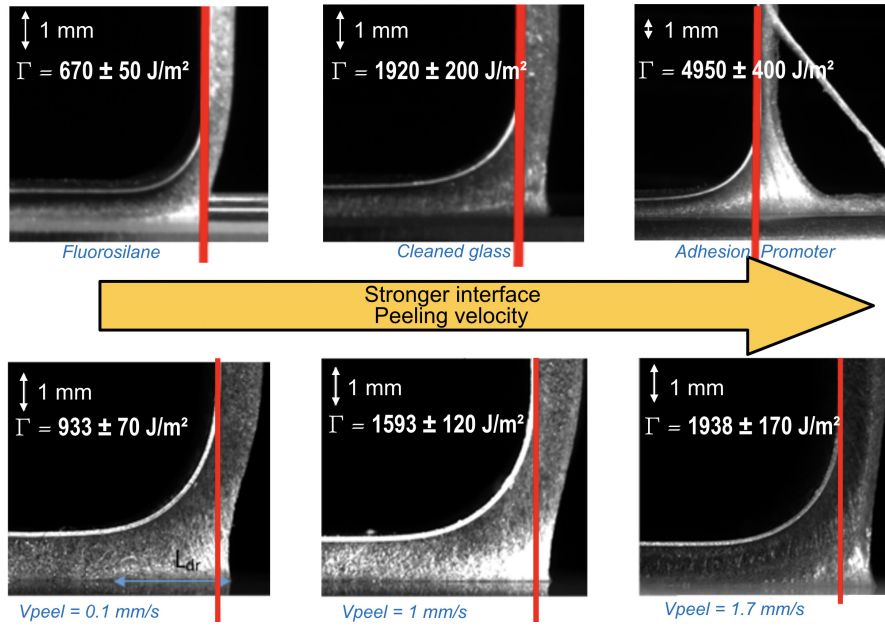
FIGURE 3.5: Debonding region shape with respect to adherence energy. On the top, the three photographs correspond to an increase in the interfacial PSA substrate adhesion. At the bottom, the three photographs correspond to a peeling velocity increase.
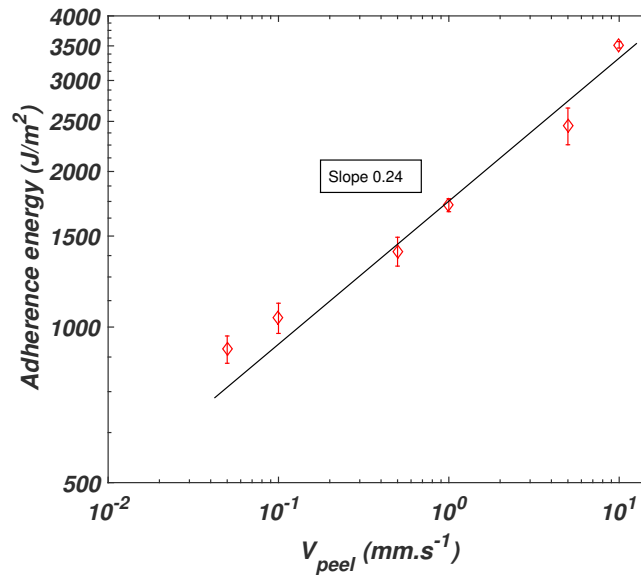
FIGURE 3.6: Evolution of the adhesion energy with respect to the peeling velocity. Samples are peeled on glass substrates (see 2.3 for substrate preparation)

through a different process. One parameter could explain this difference: the thickness of the foam PSA. For the latter, the large thickness is primarily motivated by aesthetics of the adhesive joint, but, as literature reports [71], it can have a tremendous impact on the adhesive performance.

We said previously that the debonding region of the foam PSA does not look like the one of the thin PSA during the debonding phase. To build a more comprehensive explanation, we perform three peel tests in three extremely different conditions. The goal is to visualize the debonding region for one very weak, one medium and one very strong adherence energy. On the figure 3.7 the three images are represented. In each case, the sample is exactly the same, only the experimental protocols differ.
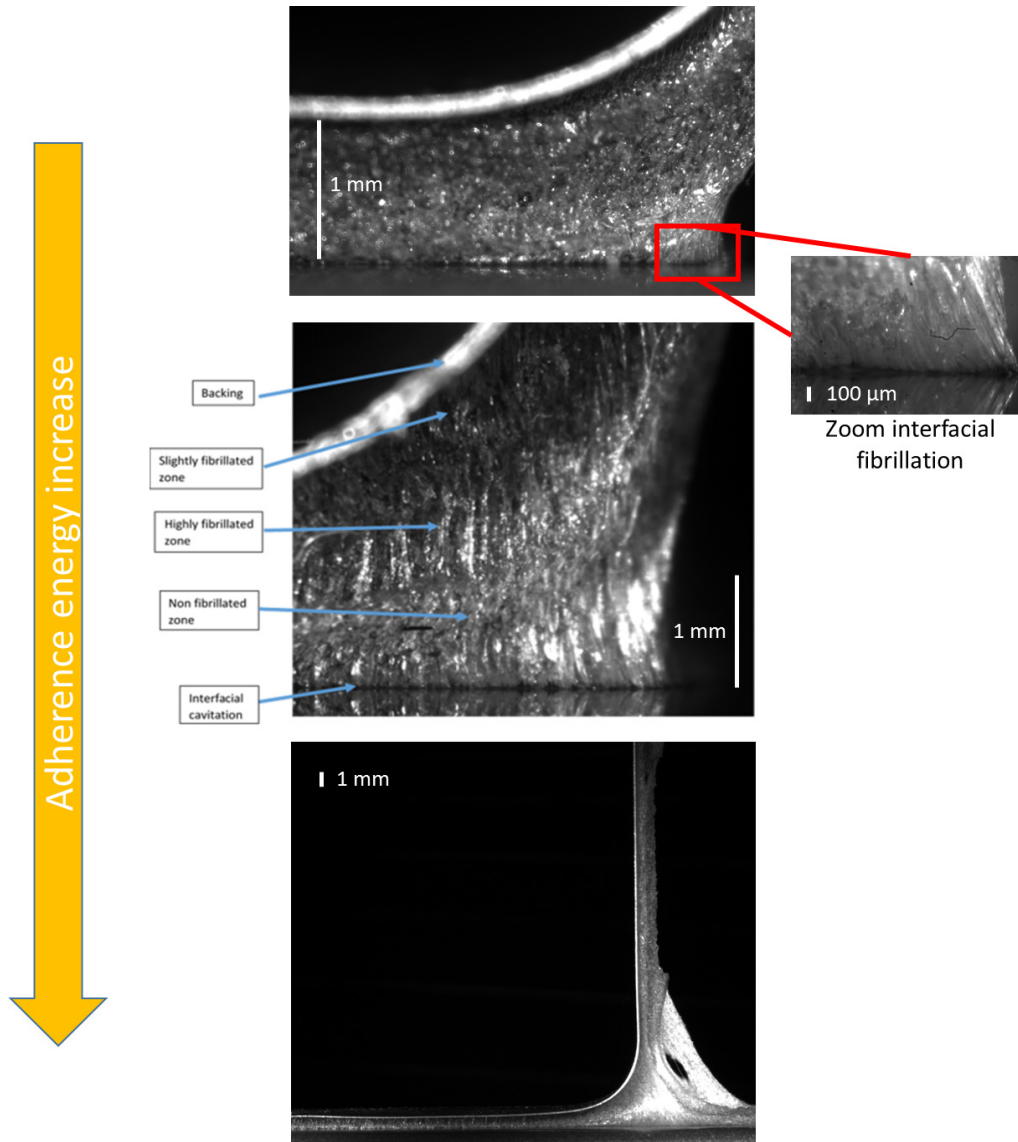
FIGURE 3.7: Debonding region of the foam PSA with respect to the increase of adherence energy. On the top, the image corresponds to a peel test at 0.1mm.s^{-1} on glass (preparation see 2.3) $\Gamma \sim 1200\text{J.m}^{-2}$, in the middle to a peel test at 1mm.s^{-1} from glass (preparation see 2.3) $\Gamma \sim 2000\text{J.m}^{-2}$, and the test on the bottom is a peeling at 1mm.s^{-1} on an adhesion promoter which chemically reacts with PSA $\Gamma \sim 5000\text{J.m}^{-2}$.

When we have a closer look at the debonding front, we observe that the foam PSA tends to orientate itself along a global fibrillation process (see figure 3.7). This orientation seems to start at the interface. For low adherence (upper image), this orientation process remains limited in a small zone close to the interface. In this zone, the adhesive material is highly stretched (zoomed view). For this configuration, it is reasonable to make the analogy with the singularity based model of fracture mechanics (see part 1.2). All the non linear large strain regime related phenomena remain concentrated

in this small (compared to the material thickness) process zone. When adherence increases (middle image), we observe that another fibrillated region appears in the bulk of the material. Interestingly, those mechanisms are not directly linked to the interfacial process zone. A non deformed zone exists between interfacial zone and bulk phenomena. The latter seem to come from the inside and is oriented towards the same direction. Knowing that a peel test is a backing adhesive load transfer (Kaelble zone see part 1.2), we can assume that such an orientation direction could be driven by local uniaxial tension conditions. However, it is worth noting that the development of bulk mechanisms does not delete the interfacial process zone which continues to exist. At even larger adherence, the whole bulk fully orientates itself along a fibrillated structure (bottom picture). Moreover, the rupture presented here is no longer interfacial (adhesive) but cohesive. The bulk process zone becomes dominant which makes the analogy with the extension of the fracture mechanics for soft matter crack description (see part 1.2 fig 1.12).

Such observations are very helpful to understand how the material dissipates energy. According to the results detailed above, it seems that dissipative mechanisms (cavitation) initiate firstly close to the interface BUT not at the interface. It consists of sphere matrix decohesions. For low adherence, their development remains limited to a small process zone at the interface. They do not grow within the material thickness. As a result, not that much energy is dissipated and the adherence performances remain limited. But, when we increase the debonding velocity and/or the interfacial adhesion level, other mechanisms (cavitations AND internal fibrillation) initiate within all the thickness and grow until all the material is orientated along a fibrillated structure. It seems that a relationship exists between the adherence energy and the deformation of this structure (proved in Chapter 4). When the adherence is high, we measure larger strains. Another point is worth noting here. In the debonding region of a $90°$ peel test, the adhesive material is significantly loaded in tension (Kaelble zone see part 1.2). Yet we only observe a very slight necking (see 4.1). For so large deformations, foam PSA, which are supposed to be incompressible in an unstressed state (see part 2.1.1 Structure identification), should exhibit a huge necking. This remark leads us to the point that the compressibility of the material could change during the debonding. This idea means that cavities appear within the bulk of the material which could deconfine the adhesive and then, reduce the necking phenomenon. Considering that the material structure is a syntactic foam architecture, it is logical to think that beads could play a role in the compressibility change. To evaluate the relevance of this idea, we have to go at a lower scale and see how hollow glass microspheres debond from the matrix.

3.1.2 At the micro scale

Micro in-situ tension

Thanks to the in-situ tensile setup described in part 2.2.3, we have the great opportunity to access this lower scale by carrying out quasi static tensile tests in the SEM machine for high strains. The large field of view observation resulted in the figure 3.8.
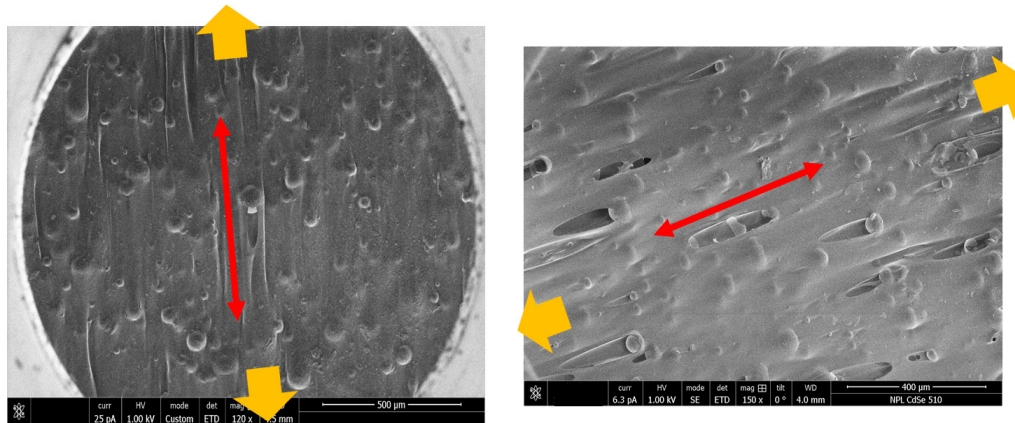
FIGURE 3.8: Orientation of the foam PSA bulk following internal microspheres debondings during tensile test at 300% deformation.

On the figure 3.8, the surface images show that most of the spheres debond from the matrix generating cavitation process. So, this phenomenon is localized around the glass beads due to local debondings. The presence of those spheres artificially engenders cavitation. What is more, we observe that the material orientates itself along the traction direction (in yellow). Although from a surface point of view, thanks to the characterization in Chapter 2, we can reasonably extrapolate these observations to the bulk of the material. Due to the large number of microspheres, this phenomenon changes the matrix structure completely and "heterogenize" it. The growth of the cavities forms walls between them, which tend to lengthen and become thinner and thinner. This mechanism can be seen as a pseudo fibrillation of the material (see the red arrows on images from fig 3.8) although the fibrils are not individual and independent as for thin PSA. These observations are in good acccordance with the observations from the flat ended probe tack and peeling we made in 3.1.1. Based on them, these results raise new questions: how are cavities formed?, how do they grow?, to what extent do they grow?. In order to answer these questions, we have enlarged individual cavities.

To observe the hollow glass microspheres debonding at the surface, we performed tensile tests for large enough deformations (around 100-150%) to debond the matrix from the glass beads and to make them appearing at the surface of the tape. On the figure 3.9 we depict intriguing phenomena.
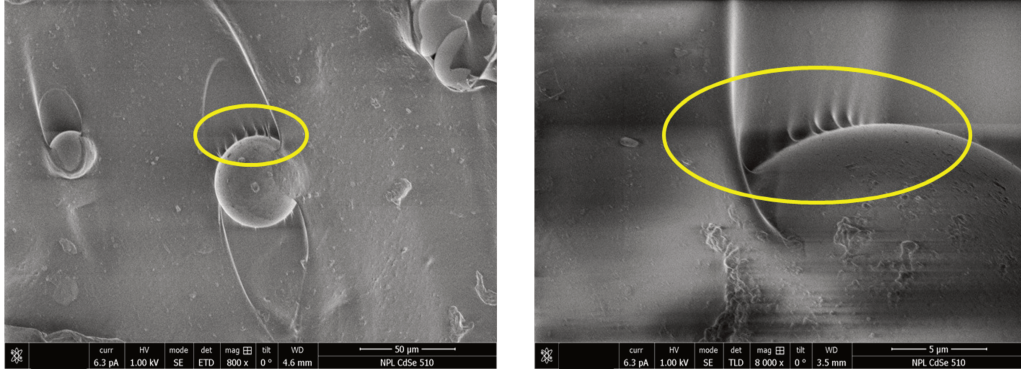
FIGURE 3.9: Hollow glass microspheres decohesion within foam PSA bulk

The images show mechanisms happening during the debonding at the interface between a sphere and the matrix. At this small scale (μm), we observe debonding instabilities. On the contrary to mechanisms occurring in foam PSA bulk, there are no smaller particles that could cause cavities. As the matrix is supposed to be incompressible, it is relevant to link this phenomena to the wrinkling studied by Mora et al. [70]. Such mechanisms can be associated to fibrillation. In our case, fibrils would have a length of about 1μm. Mora et al. [70] explains microfibrils formation by the competition existing between a reduction in the stretching energy (the fibrillated configuration decreases the stretching energy) and an increase in the shearing (microfibrils formation engenders shear). This process allows the material to adapt to the solicitations by locally deconfining. On the contrary to the material deconfinement occurring when the sphere debond from the matrix ($10^2\mu$m scale mechanisms), this second deconfinement process appears at a much smaller scale (at the interface sphere matrix, 1μm scale). According to Mora et al. [70], these wrinkling can be multiscale. Hence, if we were able to zoom in on the instabilities (microfibrils) in fig 3.9, we would certainly observe the same kind of instabilities on the microfibrils themselves (at the $10^{-1}\mu$m scale). At the sphere matrix interface, the presence of those small fibrils (dissipative mechanisms) suggests that they could contribute to the overall dissipation process by dissipating a small amount of energy themselves.

First results obtained regarding the local sphere matrix debondings then answer the following question: how do internal cavities occur? They are formed by the local debonding of the spheres from the matrix.

Thanks to our micro tension test setup, we succeed in recording videos of the local cavities growth (see fig 3.10). For a quasi static tension (incremental ramp loading), we observe that the length of the cavities increases along the tension direction and the lateral dimension tends to remain constant. This lateral dimension seems to depend on the steric hindrance of the sphere where the cavity comes from. However, the images recorded with our

setup are only surfacic. The size depicted on fig 3.10 is related to the cavity size but is not rigorously equal (slightly smaller).
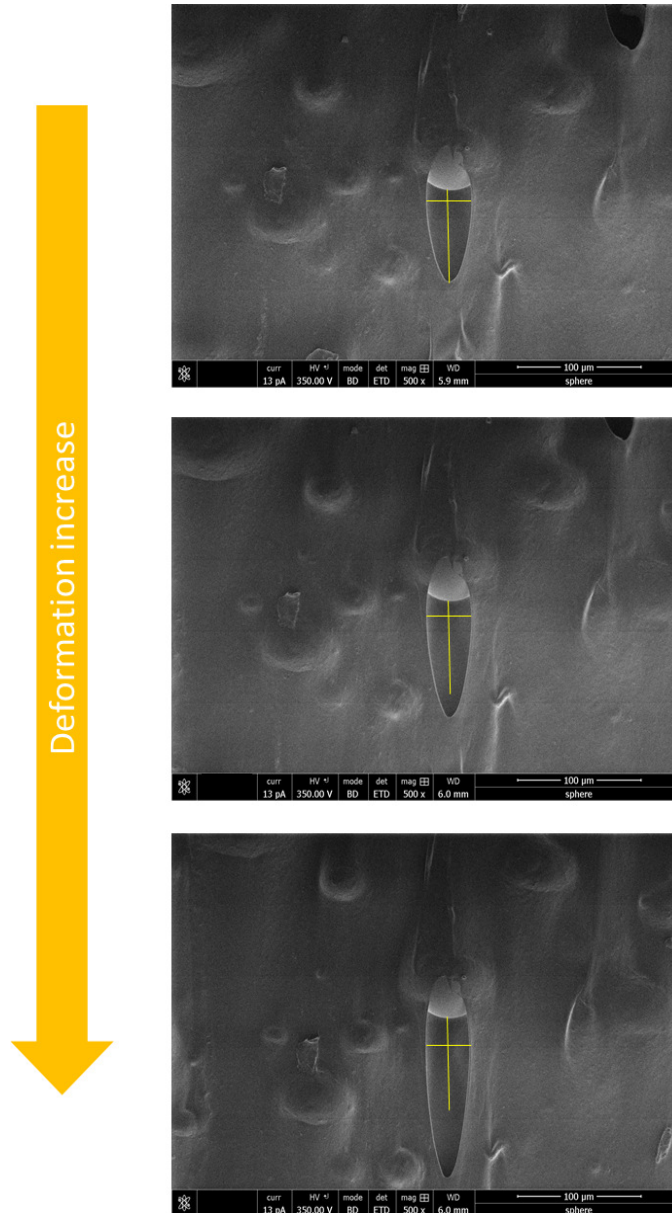
FIGURE 3.10: Bulk cavity shape evolution for a sample deformation going from 400% to 500%

On the figure 3.10, we notice that cavity grows along the tension direction. Interestingly, we observe that cavity deforms at 60% when the sample is deformed at 100%. This gap can come from effects inside the grips or from vacuum chamber conditions. We also note that there is no side effect or perturbation induced by neighboring spheres. When we extrapolate these considerations to all the cavities which appear in foam PSA we can explain the observation we made at the macroscale where we saw that all the material orientates itself when submitted to a large strain regime (for high

adherence energy cases reported in fig 3.7). Here comes the answer for the second question, how do internal cavities grow? They grow along a global uniaxial tension loading direction.

At this point we can explain that cavities are formed following the debonding of the glass microspheres from the matrix. Those cavities grow along the loading direction within the thickness of the material. Due to the syntactic foam structure such sphere matrix debonding can occur anywhere in the material bulk. If we recall the peel test results of fig 3.7, we saw that such bulk debondings occur for sufficiently high adherence energy ($\Gamma > 700$J.m^{-2}). When the structure of the foam PSA becomes totally fibrillated, for a sample tensile strain higher than 500%, the walls between the cavities (see the image fig 3.11) become thinner and thinner.
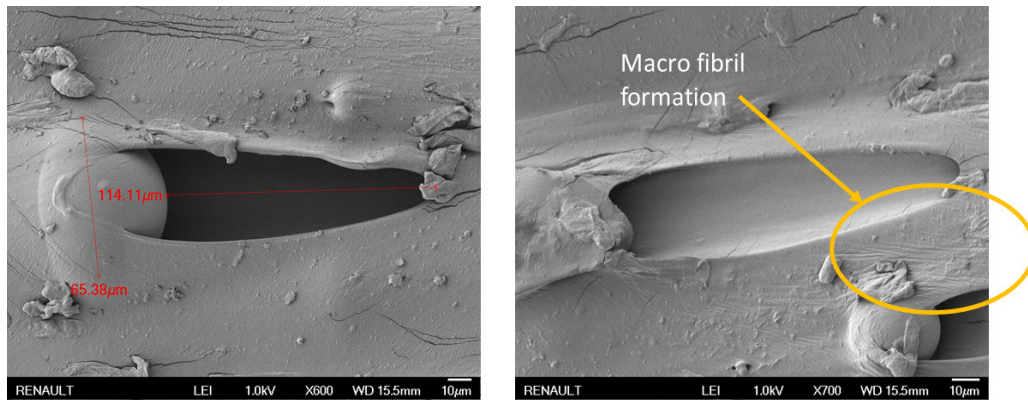
FIGURE 3.11: Mesoscale fibril formation process (μm scale

When the material reaches very large deformations (more than 600%), we observe the breakage of some spheres. An image is provided on the figure 3.12. Important to note that we have no clear evidence that the breakage occurs during the test loading (could also be due to default in the product manufacturing). However, we never distinguished broken spheres for smaller deformations. That is why we evoke the lateral pressure exerted on the spheres during the tension (in blue on the figure 3.12) as a plausible breaking cause. The pressure is so high that it becomes critical for the spheres physical integrity which, as a result, break.
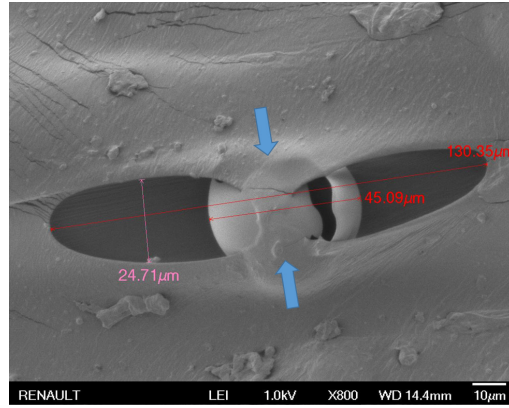
FIGURE 3.12: Hollow glass microsphere breakage

We can sum up all the knowledge gained thanks to this micro tension by the graph of the figure 3.13.
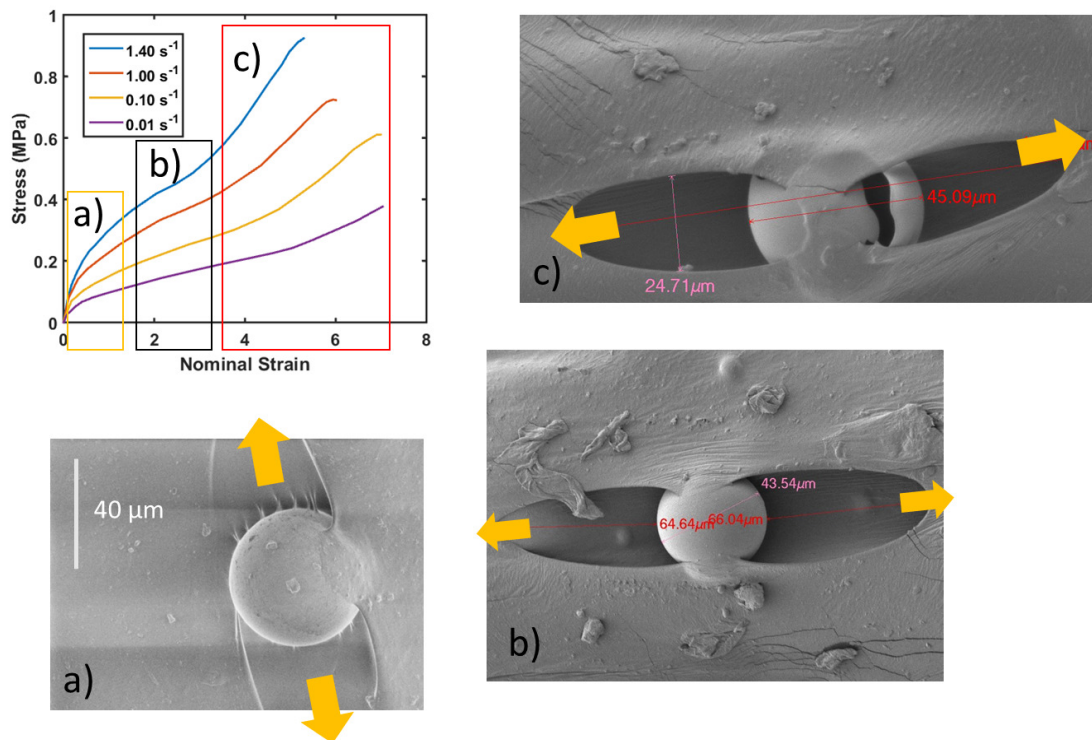
FIGURE 3.13: Bulk micro structure evolution of foam PSA during tensile tests stopped before rupture

When foam PSA are loaded in tension, syntactic foam matrix debonds from glass hollow microspheres. During those local debondings (microscale), dissipative mechanisms appear locally due to matrix material local instabilities. Hence, energy is dissipated through micro fibrillation processes. These dissipative processes can be assimilated to thin PSA cases [78]. Such local debondings lead to a material structure change which tends to orientate itself along a uniaxial direction, especially true when the adherence becomes

15% deformation
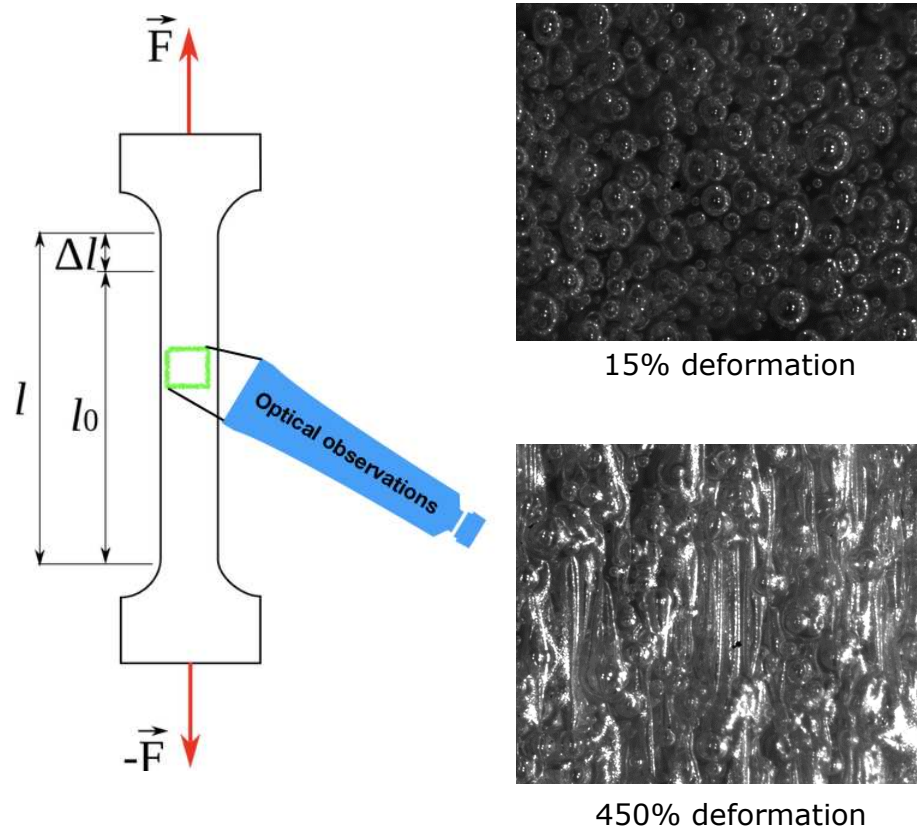
450% deformation

FIGURE 3.14: On the left, the used instrumented tension setup (Instron 5280). On the right, the optical observations corresponding to 15% deformation and 450% deformation. The stretch is vertical. The thickness of each image is 1mm. Sphere matrix debonding is observed when spherical shapes begin to deform along the tension direction.

high. During this stage, cavities following the sphere matrix debondings start to grow which step by step deconfines the adhesive. As the size of the cavities (homogeneously dispersed in the bulk) increases, the foam PSA bulk becomes more and more compressible. This process is directly related to the material loading. Eventually, for deformations higher than 500%, when all the structure is fibrillated and highly stretched, some broken spheres are reported. At the end, the material continues to deform until the fracture of the sample.

From these results, one important question pops up. What is the minimal strain to observe sphere matrix debonding? To answer this question, we carried out tensile test presented in part 2.1.3, where we instrumented our setup with high resolution optical observation devices. We then observed microspheres in our sample during a typical tension test. Observations are reported on figure 3.14.

According to our experiments, this debonding occurs at around 15% deformation. This value is very low which means that a relatively small strain

can engender sphere matrix debonding. For the use of this value of 15% in the case of peel test and flat ended probe tack test, it is important to bear in mind that uniaxial tensile test conditions differ in terms of geometrical confinement. That is why 15% deformation accounts for a maximum. In the case of peeling or tack, where the geometrical confinement is much higher, sphere matrix debondings (highly dependent on hydrostatic pressure) should only appear at lower strains.

Damage origins

According to the results we obtained from in situ tensions, we now have leads to explain damage observed in part 2.1.3. The first one regards spheres matrix debondings. If we recall the cyclic loading graph on the fig 2.14, we pointed out a softening effect seeming to take place in the foam PSA for deformations around 80-100%. Such a behavior is somewhat reminiscent with Mullins effect extensively encountered in the filled elastomers [26]. However, Mullins effect is supposed to happen at the nano scale, classically when the interface between elastomeric matrix and black carbons aggregates breaks once and rebonds at a lower adhesion level. For the foam PSA, even if black carbons are added to color the material, the concentration of the particles is too small (less than 5%) to have a mechanical influence [26, 31]. But, thanks to the in-situ tests results, we can see that this interfacial debonding bonding cycle is similar to the one occurring at the interface between the hollow glass microspheres and the polymeric matrix. When syntactic foam architecture is deformed enough to debond the spheres form the matrix, the interface reformed after each cycle, during the relaxation time, would exhibit a lower adhesion level. So, if we then reload again the adhesive, the spheres matrix interface will break more easily and the force to provide to deform the material will be lower. That seems to explain the measured softening effect. In the foam PSA, an equivalent Mullins effect would explain well the observed behavior. However, it would be Mullins effect at a length scale a thousand times larger than in the filled elastomers [26].

If our explanation is correct, the softening effect should be easily decreased if we enhance the spheres matrix interfacial rebonding after the first loading. The most straightforward solution to do so is to heat the material during its relaxation. In other terms, we stretch the material until a sufficient strain to debond most interfaces but not too much to break the spheres, we choose 450% with a strain rate of $1s^{-1}$. After the first cycle, material is relaxed and heated at 80°C during 2 hours. According to PSA supplier, this temperature is safe for the adhesive. Then the sample is cooled down at 23°C and the second cycle until 450% is carried out. Results are presented in the figure 3.15.
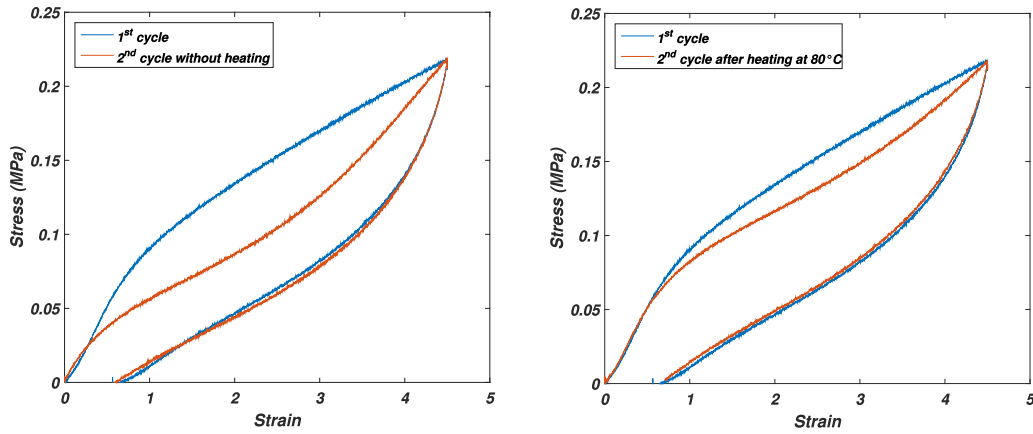
FIGURE 3.15: On the left, the two cycles are carried out at imposed strain (450%) without heating stage between the two tests. On the right, the two tests are performed at imposed strain (450%) with heating stage after the first cycle.

As we can see on the figure 3.15, such heat treatment allows to cure the material by dramatically decreasing the softening effect and therefore the damage in the material bulk. In Chapter 4 we will see, thanks to this induced healing protocol, how we can reuse a foam PSA without loosing performance.

As it stands we can say that this source of damage has a significant impact on the tape behavior. However, as long as the matrix itself is not fractured (which has never been observed in our tests), this damage seems to be partly recoverable. This potential recoverability is what differs spheres matrix interfacial adhesion level changes with the other damage source found, the breakage of the spheres.

3.2 Equivalent Fibril Model

In the previous section we identified the dissipative mechanisms which take place when foam PSA are loaded. Due to the syntactic foam structure, dissipative mechanisms occur within the bulk of the material at interfaces between the spheres and the matrix. The spheres which are close to the interface debond first. Most probably, this local debonding is caused by confinement. Then, bulk spheres begin to debond, even in small strain regime (about 15% deformation). Their development depends on material loadings rate and PSA substrate interfacial adhesion levels. We understood that the bulk cavities are generated by internal cavities nucleation which leads to fibrillation processes at the scale of the sample (mm scale). As the deformation of the foam PSA increases, internal cavities grow. Inside these larger cavities, we observed instabilities occurring on the walls forming a micro fibrillation process (μm scale). When the cavities continue to grow, walls between them become thinner and thinner which create a second bulk fibrilation process at

a larger scale (mm scale). These fibrils are then elongated until the ultimate detachment from the substrate or until a cohesive material fracture.

In the conditions where the PSA is loaded in a peel test at 90°, we present a model which is based on the dissipative process detailed above. The relevant part of the energy dissipation is made in fictional equivalent fibrils which are aligned with the material orientation. This model is called *Equivalent Fibril Model*. Energy dissipation is supposed to be piloted by the strain rate of this equivalent fibril where the measurement is detailed after. The model presented is inspired by the Gent and Petrich approach [37] and the work of Villey et al. [78, 77].

3.2.1 Hypotheses of the model

Before describing the model, we define all the hypotheses needed to build it. They all derive from one main assumption which is that most glass microspheres must be debonded from the matrix. This implies sufficient PSA substrate interfacial adhesion level and debonding velocity. Relevant couple of these two parameters gives an adherence higher than 1000J.m^{-2} for our 90° peel test setup with the chosen backing layer. In practice, we take as substrates the glass slides prepared according to the surface treatment protocol described in part 2.3. For the debonding velocities, we identified velocities higher than 0.1mm.s^{-1}.

3.2.2 Model description

As we said, the concept behind the model is that most dissipation is made through the extension of equivalent fibrils. The latter are assumed to be loaded in uniaxial tension in the debonding region. As a result, the dissipative energy should be equal to the expended energy in equivalent fibrils until the breakage. Breakage is defined when the adhesive detaches from the substrate. We assume that most energy dissipation is made through this equivalent fribrillation process. So, the energy that has to be provided to the adhesive material to debond, also called adherence energy Γ, should be close to the energy expended in one single equivalent fibril during the foam PSA peeling.

During the peeling, if confinement effects remain limited, the adherence energy measured should be close to the energy we should provide to the tape in a uniaxial tension test for the same ϵ_{max}. Thin PSA studied by Villey et al. [78, 77] are highly confined. As a consequence, fibrils occurring in the debonding region dissipate a 5-time smaller amount of energy than the material does in uniaxial tension test. As foam PSA thickness is 60 times larger than PSA from Villey et al. [78, 77, 13], it is reasonable to think that this prefactor of 5 should be lower.

In other terms, if we carry out a tension test of the material and we calculate the energy expended in the material until ϵ_{max}, we should be closer to the overall adherence energy. To do so, we have to multiply the calculated energy in tension tests (area under the curve until ϵ_{max}) by the initial material thickness a_0.

$$\Gamma(V_{peel}) \approx a_0 \int_0^{\epsilon_{max}} \sigma(\dot{\epsilon}_{equivalent fibril}(V_{peel}), \epsilon)d\epsilon \qquad (3.1)$$

This analogy with tension tests works if the tension tests are performed at the same strain rate than the one calculated on the equivalent fibril, $\dot{\epsilon}_{tension} = \dot{\epsilon}_{equivalent fibril}$. According to Villey et al. [78], in the debonding region the equivalent fibrils are supposed to have a constant strain rate and they undergo a constant stress during their loading. Hence, we have the following relationship:

$$\dot{\epsilon}_{equivalent fibril} = \epsilon_{max} \frac{V_{peel}}{L_{dr}} \qquad (3.2)$$

This equivalent fibril has an initial length equal to the initial thickness of the adhesive a_0. Its maximal extension is the extension when it detaches from the substrate. On the photograph 3.16, equivalent fibril just before detachment is drawn.
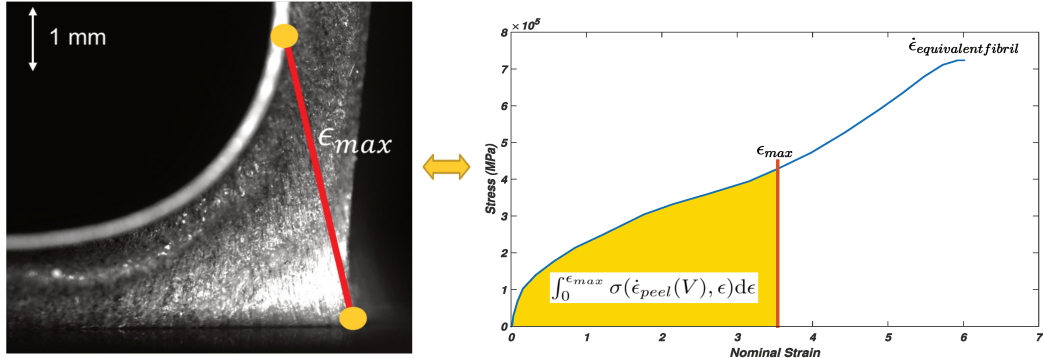
FIGURE 3.16: EFM application principle

Equivalent fibril is supposed to be aligned with the apparent material orientation that we observe on the tape surface. In this configuration we measure ϵ_{max} reported in the figure 3.17.
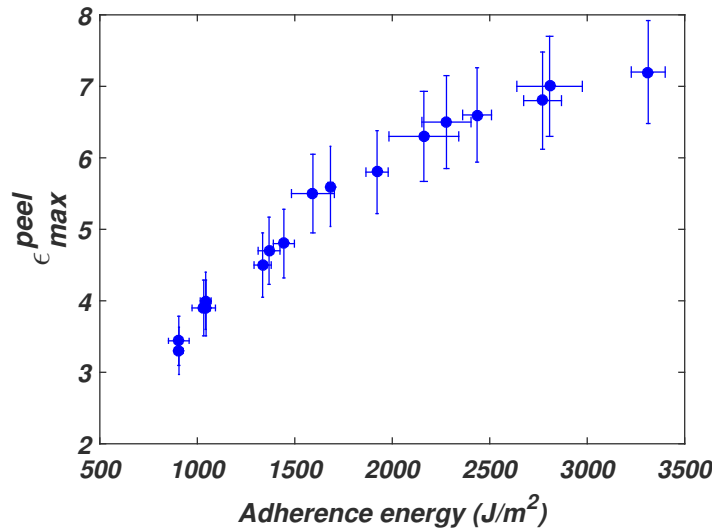
FIGURE 3.17: Maximal extension of equivalent fibrils measured in peeling at 90°

On figure 3.17, ϵ_{max} increases with the velocity: $\epsilon_{max} \sim V^{0,12}$. Once again, this observation highlights the difference with thin PSA behavior. Chopin et al. [13] reported for their materials: $\epsilon_{max} \sim V^{\alpha}$ with α being negative. ϵ_{max} evolution is consistent with the morphology study of the debonding region shape in Chapter 4. The equivalent fibrils strain rate is the spacing rate between the two fibril extremities (one on the substrate, the other on the backing) [78].

Expended energies in tensile samples (for ϵ_{max} and $\dot{\epsilon}_{equivalent\,fibril}$ coming from the peel tests) are now compared with the actual peel adherence energies. Results are presented in the figure 3.18.

For adherence energies higher than 2000J.m^{-2}, the EFM fits very well the adherence energy measured during the peeling. In this domain, dissipated energy can be assimilated to the energy expended in the uniaxial tension of equivalent fibrils. In those conditions, the maximal extension and the strain rate of the equivalent fibril pilot the dissipation. Knowing that dissipated energy is related to adherence energy, the EFM provides us with a new way of describing adhesive joint performance for adherence energies higher than 2000J.m^{-2} (with the chosen backing). It is worth noticing here that these peeling conditions correspond to industrial specifications. For lower adherence, EFM deviates. We propose an explanation for this deviation in the following section.

3.2.3 Model limitations

EFM seems to be relevant for the adhesive peeling behavior description except for some limitations. The first one is the validity domain. As we saw
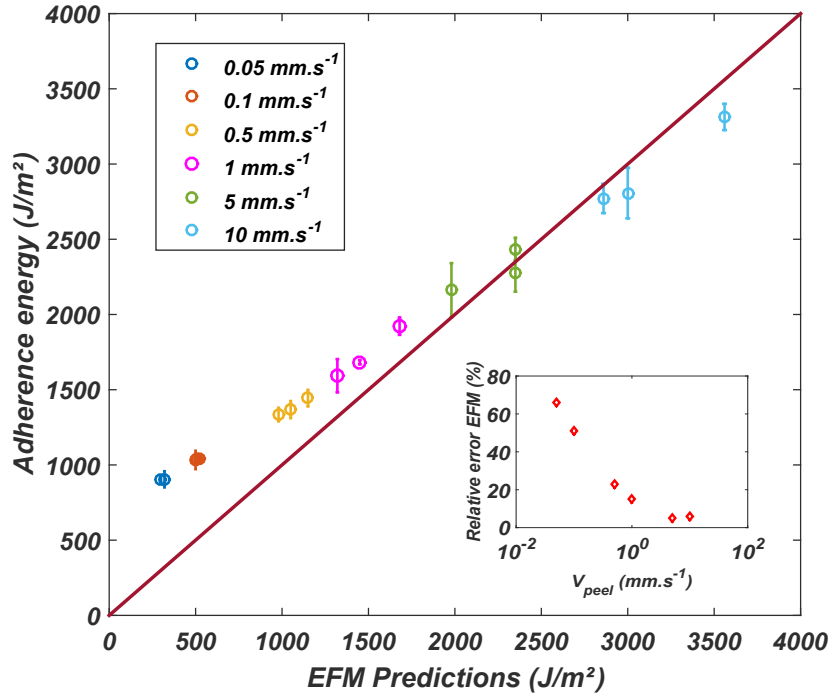
FIGURE 3.18: EFM predictions with respect to actual adherence energies measured with peel tests over 2 decades of debonding velocities

the model works only for a fully fibrillar structure where hollow glass microspheres are totally debonded from the matrix. This condition eliminates the low adherence cases ($\Gamma < 2000\text{J.m}^{-2}$) where all bulk cavities are not highly deformed and very high adherence cases ($\Gamma > \approx 5000\text{J.m}^{-2}$) where internal fracture occurs.

The other limitation comes from the fact that fibrils in the case of Villey et al. [78, 77] are individual and independent. They develop as a continuum within all the material thickness. In the foam PSA case, we saw that such bulk fibrillation process is totally different (see part 3.1). Large fibrils elongated within all the material thickness are purely made for modeling purpose. This major difference could explain most of the deviation we observe on the figure 3.18.

From a general point of view, even if we highlighted its main limitations, the EFM stands as a relevant quantitative model to describe the foam PSA behavior for the 90° peel test loading conditions. The EFM shows that most energy is dissipated in the unconfined uniaxial extension of equivalent fibrils. Dissipation seems to be piloted by the strain rate of this equivalent structure. The goal is now to explain more quantitatively those results. We base our work on the use of the non linear rheological behavior of foam PSA.

3.3 Non-linear rheological approach of adherence explanation

Chopin et al. [13] presented a method based on the non linear rheology of thin PSA fibrils to explain quantitatively the work of Villey et al. [78, 77]. EFM results showed for an adherence energy higher than about 2000J.m^{-2}, the strain rate and so the rheology of a single virtual fibril pilots the energy dissipation. Also, Chopin et al. [13] explains thin PSA adherence down to one detail. There is a prefactor of 5 to match with experimental data. This prefactor is explained by the extreme confinement of thin PSA. The idea we had was then to adapt this work to our weakly confined foam PSA.

The descriptive method of Chopin et al. [13] is made according to a classic linear TTS protocol extended to non-linear rheological measurements. These measurements are provided by uniaxial tension tests at different strain rates and temperatures. The method used is based on the possibility to collapse tension test results (strain stress curves) on a single mastercurve for any arbitrary chosen strain rate and temperature.

We started by performing tension tests for different strain rates and different temperatures. We observe that all strain stress curves collapse into a master curve arbitrarily defined by a strain rate of 0.05s^{-1} and a temperature of 23°C. Collapsing is made thanks to a stress normalization as depicted in the figure 3.19.
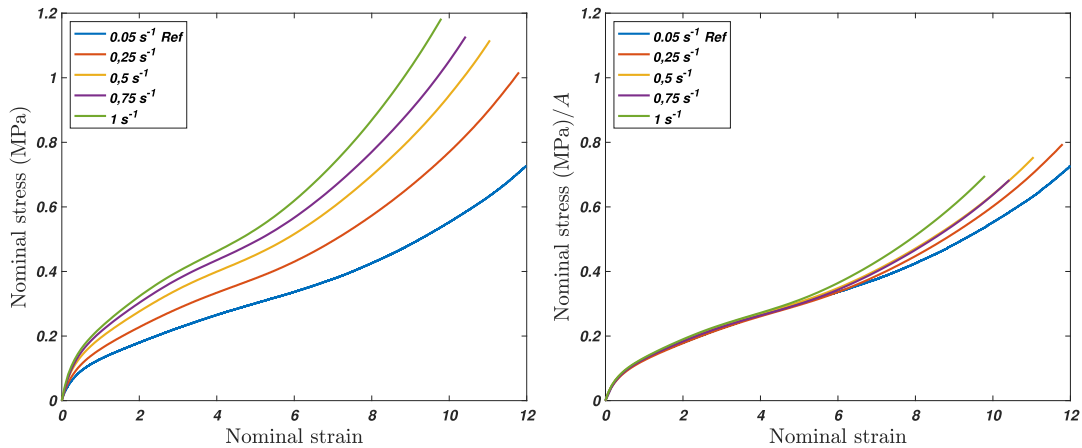
FIGURE 3.19: The graph on the left corresponds to the tension test results when varying strain rates. The graph on the right shows the normalized stress with respect to the nominal strain of the same tests. Normalization is made using the prefactor $\mathcal{A}$

From the graphs in figure 3.19, we obtain the rescaling parameter $\mathcal{A}$ plotted with respect to the strain rate in the second graph from figure 3.19. Rescaling is made without taking into account the hardening effect. The first main result is here that rescaling stress strain curves from the uniaxial tension test

to a master curve works very well up to strains of 7 and for temperatures going from 20°C to 45°C.

We then combine all the shift parameters for different temperatures and strain rates and apply to them TTS parameters coming from the linear small strain measurements from Chapter 2. We then plot the shift parameter $\mathcal{A}$ with respect to $a_T.\dot{\epsilon}$, in the main graph from the figure 3.20.
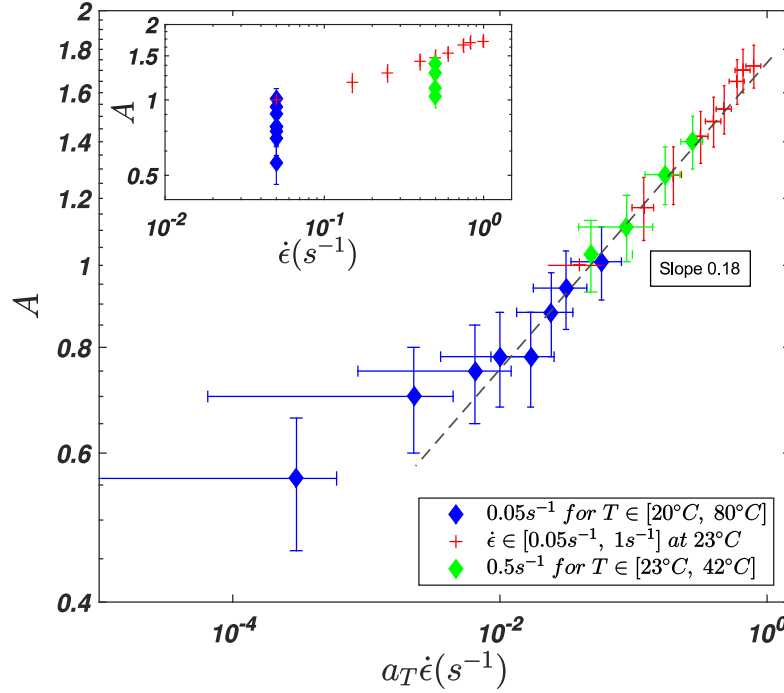
FIGURE 3.20: The two graphs represent the evolution of the shift factor $\mathcal{A}$. The small graph regards its evolution with respect to $\dot{\epsilon}$ and T. On the main graph, $\mathcal{A}$ is plotted with respect to the normalized strain rates $a_T.\dot{\epsilon}$.

On fig 3.20, we observe that above a certain abscissa, $\mathcal{A}$ can be described as a power law of the TTS rescaled strain rate (the choice of the power law is common to compare with other PSA). In other terms, from this specific value, we have:

$$\mathcal{A}(a_T.\dot{\epsilon}) \sim (a_T.\dot{\epsilon})^{0.18} \tag{3.3}$$

This result shows that most of the rate and temperature dependent elements of foam PSA behavior can be represented by this rheological function $\mathcal{A}$. Another relevant point to mention is that the specific validity domain of the equation (3.3) corresponds to the equivalent fibrils strain rates met when studying the peeling.

Based on the conditions of EFM application, we know that adherence energy should be described by the following relationship:

$$\Gamma(V_{peel}) \approx a \int_0^{\epsilon_{max}} \sigma(\dot{\epsilon}_{equivalent\,fibril}(V_{peel}), \epsilon, T) d\epsilon \tag{3.4}$$

However, thanks to the equations 3.3 and 3.4 we have:

$$\sigma(\epsilon, \dot{\epsilon}, T) = \mathcal{A}(a_T.\dot{\epsilon}).\sigma^{ref}(\epsilon) \sim (a_T.\dot{\epsilon})^{\alpha}.\sigma^{ref}(\epsilon) \tag{3.5}$$

where $\alpha = 0.18$.

Thus, equation 3.5 becomes:

$$\Gamma(V_{peel}) \approx a.(a_T.\dot{\epsilon})^{0.18} \int_0^{\epsilon_{max}(\dot{\epsilon})} \sigma^{ref}(\epsilon) d\epsilon \tag{3.6}$$

Using the same data from the EFM calculations, we then obtain the predicted adherence energy levels given by equation 3.6. A comparison of this description with the actual measurements provided by peel tests is presented in the figure 3.21.
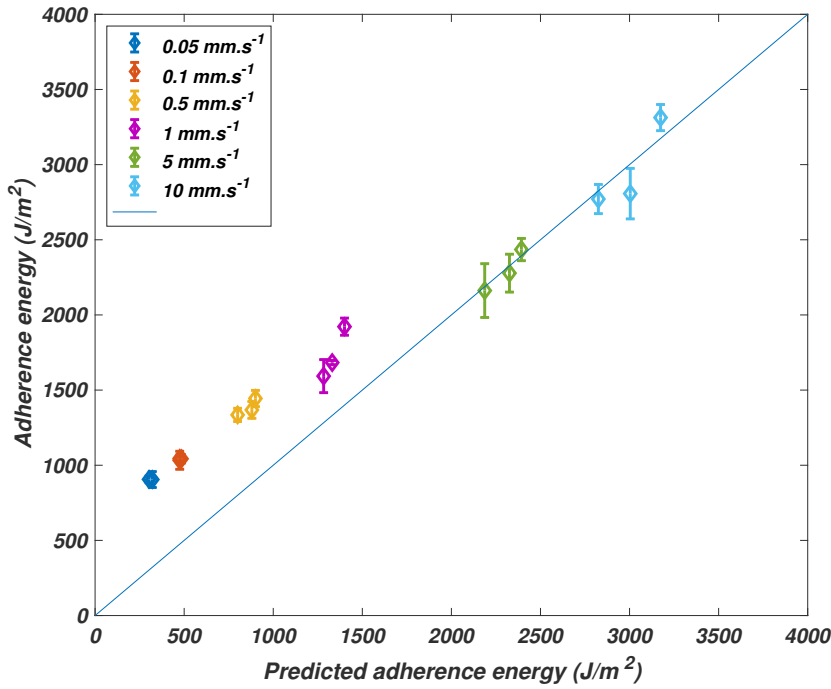
FIGURE 3.21: The figure presents the gap between adherence energies predicted by the non linear rheological based method and the actual data obtained from peel test experiments. On the small graph, relative errors between model and real data are plotted.

On the graph from figure 3.21, we observe that the description is even better than EFM for high adherence energies ($\Gamma > 2000 J.m^{-2}$). For lower adherence energies, the error is the same. This shift seems to be explainable by

the structure of the tape debonding region. For such peeling adherence levels, the foam PSA is not enough fibrillated or not totally orientated (see EFM limitations). For this reason the non linear rheology based model predicts underestimated adherence energy values. Equivalent fibrils do not deform enough to dissipate enough energy. Such results quantitatively support the fact that the foam PSA non linear rheology pilots most of the energy dissipation as we indicated in part 3.1. Because we know foam PSA performance is directly driven by its ability to dissipate energy, non-linear rheological behavior of the tape is then of prime interest when assessing bonding assembly strength.

In this section, we saw how the non-linear rheological behavior of foam PSA was relevant to quantitatively describe adhesive performances. To use it with our material, we first evaluated the relevance of using TTS parameters obtained in linear small strains regime for the non linear high strains domain. To achieve this, we determined the linear rheological function $\mathcal{A}$ existing between the non-linear shift factors and $a_T.\dot{\epsilon}$ (the strain rate normalized by linear TTS parameters a_T). We then estimated the adhesive joint resistance in applying our rheological function $\mathcal{A}$ to the adherence energy calculation (see equation 3.6). The comparison with actual adherence energy measurements was reasonably good for high adherence energies ($\Gamma > 2000 \text{J.m}^{-2}$). Nevertheless, errors observed for lower adherence levels are in good accordance with EFM conclusions. For energies lower than a certain value ($\Gamma < 2000 \text{J.m}^{-2}$ in our case with our backing), the debonding region is not totally straightly oriented which questions the concept of an equivalent fibril.

In order to broaden these observations to other loading conditions, we present in the following part a transposition model to extend our results to the flat ended probe tack test.

3.4 Transposition Peel/Tack Model

By definition, flat ended probe tack test and peel test are inherently different. As we saw in part 2.2, the first one is classically used to study the initiation of the debonding and the second one focuses on the debonding steady state crack propagation. However, we present here a transposition model which allows to transpose peel tests results to flat ended probe tack test. Such a transposition model (TM) is based on the EFM presented before and on the following hypotheses on the foam PSA behavior in confined tension.

3.4.1 Hypotheses of the model

Flat ended probe tack test can be seen as a confined tension loading. Geometrically, the adhesive disk has a diameter 8 times larger than its thickness. In an incompressible material, such a confinement level would result in a huge

hydrostatic pressure at the material center leading to internal fracture during probe tack like experiments (see chapter 2). However, the syntactic foam architecture of foam PSA prevents such a catastrophic situation from happening thanks to sphere matrix debondings. Indeed, we saw in part 3.1 that when we load foam PSA, voids occur within the bulk of the material. These voids release the confinement effects. As the material is loaded, it becomes more and more compressible and orientates itself along the tension direction in the debonding region. The main assumption we make for the application of the Transposition Model is that all the material bulk is cavitated before the occurrence of the PSA substrate detachment. That is why we focus TM for a peel velocity higher than 0.5mm.s^{-1}.
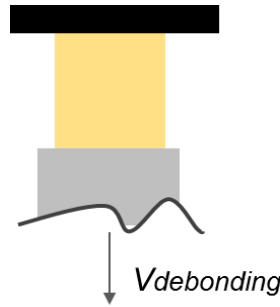
FIGURE 3.22: Flat ended probe tack test simplified model

In these conditions, we can define equivalent fibrils in the same way as in the EFM. Considering the loading geometry of the flat ended probe tact test (see figure 3.22), we calculate the equivalent fibrils extensional strain rate as:

$$\dot{\epsilon}_{equivalent fibril} = \frac{V_{debonding}}{a} \tag{3.7}$$

where a is the disk initial thickness.

3.4.2 Model description

As previously explained, the goal of the transposition model is to find a method to transpose adherence results obtained in peel to the probe tack and viceversa. This transposition is based on the application of the EFM to the debonding region of the peel test. To do so, adherence regime must belong to the EFM validity domain (adherence energy $\Gamma \in [1.5 \, ; 4\text{kJ.m}^{-2}]$).

In the EFM validity domain, the work of Villey et al. [78, 77] gives us a simple formulation (see eq. 3.2) to calculate the extensional strain rate of equivalent fibrils in the peel test.

The essence of the Transposition Model (TM) is thus to equalize this strain rate with the strain rate in the probe tack test. To achieve this, whether it

is in peel or tack tests, the only parameter we can experimentally impose is the debonding velocity. In the peel test, changing $V_{debonding}$ changes also L_{dr} and ϵ_{max} so we prefer equalizing the strain rates by adjusting the tack debonding velocity, a being a constant. By doing this, fictional equivalent fibrils have theoretically the same strain rate. According to part 3.2 and 3.3, energy dissipation should be mainly piloted by these equivalent fibrils strain rates. Since the performance of a PSA adhesive joint depends on the amount of energy it can dissipate, we should measure in the two adhesion tests (peel and tack) the same adherence energy. Of course, this statement should only be true if the interfacial PSA substrate adhesion level is the same between the two tests. Through the experiments, we can meet this conditions by using glass slides treated according to the protocol 2.3. In applying this method, we measure the adherence energies for both tests. These measurements are reported in figure 3.23.
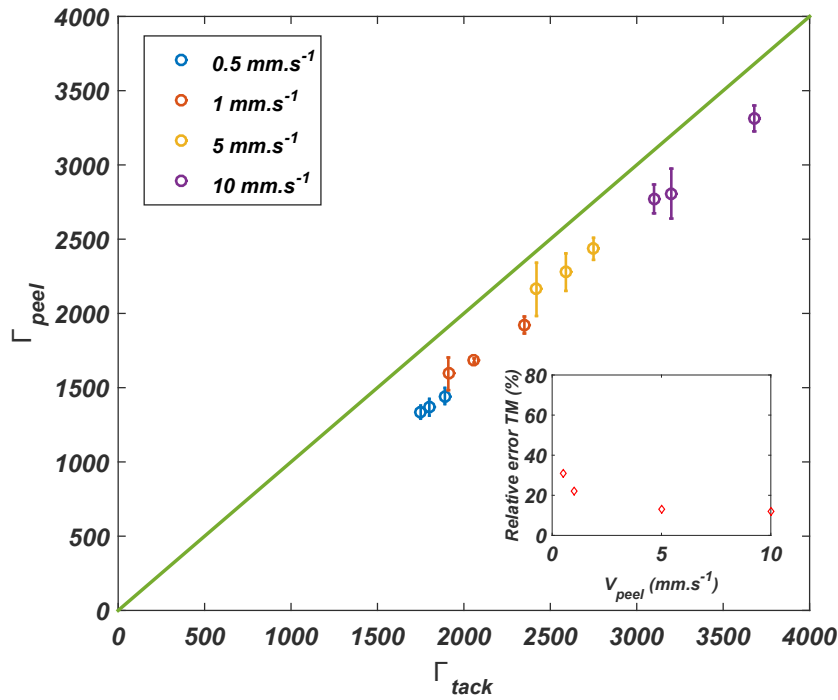
FIGURE 3.23: Adherence energies measured with the peel test with respect to the flat ended probe tack test. Experimental conditions are based on Transposition Model hypotheses

We can see on this graph (fig 3.23) that the results are very similar. The loading conditions of this test correspond to a confined tension. Our result reinforces then our description of the peel debonding region for high adherence regime. There, the debonding region can be assimilated as uniaxial stress application. That is in good accordance with the foundation based model of Kaelble (see figure 1.13).

It is worth noticing that we observe a small enhancement of the adherence energy in the probe tack test. It is mainly due to the fact that the contact
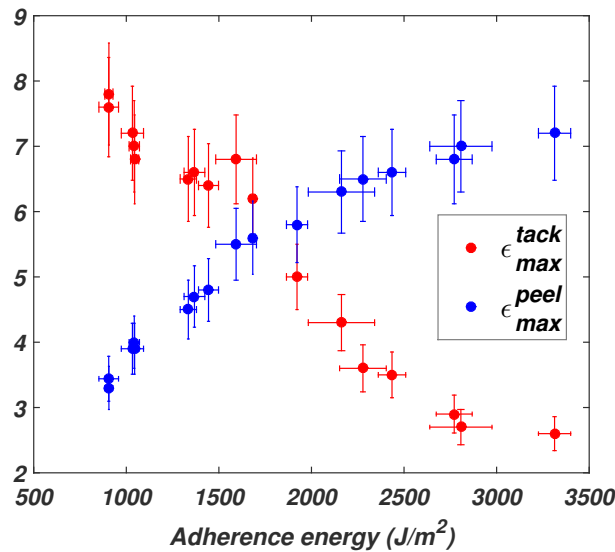
FIGURE 3.24: Maximal strains measured in peeling and in probe tack tests with respect to the adherence energy

formation stage of the two tests differs quite a bit. The contact formation in the peel test is made manually whereas in the flat ended probe tack test, the contact is made automatically. Thus, interfacial adhesion levels are likely to differ. Even if this difference occurs, a clear tendency can be observed.

3.4.3 Model limitations

In terms of limitations, the first one we can highlight is the same as for the EFM. The Transposition Model remains valid only for a certain adherence energy range. But under this condition, assimilating foam PSA as a fully fibrillated material where energy dissipation is piloted by fibrils strain rates seems to be relevant.

The other limitation comes from the fact that the contact formation stage between the two adhesion tests can be critical. Indeed, for the peel test, the application is manual which can lower the interfacial adhesion level (see part 2.1.2). Compared to the probe tack test where every parameters of the contact formation is controlled, it can make a huge difference.

The last limitation is met since the flat ended probe tack test and the peel test do not describe the same stage of the debonding evolution. Hence some hypotheses of constant equivalent fibril strain rates and stresses can be questionable. Especially since we observe the maximal deformations of the equivalent fibrils for the two tests. On the graph figure 3.24, we clearly see that their evolution with the adherence energy is totally opposite.

This result is counter intuitive and lets us puzzled. The only explanation seems to take into consideration boundary effects in the tack test which could change the debonding front propagation. But this explanation has to be proven. This behavior stays an open question for this PhD work.

As for the EFM, the Transposition Model (TM) provides another approach to describe energy dissipation during the foam PSA debonding. To go further, the transposition model should be implemented to other adhesion tests such as cleavage. This model also strengthens the relevance of regarding the foam PSA bulk self orientation during uniaxial loadings at the scale of the material thickness. Thanks to this configuration, we also bring to light a major change in the way PSA debond. If the strain rate of equivalent fibrils seems to be the relevant transposition parameter, the differences observed on the maximal extension vanish the validity of this concept for tack test. Going beyond this major scientific limitation, in a purely industrial point of view, it provides an easily implementable model to move to a test which it is not used yet, the flat ended probe tack test.

3.5   Conclusion

Chapter 3 gives answers to many questions we had when we finished characterizing the foam PSA behavior. First, we identified the dissipative mechanisms taking place in the tape during the debonding. These mechanisms occur at length scales going from $\sim \mu$m to $\sim$mm. During the debonding, cavitation appears first locally in the bulk in a region close to the PSA substrate interface. This cavitation is due to local sphere matrix debondings engendered by the material confinement. Then, when deformation increases in the bulk, another cavitation process develops within all the material thickness. Cavities additionally appear between the glass microspheres and the polymeric matrix. If the interfacial PSA substrate adhesion level is strong enough, bulk cavities grow. During this growth, instabilities are formed on the cavities walls. Such instabilities result in the creation of micro fibrils. Although microscopic, this process is likely to contribute to the overall energy dissipation. At some point (second transition regime studied in Chapter 4), bulk cavities are large enough to deconfine the material. As the loading is performed, foam PSA confinement decreases. The walls between cavities become thinner and thinner which create large fibrils ($\sim$mm). Thanks to this geometric configuration, a larger amount of energy can be dissipated. This geometric configuration change can then allow the adherence energy to increase. Eventually, we observed that the spheres matrix debondings are not fully reversible. A damage effect, similar to "Mullins effect" met in filled elastomers, was pointed out during cyclic loadings where spheres are debonded and then rebonded during material relaxation.

Depending on the adherence energy reached in peeling, we saw the structure of the adhesive being more or less "oriented". This orientation conditions the validity domain of the Equivalent Fibril Model (EFM). It consists of a model describing the energy required to debond foam PSA. It supposes that we can define equivalent fibrils along all the material thickness elongated in uniaxial tension in the debonding region. The concept laying behind is that most of the energy dissipated by the material is similar to the energy expended by those equivalent fibrils during their uniaxial extension. The amount of energy dissipated is piloted by their strain rate. We quantitatively explained this model by a non linear rheological approach.

The last model is the Transposition Model (TM). It is an extension of the EFM to the flat ended probe tack test. It supposes that results can be transposed between these two tests by equalizing the strain rate of the material in the probe tack test and the strain rate of the equivalent fibrils in peeling. A good transposition of the adherence energy can be made. However, maximal material deformation in tack and strain at rupture of the equivalent fibrils follow two opposite trends. This point still remains puzzling for us.

Chapter 4

Linking debonding region shape and adhesive performance

4.1 When adhesive performances depend on the tape morphology

Studying the geometry of the debonding region requires the observation of the material during a complete debonding process. Whether it is for the mechanical loading conditions or for images recording system, our instrumented peel test setup seems to be perfectly suitable. We had already hints regarding the coupling between the size of the foam PSA debonding region size and the adherence energy in Chapter 3 (see fig 3.5). However, there were only qualitative hints. In the following section, the objective is to quantitatively explain the relationship between the morphology of the foam PSA in a peeling and the adherence energy.

In this part, we start by studying the deformation of the debonding region thanks to the evolution of relevant geometrical parameters. Then, we explain such evolution by a substantial change in the material properties occurring during the debonding. Eventually, we build a curve which could account for an adherence mastercurve for the foam PSA materials.

4.1.1 Foam PSA geometry and adherence energy: how to model the tape geometry during a peel test at 90°?

The instrumented peeling setup presented on the figure 2.18 allowed us to collect numerous videos of the peeling experiments. Here, we focus on the variations of the debonding region with respect to adherence energy evolution. In order to describe the debonding region geometry of the foam PSA, we choose three relevant geometrical parameters in addition to the debonding region length L_{dr} and the equivalent fibril deformation at rupture ϵ_{max} used in part 3.2:

- According to the literature [10, 78, 77], *the radius of curvature of the backing* r_c (represented in green on the figure 4.1) is directly linked to the debonding behavior of the tape. Indeed, in peeling test conditions, the energy to break the interface (which means to debond the adhesive) is directly transmitted

by the backing to the tape. Energy balance of beam bending in large strain
(elastica model using the Euler formulation) gives the following relationship
for the weak adherence case:

$$r_c = \sqrt{\frac{EI}{F_{peel}}} \tag{4.1}$$

Here, only the contribution of the peel force in the bending of the backing
is taken into account.

- The second parameter is more specific to our system. It is the length
defined between the apex of the curved edge of the debonding region and the
line drawn between the detachment point and the end of the curved region.
This length is called *the suction length e* (represented in yellow on the figure
4.1).

- The third parameter has been used in the literature [8] where it points
out the existing link between the adherence energy level and the angle formed
by the last fibril and the substrate. Influenced by this work, we use this pa-
rameter for our thick and unconfined sample. Hence, we define our third
geometrical parameter: *the interfacial debonding angle α* (represented in red on
the figure 4.1).
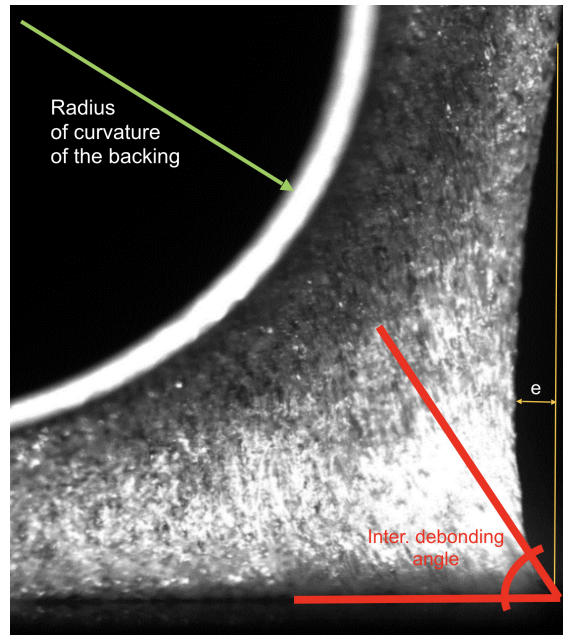
FIGURE 4.1: Geometrical parameters chosen to study the vari-
ations of the debonding region size

The evolution of these parameters with respect to the adherence energy
shows how the shape of the debonding region changes regarding adherence.
According to part 1.2.2, this specific region gathers all the dissipative mecha-
nisms identified in Chapter 2 and Chapter 3. A change in its geometry can be
directly reported to a change in the amount of the dissipated energy. AND,

changing this amount of dissipated energy affects extraordinarily the performance of the whole adhesive joint (see part 1.2.2).

The evolution of the first parameter is depicted in the figure 4.2. According to the equation (4.1), the radius of curvature should decrease with the increase of adherence energy. This trend is followed by thin and confined PSA [18].
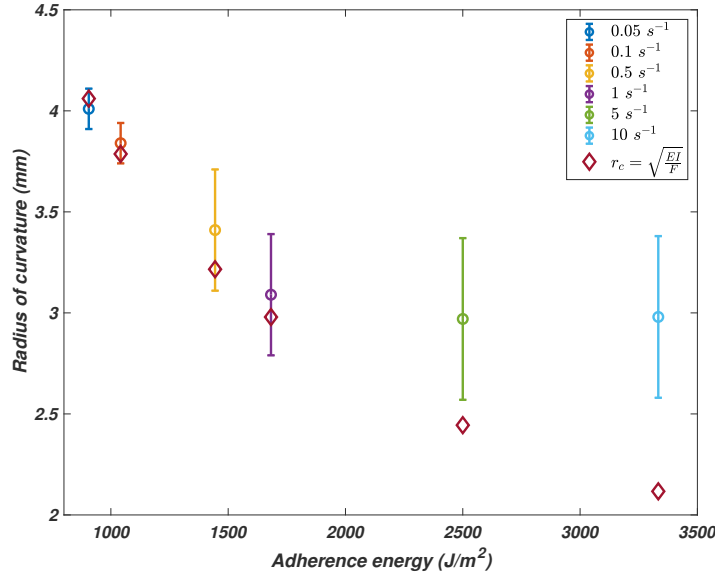
FIGURE 4.2: Radius of curvature of the backing layer with respect to the adherence energy increase

As we see on the figure 4.2, the radius of curvature of the backing follows the theoretical prediction for low adherence energies which could be expected due to the nature of equation 4.1. For adherence higher than a limit defined by $\Gamma \approx 2000\text{J.m}^{-2}$, the peel force increases but it has no effect on the backing curvature. This observation is suggests that we can no longer consider the bending of the backing layer only engendered by the peeling force. Hence, the only explanation we found is a change occurrence in the debonding region. Such change would load the backing layer. The loading due to the adhesive would be opposite to the peel force contribution. At some point, this loading is even dominant since the radius of curvature of the backing layer re-increases.

The second parameter we investigate is the suction length, *e*. We define it specifically for the purpose of the foam PSA study. This length represents how much the bulk of the foam PSA is curved. In other words, it should directly depend on the vertical deformation of the debonding region. It is worth noting that we neglect deformations in the other lateral direction that can occur on the sides of the tape. Such a hypothesis is motivated by the fact that, through the experiments, no significant lateral deformation is observed. Hence, if the adherence energy increases, the suction length should increase

as well. Measurements of this suction length with respect to the adherence energy are represented on the figure 4.3.
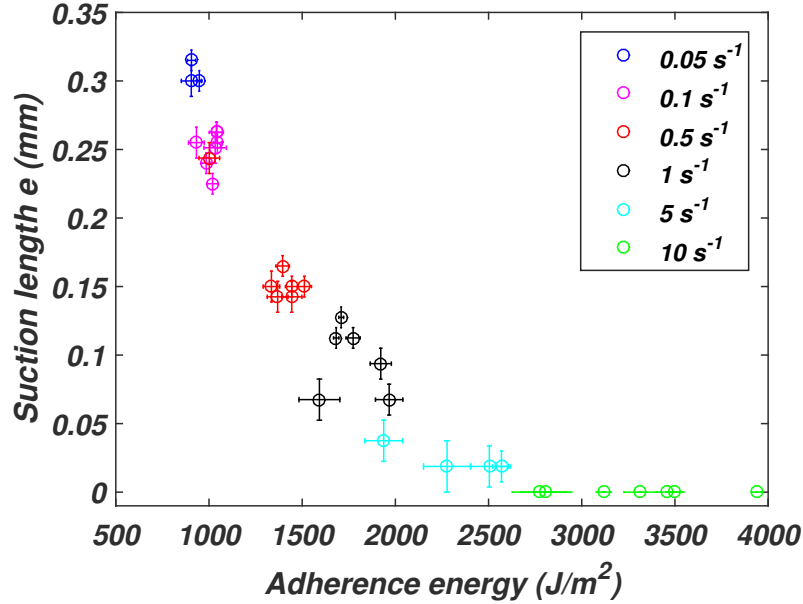
FIGURE 4.3: Suction length e with respect to the adherence energy increase

On the figure 4.3, the suction length seems to depend on the adherence energy but this dependency stops at, once again, approximately $\Gamma \approx 2000 \mathrm{J.m}^{-2}$. Such a result must be compared to the evolution of the radius of curvature of the backing. When r_c stabilizes (for $\Gamma \approx 2000 \mathrm{J.m}^{-2}$), it corresponds to the point where the suction length e goes to zero. It means that the edge of the debonding region is no longer curved. We illustrate on the figure 4.4 the evolution of the ratio $\frac{e}{r_c}$ with respect to the adherence energy.

Interestingly, for the adherence energy levels under $\Gamma \approx 2000 \mathrm{J.m}^{-2}$, the ratio $\frac{e}{r_c}$ decreases with the adherence energy. Above, this ratio becomes zero. As we see in the figure 4.4, this regime corresponds to the stabilization of the radius of curvature of the backing. Because in this regime adherence energy increases for the same interfacial adhesion level, it means that more energy is dissipated in the debonding region. However, r_c remains constant (before increasing for even higher adherence). Thus, such results give an indication to explain the increase of size by a behavioral change in the bulk of the foam PSA. We observed in figure 3.7 that adherence increases corresponds to strains becoming larger and larger in the debonding region. However, in part 3.1 3.10, we saw that large strains engender the growth of bulk cavities. Those cavities would affect the behavior of the all foam PSA by making it less sensitive to volumetric changes. So, the morphology evolution of the debonding region of the foam PSA could be due to a deconfinement phenomenon. Cavities would reach a critical size to which the continuum would be lost. Based
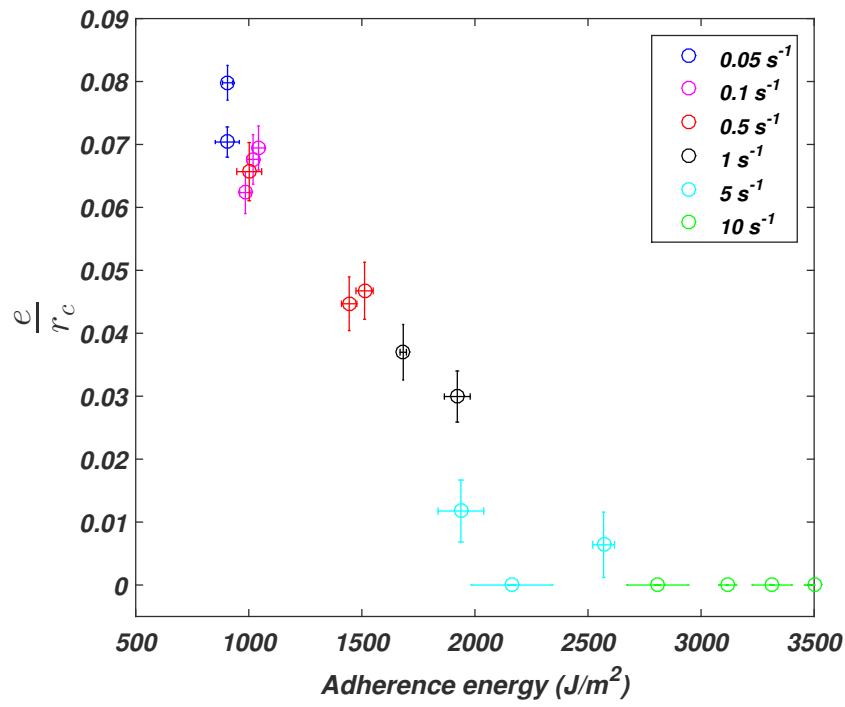
FIGURE 4.4: Ratio $\frac{e}{r_c}$ with respect to the adherence energy increase

on our results, this loss would occur at an adherence level around $2000\mathrm{J.m}^{-2}$ (for the chosen backing).

To go further, we now observe the variations of the interfacial debonding angle, presented in the figure 4.5.
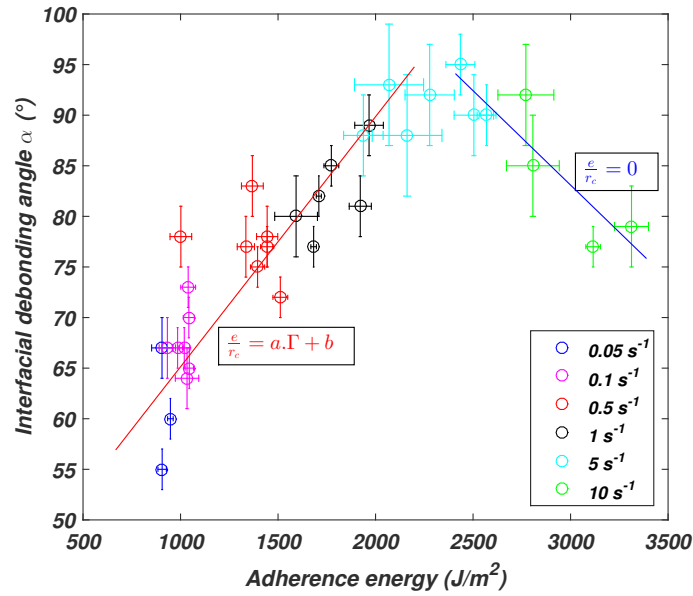
FIGURE 4.5: Interfacial debonding angle α with respect to the adherence energy increase

On the graph of the figure 4.5, we can then draw the lines representing the two regimes described above. A transition occurs at $\Gamma \sim 2000 \text{J.m}^{-2}$. This transition corresponds to the particular value of the adherence energy where the $\frac{e}{r_c}$ ratio goes to zero. The bottom line regards the regime where the debonding region edge is curved (figure 4.6 a), which contrasts with the upper regime ($\frac{e}{r_c} = 0$). There the debonding region is highly stretched (figure 4.6 c).
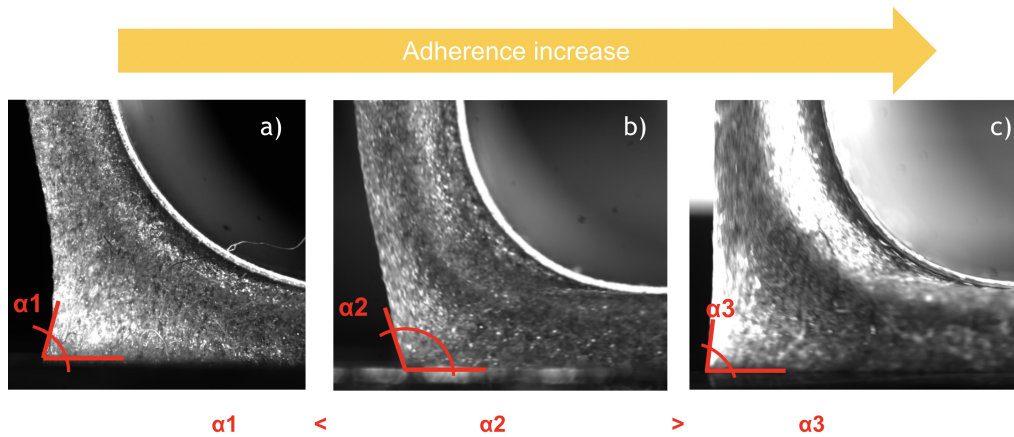
FIGURE 4.6: Morphology change with respect to the adherence energy increase. Figure a) regards the regime for low adherence where $\frac{e}{r_c}$ linear. Figure c) regards the case of high adherence energy where $\frac{e}{r_c} = 0$. Figure b) regards the transition zone where α reaches its local maximum.

The two last parameters are the ones we used in the EFM form the part 3.2. We plot the debonding region length L_{dr} with respect to the adherence energy (see figure 4.7).
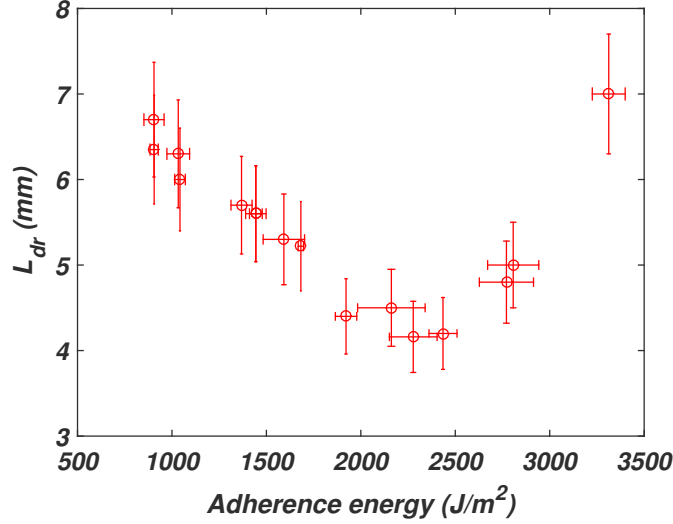
FIGURE 4.7: Debonding region length L_{dr} with respect to the adherence energy increase

On figure 4.7, we observe also a singularity around peeling velocity corresponding to the adherence energy $\Gamma \approx 2000\text{J.m}^{-2}$. These remarks give more weight to the hypothesis of the deconfinement phenomenon occurring in the bulk.

The figure 3.17 shows that maximal strain at rupture is the only parameter which is not affected by the change of the material behavior. In other terms, in the unstressed state, the foam PSA is incompressible (we can assimilate this situation to a Poisson's ratio ν close to 0.5) but when it deforms, it becomes more and more compressible (ν decreases). This decompressibility process deconfines the material which at some point (in our case, $\Gamma \approx 2000\text{J.m}^{-2}$) behaves more and more like a fibrillated material (thin PSA in a large strain regime [78]). The observed stabilization of the radius of curvature and the size of the debonding region tends to indicate a change in the material bulk. Due to the annihilation of the necking (suction length e reaching 0) we can relate this change to a compressibility evolution. Based on our results of the Chapter 3 (part 3.1), bulk deconfinement is likely to occur when adherence energy increases. However, we note that for the same critical adherence energy ($\Gamma \approx 2000\text{J.m}^{-2}$) no modification is observed on the maximal strain at rupture of the equivalent fibrils (ϵ_{max} in part 3.2). Hence, we can evoke that such effect would maybe correspond to the creation of a "real" equivalent fibril which would result in complete material deconfinement. Thus, the bulk cavities would be large enough to give birth to real tridimensional fibrils having a length close the material thickness (geometrical configuration of the thin PSA).

By focusing on these five parameters, we pointed out a regime change occurring in the foam PSA for an adherence of about 2000J.m^{-2} (with our backing). This change seems to be linked with the growth of bulk cavities which takes place when the material is loaded in large strains. Such a phenomenon appears at the scale of the microspheres but it affects the shape of the debonding region. In this section, we found a method based on our five parameters to point out this change. Recalling Villey et al. [78, 77] and Chopin et al. [13], the size of the debonding region for thin PSA decreases with the increase in adherence, we see that foam PSA behave as the opposite.

To sum up, we postulate the formations of "real" equivalent fibrils standing all over the material thickness for a sufficient adherence ($\sim$ 2000J.m^{-2}). In this configuration, the material continuum of the tape is lost and it can be assimilated as a compressible medium. A fingering model seems to describe well the new behavior of the foam PSA: the EFM (built in part 3.2). In such conditions, part 3.3 gave us the quantitative explanation that the dissipated energy is then piloted by the large strain non-linear rheology of the whole material (not only the rheology of the matrix).

4.1.2   Theoretical analysis

Analytical calculations

In order to justify from a theoretical point of view the transition observed in the previous part (see fig 4.5), we describe the shape of the debonding region on the sketch in the figure 4.8.
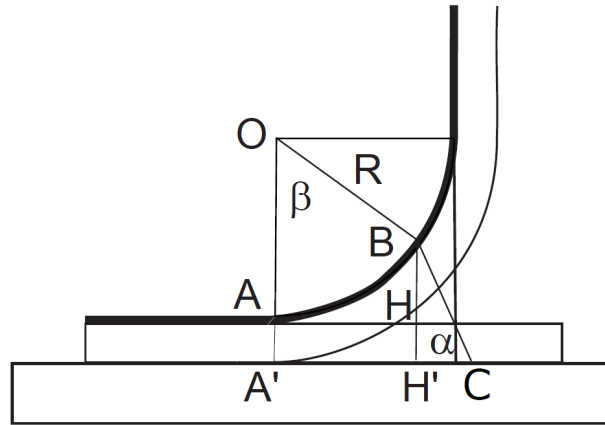
FIGURE 4.8: Schematic of the debonding region in a peel test at 90°

We can define two limiting cases:

- 1st case, for weak adherence the debonding region is small in front of the radius of curvature. In this case we can consider that the last fibril is vertical before the detachment. In this configuration the last fibril is BH'. Equilibrium equations give:

$$l \equiv AH \sim R sin(\beta) \tag{4.2}$$

$$a_f - a_0 \equiv BH \sim R(1 - cos(\beta)) \tag{4.3}$$

$$\frac{EI}{R} \sim FR - b\sigma_0 l^2 \tag{4.4}$$

$$\frac{F}{b} \sim \sigma_0(a_f - a_0) \tag{4.5}$$

When $l \ll R$ we can use the approximate relationship $R(a_f - a_0) \sim l^2$. The two terms on the right of equation 4.4 have the same scaling and their difference will have the same scaling too. The radius of curvature will thus be determined by the Euler equation:

$$R = \sqrt{\frac{EI}{F}}$$

as already described in part 4.1.1.

Considering equation 4.3, when the adherence increases, the observed increase of a_f leads to an increase of the angle β, which tends to 90° leading to the loss of validity of this first model based on weak adherence.

- 2nd case, for strong adherence the debonding region increases in size and l was observed to saturate at the maximum fibril extension $a_f - a_0$. This effect can be modeled by considering that the curvature of the backing becomes dominated by the tension force exerted by the adhesive in the debonding region.

If we focus on the backing layer only (black on fig 4.8), the elastica model gives:

$$EI\frac{d\alpha}{ds} = M \tag{4.6}$$

$$\frac{d\vec{M}}{ds} = -\vec{T} \wedge \vec{t} \tag{4.7}$$

$$\frac{d\vec{T}}{ds} = -\vec{q} \tag{4.8}$$

where $\vec{T}$ is the force transmitted through a section of the tape and $\vec{q}$ is an external force per unit length (along the tape).

Considering that the peel force turns at 90° with the backing describing an arc circle under the action of the stress σ_0 applied all along the debonding region, the third line equation gives:

$$\frac{d\vec{T}}{ds} = \frac{T\sqrt{2}}{R\frac{\pi}{2}} \sim \frac{F}{R} \sim \frac{\sigma_0 bR}{R} \tag{4.9}$$

hence,

$$R \sim \frac{F}{b\sigma_0} = a_0\epsilon_f \tag{4.10}$$

In this high adherence regime, the radius of curvature departs from the Euler equation and tends to follow the maximum fibril extension $a_f - a_0$, which slightly increases with the adherence.

Alternatively, this can be interpreted by using the Laplace law on the bent part of the backing. It results in:

$$\frac{\gamma}{R} = \Delta P \tag{4.11}$$

Considering the geometry of the system, we have then the same result:

$$\frac{F/b}{R} = \sigma_0 \quad \Rightarrow \quad R = \frac{F}{\sigma_0 b} \tag{4.12}$$

From equation 4.14, we use the saturation condition on R to deduce:

$$\frac{F}{b} = a_0\sigma_0\epsilon_f \tag{4.13}$$

In order to determine the condition of transition between these two regimes we should evaluate the relative importance of the bending energy and the traction stress acting on the debonding region.

$$FR << b\sigma_0(a_0\epsilon_f)^2 \tag{4.14}$$

$$\sqrt{FEI} << b\sigma_0(a_0\epsilon_f)^2 \tag{4.15}$$

$$\sqrt{EIa_0\sigma_0\epsilon_f b} << b\sigma_0(a_0\epsilon_f)^2 \tag{4.16}$$

$$\sqrt{Eh_b^3} << \sigma_0^{1/2}(a_0\epsilon_f)^{3/2} \tag{4.17}$$

$$h_b << \left(\frac{\sigma_0}{E}\right)^{1/3} a_0\epsilon_f \tag{4.18}$$

Theoretically, this relationship captures in scale laws the transition observed.

Static FEM calculations

We saw that focusing on the geometry of the backing allowed us to find this transition regime. Now we will explain it. Previously, we pointed out one plausible origin: the material deconfinement. During the peel test, we already highlighted the decohesion between the hollow glass microspheres and the matrix, which is likely to occur as the strain in the debonding region increases. In part 3.1, we concluded that debondings lead to a material

structure change which seems to orientate along a tension direction driven by backing adhesive load transfer. During this stage, the formed bulk cavities grow which changes the structure of the adhesive. From being an incompressible material in its unloaded state, it becomes more and more compressible during the loading (part 4.1.1). We evaluate the relevance of this hypothesis by computing a finite element model (FEM) describing the effect of changing the compressibility during the peel test. The goal was to point out the transition observed in the figures 4.2, 4.4 and 4.5. In practice we model the material in a quasi-static peel loading without crack propagation. Such an assumption considerably reduces the model complexity.

In Chapter 2 and Chapter 3, the material behavior has been extensively studied. To recall, the foam PSA have a hyper(visco)elastic behavior with damage. So, to make FEM simpler, we neglect the time-dependent phenomena and reduce the problem to the debonding region deformation prior to the crack propagation. To focus only on mechanisms occurring due to compressibility changes, we use the simplistic Neo-Hookean law, widely-used for hyperelastic material. Thanks to this model, we evaluate the impact of changing the material compressibility. In practice, changing the compressibility in a Neo-Hookean model regards the volumic term of the energy density, D. In this model, the energy is computed as follows.

$$U = C_{10}.(I_1 - 3) + \frac{1}{D}.(J^{el} - 1)^2 \tag{4.19}$$

The more D is small, the more the material is sensitive to an infinitesimal volume change. Hence, the higher D is, the more compressible the material is. We go from a quasi incompressible material (D very small) and we fixed arbitrary $D = 100$ which defines a highly compressible material (ν well below 0.49) . We compute FEM calculations based on the peel test at $90°$. The goal here is to observe how the change in compressibility affects the the shape of the debonding region of the foam PSA (see figure 4.9).

Shapes in FEM and in the real test are then compared. We observe that triggering the compressibility of the material (i.e. triggering Poisson's ratio ν) changes the shape of the debonding region as it happens in the real case. These two images regard the two regimes observed previously: one belongs to the $\frac{e}{r_c}$ linear like regime and the other to the $\frac{e}{r_c} = 0$ regime. Such results support the relevance of a compressibility change during the peel test in our material. When we increase the deformation, compressibility increases. This phenomenon is captured by the geometrical parameters above (see part 4.1.1). Deconfinement increases compressibility which makes the self orientation of the debonding region easier. This regime (for Γ above 2000J.m^{-2}) where the material is straightly oriented corresponds to the EFM validity domain presented in Chapter 3. This configuration represents a situation where all the thickness of the material is highly stretched. Hence, based on Chapter
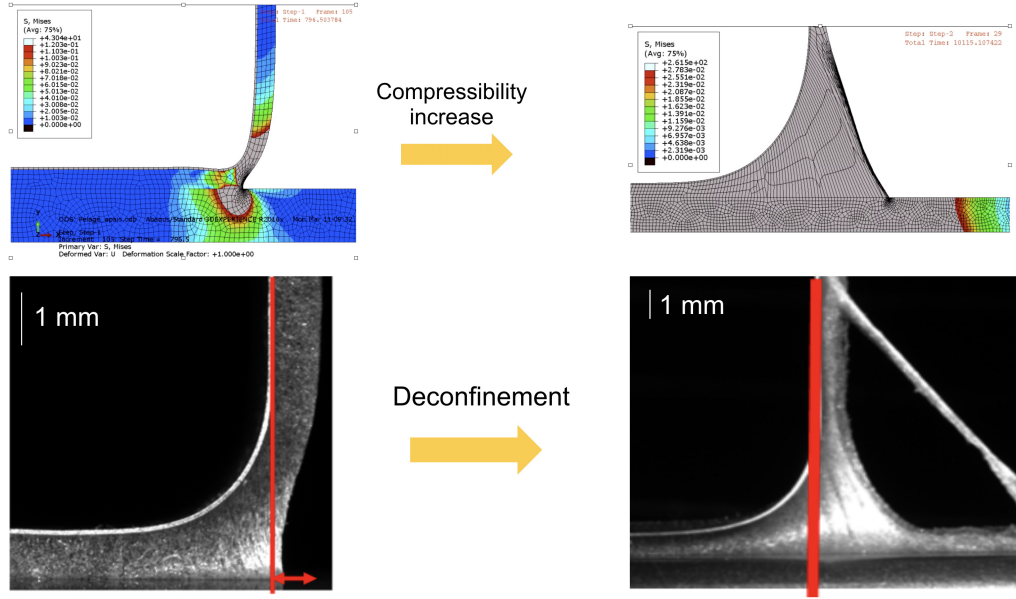
FIGURE 4.9: The two figures on the top describe FEM calculations carried out for two cases. On the left the material is supposed to be quasi-incompressible. On the right the material is highly compressible. In both calculations, a peel test with similar experimental conditions is performed. The two photographs on the bottom correspond to real situation where adherence is low (left) and adherence is high (right).

3, it means that the main dissipative mechanisms are activated all through the thickness. The foam PSA detachment is piloted by the maximum equivalent fibrils extension $\epsilon_{rupture}$ (see part 3.2).

4.1.3   Debonding region shape when triggering the PSA substrate interfacial adhesion

In the part 4.1.1, we have pointed out the singularity created by a deconfinement of the foam PSA. This major result of the PhD has been then demonstrated by the theory and FEM calculations (part 4.1.2). However, one limit subsists. The studied range of adherence does not take into account very small and very high adherence energy levels. To extend our research on these particular domains, we trigger interfacial adhesion. We use the silanization technique depicted in part 2.3. Those tests completed our data-sets on the evolution of the geometrical parameters presented above.
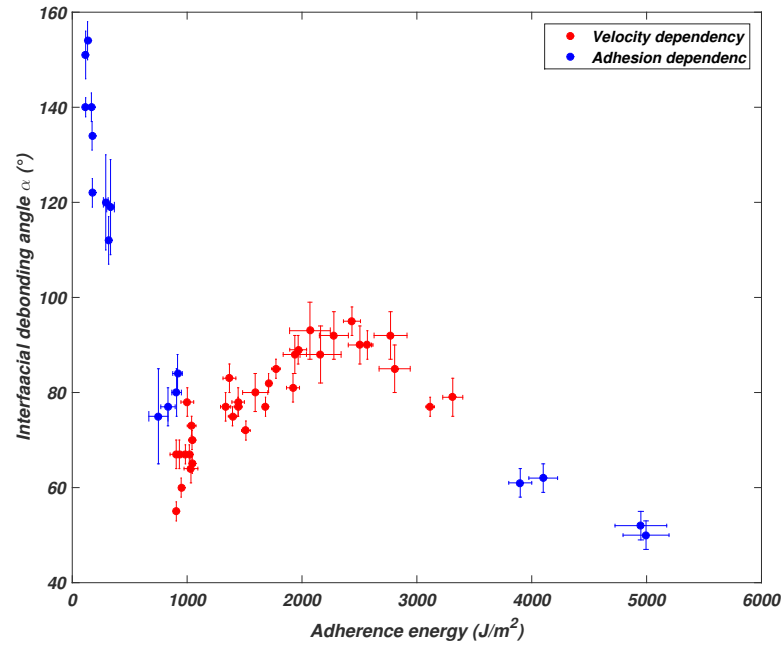
FIGURE 4.11: Interfacial debonding angle α measured in triggering the peeling velocity (in red) and substrate surface chemistry (in blue) with respect to the adherence energy
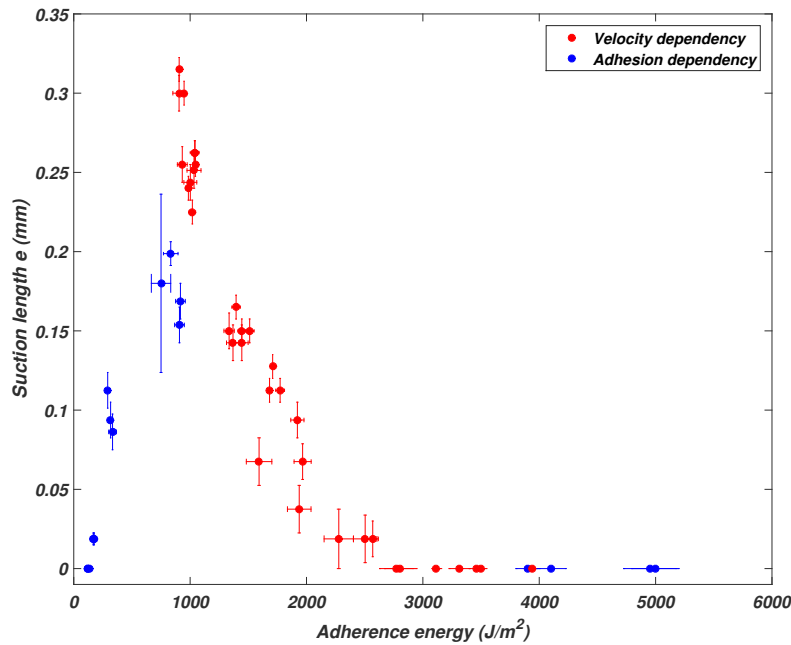
FIGURE 4.10: Suction length measured e in triggering the peeling velocity (in red) and substrate surface chemistry (in blue) with respect to the adherence energy

When reaching very high adherence we observe on figure 4.10 that the suction length goes to zero. Such behavior is easily explained by the total
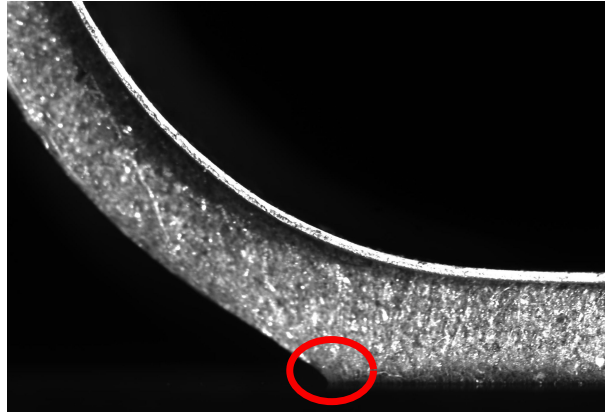
FIGURE 4.12: Peel test at 90° for a weak adherence case.

deconfinement of the material (see part 4.1.1). More intriguing is the decrease observed for weak adherence. This decrease occurs at $\Gamma \approx 1000\text{J.m}^{-2}$. No suction can be observed. This adherence energy (value depending on the backing choice) accounts for a second transition regime. This behavioral change is also observed on figure 4.11, with the evolution of the interfacial debonding angle. Around 1000J.m^{-2}, the angle starts to increase dramatically. From this point, when adherence decreases, distinguishable interfacial debonding angle is confounded with the material angle. We can no longer measure the interfacial debonding angle. A singularity seems to exist (see figure 4.12) at the interface where all the deformation remains localized (red circle). This transition allows to capture the instant where a singularity tends to overcome bulk dissipative processes (see figures 4.10 and 4.11).

The emphasis is now laid on capturing this transition thanks to the other geometrical parameters evolution with respect to the adherence energy. Results are presented on figure 4.13.
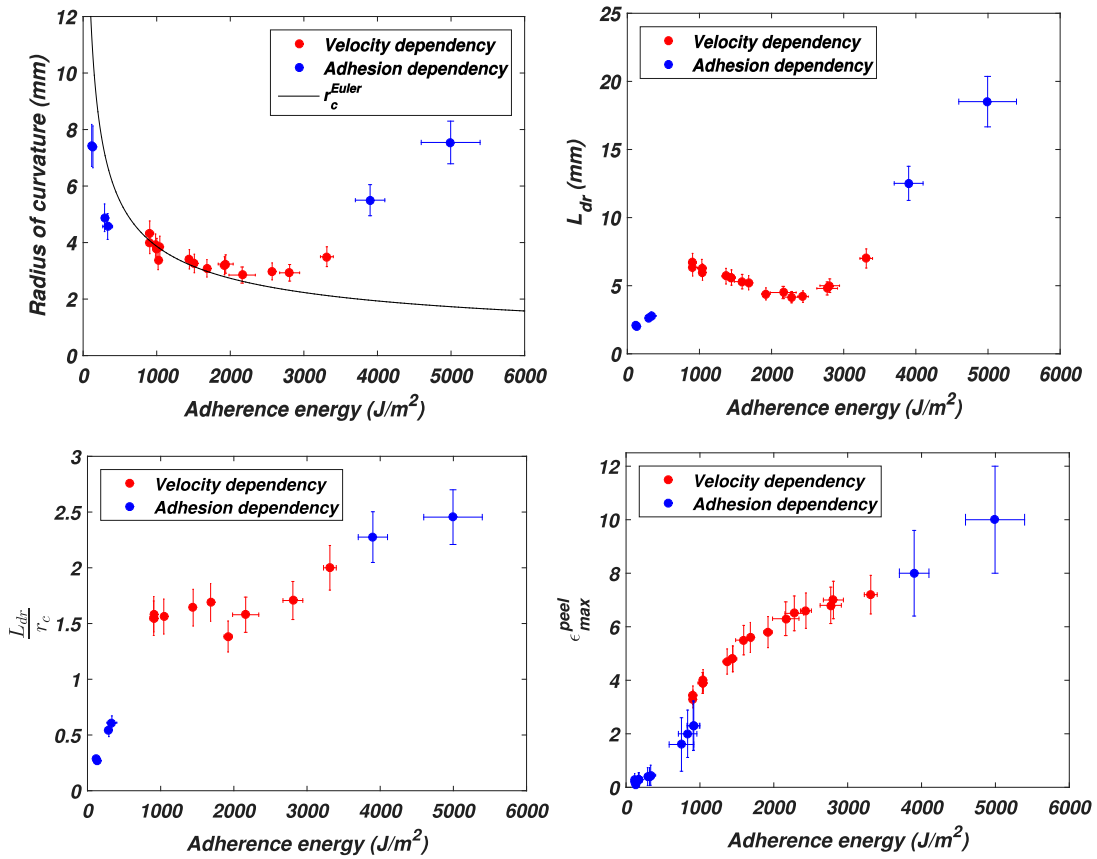
FIGURE 4.13: Radius of curvature r_c, debonding region length L_{dr}, ratio $\frac{L_{dr}}{r_c}$, maximal extension ϵ_{max}^{peel} evolutions with respect to the adherence energy. Peelings at $90°$ in triggering the peeling velocity (in red) and substrate surface chemistry (in blue).

On the top left graph of the figure 4.13, we observe that the radius of curvature of the backing decreases until the deconfinement at 2000J.m^{-2}. Interestingly, it is not affected by the singularity transition at 1000J.m^{-2}. We also observe that this parameter follows the elastica prediction given by the equation 4.1 for small adherence. This prediction describes the case where the curvature of the backing is only due to the peel force. There is no contribution of the dissipative region in its bending. This finding supports the idea that, for small adherence, debonding dissipative processes can be assimilated to a small region close to the debonding front propagation (singularity based model). In this approach, the amount of energy dissipated is limited by the small size of this region.

On the top right graph of figure 4.13, the debonding region length seems to increase until the first transition at 1000J.m^{-2} and then decreases until the second transition at 2000J.m^{-2}. Such evolution can be explained by the development of bulk mechanisms (see sphere matrix debondings in part 3.1). This development creates another dissipative region, in addition to the singularity of small strain, which initiates in the bulk and grows throughout the

all material thickness. We can see the domain between the two regimes (between 1000J.m^{-2} and 2000J.m^{-2}) as similar contributions of the singular and the bulk mechanisms on the debonding region shape. At the second transition the contribution of bulk mechanisms becomes dominant and drives the increase of the debonding region length thanks to fibrillar structure elongation.

This competition between interfacial singular phenomena and bulk mechanisms is also observed on the bottom left graph of figure 4.13. Between the two transitions, The ratio $\frac{L_{dr}}{r_c}$ stabilizes. Here, we see the debonding region length value as the contribution of the bulk mechanisms on the debonding region shape. For this adherence range, we see the radius of curvature as the contribution of the peel force on the debonding region shape. Hence, this stabilisation wcould reasonably account for the similar contribution of each mechanisms.

The last parameter regards the maximal extension of equivalent fibrils in the peel test (see bottom right on figure 4.13). Here, no special influence of one transition or the other is reported. This mostly come from to the validity domain (only after the second transition) where we can actually talk about equivalent fibril existence.

To go further in investigating the link between the debonding region shape and the adherence energy, we evaluate in the next section the relevance of those observations when the adherence energy varies due to substrate contamination and material damage.

4.2   Tape repositioning industrial issue

Tape repositioning has been found as being a relevant and straightforward method to randomly contaminate the substrate and to randomly damage the bulk of the foam PSA. The idea is here to use these effects to expand our conclusions regarding the relationship existing between the morphology of the foam PSA dissipative region and the aadherence energy.

4.2.1   Description of the industrial issue

In its mass production oriented system 4.14, Group Renault faces a particular problem regarding bonding application: tape repositioning. Indeed, when a part is not properly aligned or not in the correct location, the part (and so the tape) must be debonded form the car. The question underlying this section is to observe and to explain how repositioning affects the adherence of the foam PSA.

FIGURE 4.14: Operator on a production line bonding letters
onto a trunk

In these applicative processes, misalignment can occur. In such cases, the aesthetics of the car is irremediably affected. In the case of sensor bondings, the issue is even more dramatic. A misalignment can result in inaccuracies when scanning the car environment. In the framework of the autonomous vehicle, that kind of error is likely to be lethal. Alignment is then of prime interest. That is why repositioning protocol was introduced in best practices of factories. However, we had an hint based on internal reports concerning the impact of such an operation on the adhesive performance. Our question is thus simple. **Can we re-bond a tape which has already been debonded from a substrate without performance losses?**

4.2.2 Impact of repositioning a foam PSA on its adhesive performance

In order to answer the question detailed above, we develop a straightforward experimental strategy based on the peel test at 90°. As repeatable substrates, we use the glass slides treated according to the protocol detailed in part 2.3. The debonding velocity is set at 1mm.s^{-1}. The test campaign consists in performing many peel tests using the same tape on the same substrate. First results are shown on the figure 4.15.
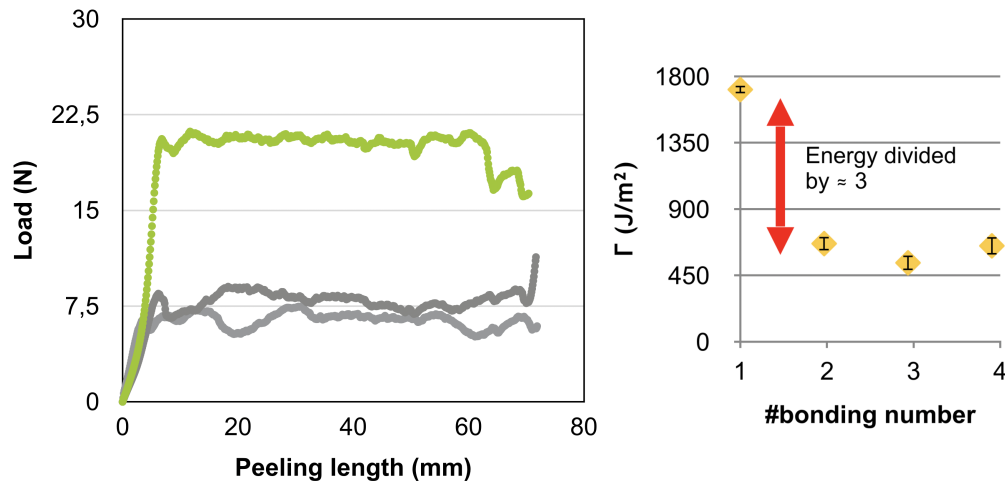
FIGURE 4.15: On the left graph, peeling results obtained for the three first bonding/debonding cycles. In green is the first test and in grey are the two others. On the right graph, adherence energy reached during the peel tests with respect to peeling number

As a clear answer, repositioning a foam PSA alters considerably the adherence performance. So, a second question pops up: where does the adherence decrease come from?

4.2.3 Looking at an industrial issue through a researcher's eye

To answer the previous question, we establish a strategy to isolate the origin of the adherence decrease. Firstly, we carry out cyclic bonding debonding peelings where we use the same substrate for the tests but take a new PSA sample for each new bonding. Hence, we only observe modifications due to potential substrate surface changes, which we will call an extrinsic source of adherence decrease. Secondly, we focus on changes which could occur within the bulk of the tape itself. To do so, we carry out cyclic bonding debonding peelings where we use the same PSA sample but take a new glass slide for each new bonding. This source of adherence decrease will be called intrinsic.

For the first test campaign (extrinsic source of adherence decrease), we observe that, on average, 1.4 of the overall adherence energy is lost between the first and the second test (see figure 4.16).
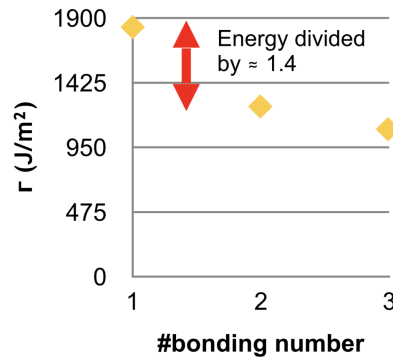
FIGURE 4.16: Adhesion energy as a function of repetition number of peel tests. This effect is ascribed to surface contamination.

We have repeated the experiments for various velocities. The results are shown in figure 4.17.
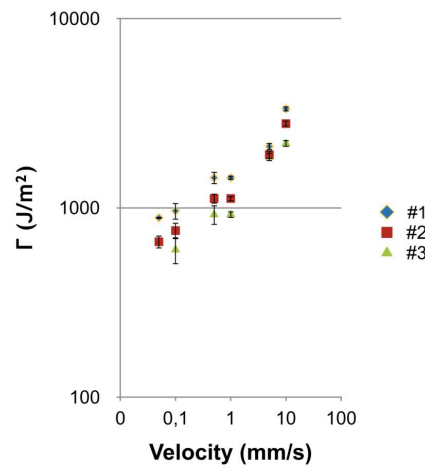
FIGURE 4.17: Adhesion energy as a function of repetition number over a two decades of peeling velocities

According to these results, we are convinced that something is taking place at the interface between the tape and the substrate during the first debonding. With the naked eye, no traces of surface modifications can be seen (adhesive failure). SEM was used to go at a lower scale. The obtained images are presented below on the figure 4.18. They show locations at the edge of the area of application of the tape after it has been peeled off.
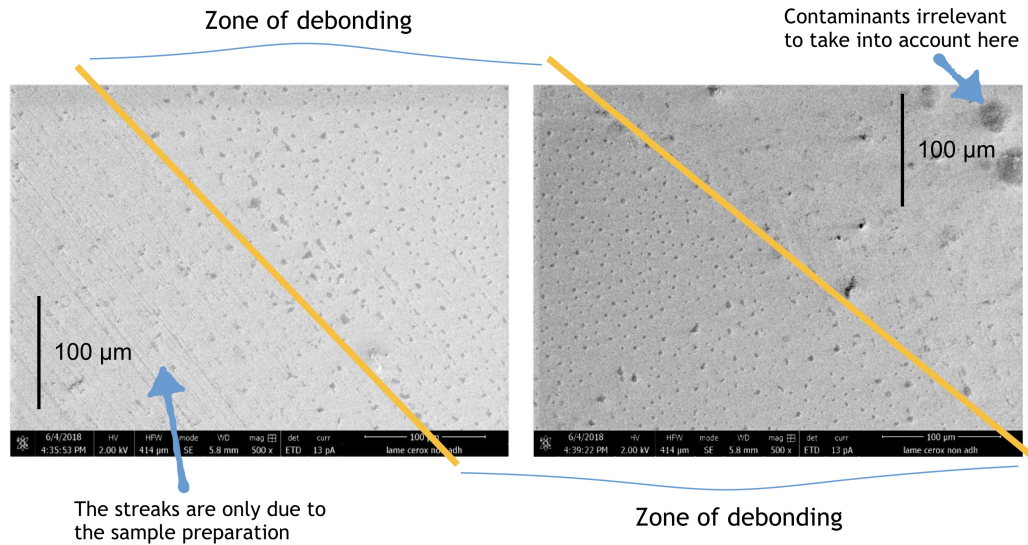
FIGURE 4.18: SEM observation of the substrate surface after debonding. The zone of debonding corresponds to the area where the foam PSA was peeled off.

On the images from the figure 4.18, contamination of the substrate is explained by small dots having a diameter around 2 to 3 micrometers which remain on the surface after the first peeling. To characterize them, EDX has been useless because of the minute area effectively covered by the contamination. However, due to the aspect, we can think that pollution dots are made of polymeric material coming from the matrix. On some dots, we also distinguish bean shapes. Such a particular shape reminds us of the morphology of the TiO_2 nanoparticles (see figure 4.19). This explanation sounds reasonable knowing that a certain amount of TiO_2 particles is added to foam PSA to color them (see Chapter 2). A plausible explanation of those small material deposition could be the presence of the microspheres close to the interface. If we recall the image from figure 3.3, we see that cavitated material configuration will change the local confinement of the matrix at the interface. This situation is described on figure 4.20. We observe (left image) the surface of the foam PSA when it debonds in a tack test. We see (see part 3.1) that most of the microspheres close to the interface debond. As a consequence, the material close to the interface is cavitated. This configuration is reported in the schematic (right image) where we represent a section of the adhesive close to the interface. The orange arrows represent the loading of the probe tack test. In white, we present two typical cavities close to the interface which grow following the sphere matrix debonding. We can observe that this process creates narrow material regions between the cavity and the interface (highly confined). Such highly confined regions remind us of a thin PSA loading case. During debonding, these small regions are likely to fibrillate. The observed dots could be then the feet of those fibrils after debonding.
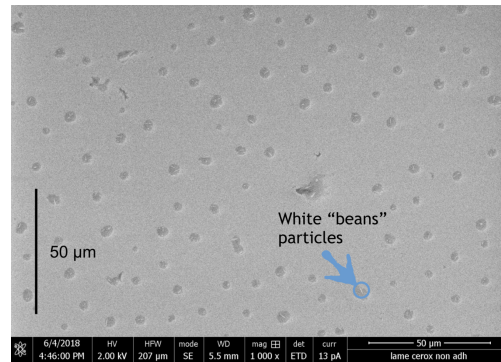
FIGURE 4.19: SEM observation of the contaminated surface. Zoom in the dots with the "beans" particles.
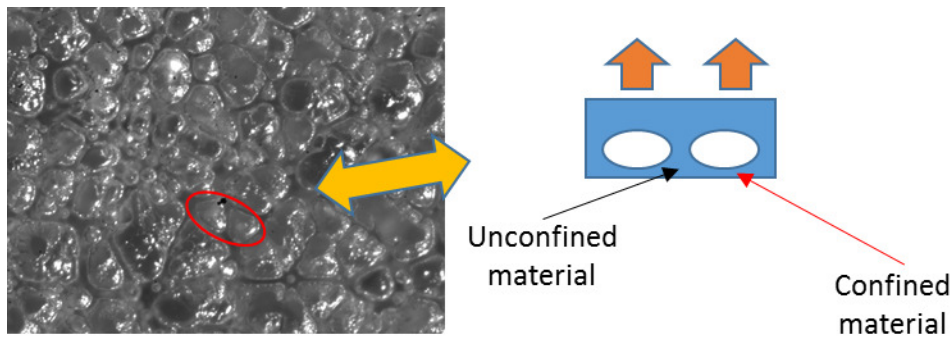
FIGURE 4.20: Local geometrical confinement change due to internal cavitations of the hollow glass microspheres close to the interface.

So, the first cause for the adherence decrease we bring to light is extrinsic. It consists of a contamination at the microscale of the substrate surface by the adhesive itself. It accounts for approximately 40% of the total adherence loss.

For the second test campaign (intrinsic source of adherence decrease), we perform bonding debonding peelings with the same tape but we take a new substrate for each new debonding. The results obtained are presented in the figure 4.21.
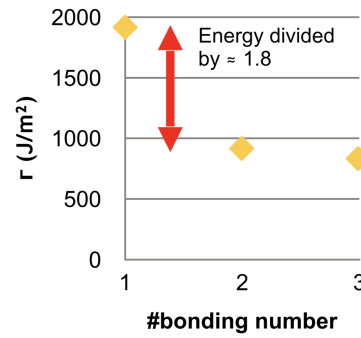
FIGURE 4.21: Impact of the tape bulk damage on the adherence
energy level

In that case, we observe an average adherence energy decrease of 1.8.
This coefficient of 1.8 is interesting because it accounts for approximately
60% of the total adherence energy decrease. Multiplied by the 1.4 found for
the surface contamination effect, we almost reach the coefficient 3 measured
for the overall adherence loss. As mentioned previously, we extended the
experiments over two decades of peeling velocities. On the graph from the
figure 4.22, we can clearly observe that the loss is not rate dependent.
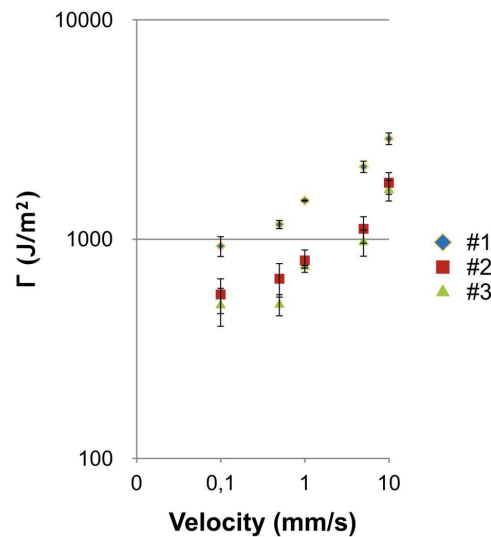
FIGURE 4.22: Adherence energy as a function of the peel ve-
locity for three successive experiments with the same tape on
three fresh substrates. The strong decrease between exp 1 and
exp 2 demonstrates the impact of the material damage during a
peeling at 90°.

These results highlight damage occurring in the material itself. Based on
the conclusions of the part 3.1.2, we could ascribe damage to sphere rupture.
However, for the adherence energy reached in these tests, the deformation
in the bulk of the material never reaches a large enough level to observe
a lot of spheres breakage. In addition, optical microscopic observations of
the samples after the peeling tests never end up with broken glass spheres

views. A second explanation could be the softening effect studied in 3.1.2. Deformation level to reach to activate this effect is easily met in the peel experiments. Such effect would consist of an interfacial adhesion change between the spheres and the matrix. After the first debonding, most spheres are debonded. However, after the first cycle, the sphere matrix interface has to reform. This reformation would result in a lower interfacial adhesion (see figure 3.13).

Following the same experimental protocol as for the second peel test campaign (same tape peeled many times on a new substrate for each debonding), we now heat the peeling sample (adhesive + backing) at 80°C for 15 minutes between each peeling and let it cool down to room temperature. Once the sample has the right temperature, we bond it before carrying out the next peeling.
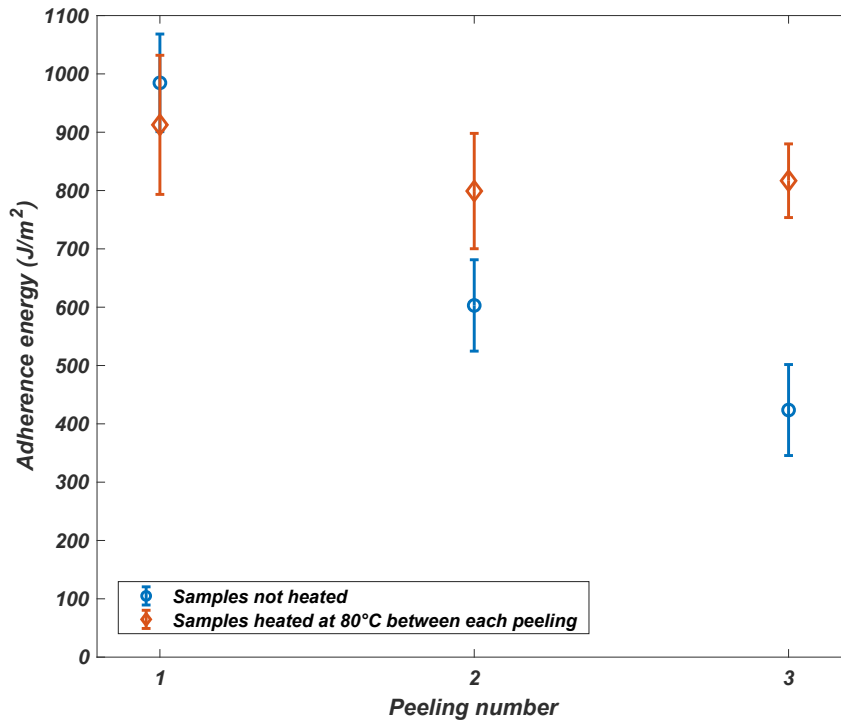
FIGURE 4.23: Induced healing by heating peeling samples before rebonding it

On the graph of the figure 4.23, we observe that heating the sample greatly helps to recover the performances. This observation convinces us to consider the softening effect due to sphere matrix debonding as the main origin for the internal damage observed in peeling foam PSA. However, this effect can be eliminated if we we dope the sphere matrix interfacial reconstruction by heating the peel sample before repositioning.

Based on the two identified kinds of adherence losses, we can now provide insdustrialists with a more robust repositioning protocol. We saw that such a decrease firstly comes from substrate surface pollution by the PSA polymer itself. To address this issue, we found out that isopropanol (IPA), which is contained in wipes used by operators in automotive production lines, is a good solvent for the PSA matrix. So, the first solution is to clean the substrate thoroughly (here the body of the car) before the second bonding. This first step saves approximately 40% of the adherence energy. Then, we highlighted the softening effect occurring in the PSA bulk. Softening can be lower in inducing material healing by heating it at 80° prior to rebonding it. This second step saves approximately 60% of the adherence energy.

Thanks to these two test campaigns, the two main causes have been well identified. One is extrinsic: **the substrate surface pollution** and one is intrinsic: **the PSA internal damage**. Such an identification is not only an added value in the understanding of foam PSA functioning, it also paves the way to build a more robust industrial protocol to reposition parts without adherence energy loss.

4.2.4 Debonding region shape after the foam PSA repositioning

As we detailed previously, basic tape repositioning lower the adherence energy. Adherence decrease comes from a substrate surface contamination and a material damage. The question which pops up now is: Does these adherence variations can affect the debonding region shape? Thanks to the parametric study conducted in part 4.1, we analyse the evolution of the morphology of the debonding region with respect to the adherence. We study separately adherence variations due to contamination effect and adherence variations due to material damage. Parameters evolutions are represented in the graphs from the figures 4.24 and 4.25.

Interestingly, all results seem to collapse on same curve than the one found in the part 4.1.3. Such result is of prime interest since it shows that the link between the foam PSA debonding region morphology and the adherence seems to remain the same whatever the source of the adherence triggering is.
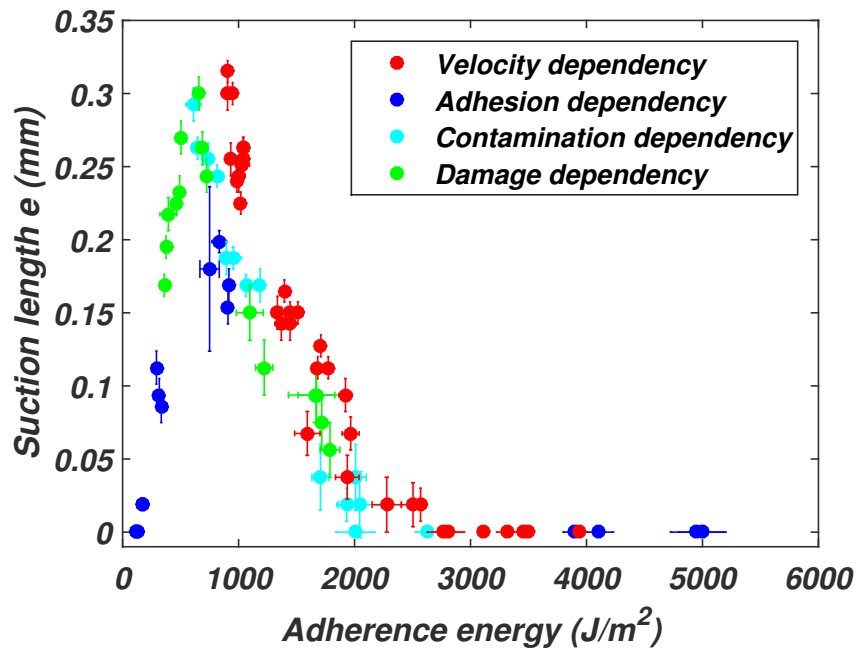
FIGURE 4.24: Suction length e measured in triggering adherence energy thanks to the peeling velocity (in red), substrate surface chemistry (in blue), the substrate surface contamination (in cyan) and using damaged adhesive (in green)
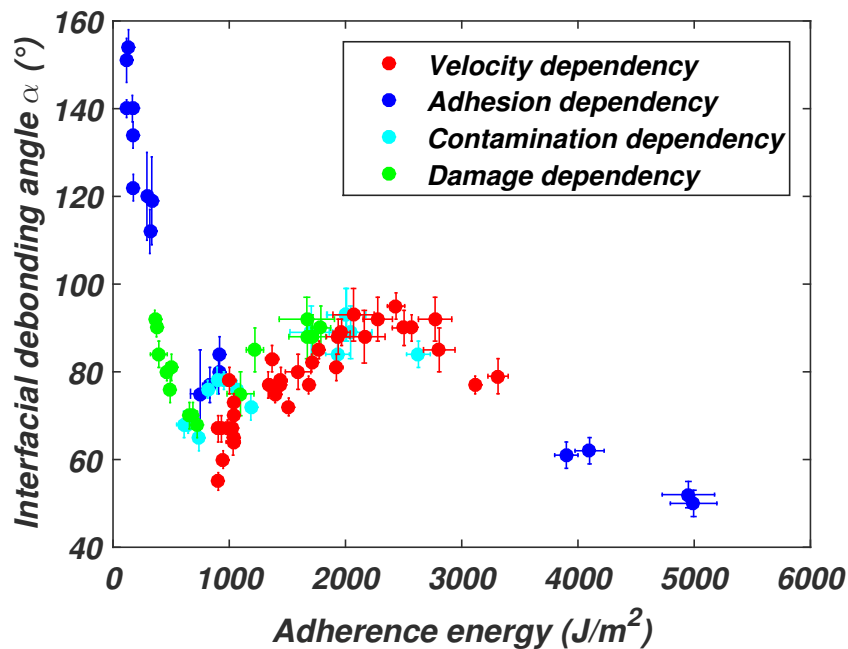
FIGURE 4.25: Interfacial debonding angle α measured in triggering adherence energy thanks to the peeling velocity (in red), substrate surface chemistry (in blue), the substrate surface contamination (in cyan) and using damaged adhesive (in green)

4.3 Conclusion

The goal of the Chapter 4 was to quantitatively link the debonding region shape and the foam PSA performance. Recently, Barrios et al. [8] hinted such a link for classic thin PSA. We started by defining five geometrical parameters to study the evolution of the debonding region morphology during peelings. Three parameters are commonly found in the literature: the radius of curvature of the backing, the maximal fibril extension, the debonding region length. One was proposed by Barrios et al. [8], the interfacial debonding angle. We propose the last one specifically for the foam PSA: the suction length. Variations of these parameters with respect to adherence energy allowed us to distinguish one main transition regime (≈ 2000J.m^{-2} for our backing). It corresponds to the point where the bulk of the foam PSA is deconfined by the strain induced by the debonding. Thus, a fibrillating equivalent system takes place (captured by the *Equivalent Fibril Model* (EFM). As a consequence, a larger amount of energy can be dissipated throughout all the material thickness and higher adherence levels can be reached. This confinement transition was explained by theoretical and FEM calculations. To support our interpretation, we note that this transition fits well with the validity domain of the EFM. Regarding dissipation process, we can reasonably said that it corresponds to the point where bulk mechanisms mostly dominate the overall energy dissipation process. Thanks to our study, we also identified another transition point (≈ 1000J.m^{-2}) in foam PSA behavior. When adherence decreases, this second transition corresponds to the point where bulk mechanisms are weakly activated (bulk deformation is light) and so, easily dominated by local PSA substrate interfacial dissipative region. Most of the dissipation is made in a region close to the interface. This configuration is close to a singularity based model in fracture mechanics. We explored a so wide adherence energy range by triggering separately the peeling velocity and the substrate surface chemistry. Both protocols generate results collapsing on the same curve. Hence, the morphology of the debonding region shape in the foam PSA seems to be driven by the adherence energy.

To broaden our study of the debonding region shape, we then emphasized how the debonding region (and so the adherence) is affected by the repositioning process. First results pointed out a catastrophic influence of the bonding debonding cycles on the adhesive joint performance. Adherence energy is divided by three after the first cycle. We highlighted two causes to explain that. Firstly, $\approx 40\%$ of the energy is lost due to a contamination of the substrate by the foam PSA itself. This contamination consists of small dots (1 to 3μm diameter made of acrylate polymer and TiO$_2$ nanofillers) which stays on the substrate after the foam PSA debonding. Secondly, $\approx 60\%$ of the adherence loss comes from damage of the bulk of the foam PSA. During the debonding, the material is highly stretched which debonds the microspheres from the matrix (see the pseudo Mullin's effect in conclusions of Chapter 3). Hence, when the adhesive is deformed during the second debonding, it

deforms more easily and dissipates less energy. As a matter of fact, the adherence decreases. Both of these two effects are not rate dependent. Based on these results, we then built a repositioning protocol to overcome these two troublesome phenomena. For peel tests, with low adherence levels due to random substrate surface contamination or random material damage, we observed a collapse of the geometrical parameters evolution on the same curves than the ones from part 4.3. Such observations have to be taken cautiously but they hint interesting perspectives. Anyhow, they support our idea that the debonding region shape in the foam PSA seems to be driven by the adherence energy.

Chapter 5

Conclusions and perspectives

The main objective of this PhD was to explain how foam PSA for automotive applications dissipate energy during the debonding. When studying PSA, the keystone is energy dissipation. Since the early stages of the research on adhesion, understanding energy dissipation has been crucial. Phenomenological and rheological approaches have provided us with results that form the basis for this work. Furthermore, the recent advances in fracture mechanics applied to soft matter brought new tools to assimilate debonding situations to material fracture. Regarding the field of PSA, the latest breakthroughs concerned classic thin tapes. Such materials are extremely thin ($\sim$ 10μm). However, researchers showed that the thickness was a critical point in the PSA adhesive performance. Being at least 100 times thicker ($\sim$ mm), foam PSA account for a perfect system to assess the relevance of extending current theories. Designed for high performances, such materials make it possible to cover phenomena occurring for a wide range of adherence energies. In this thesis, we have been then able to activate all types of dissipative mechanisms from very weak to very strong cases. It enabled us to characterize exhaustively material dissipation.

The context of this research was automotive applications. In this domain, bonding is gaining tremendous momentum as an assembly technique. Understanding quantitatively the adhesive problem is mandatory for industrialists to develop this technique. From a mass production oriented point of view, it enables to produce faster at lower costs. More specifically, numerous sensors in autonomous vehicles are attached onto the body of the car thanks to foam PSA. Quantitative explanations of tape functioning are then of prime interest for safety issues: understanding the debonding process to prevent rupture from occurring on cars.

Since foam PSA are much thicker than thin PSA, the first step was to understand the material structure. Characterization techniques like SEM, EDX or X ray μ-tomography, allowed us to describe the material structure as a syntactic foam architecture. Foam PSA are composite materials made of a polymer matrix and filled with hollow glass microspheres having a micrometric size. Even if the structure differs from thin PSA, foam PSA exhibit a similar small strain rheology. Such behavior is fundamental for the bonding process where adhesive substrate contact is formed. Although having a different mesoscopic structure, foam PSA follow the requirements provided by

the literature to adhere easily. The non-linear large strain regime exhibits a strong viscoelasticity that enforces the occurrence of dissipative mechanisms at several scales.

To study dissipative mechanisms during debonding, we based our research on two tests: the flat ended probe tack test and the peel test at 90°. Both tests were instrumented with an image recording systems to observe directly the development of dissipative mechanisms at the mesoscale ($\sim 100 \mu$m). To observe dissipative mechanisms occurring at a lower scales, we designed our own SEM in-situ tension test setup.

Our strategy led us to identify how foam PSA dissipate energy. During the debonding, if the interfacial PSA substrate adhesion is strong enough, we first observe sphere matrix decohesions in the neighborhood of the adhesive substrate interface. These decohesions engender cavities which grow due to the effect of high negative hydrostatic pressure. The latter depends on the material geometrical confinement. As the strains in the debonding region increase, we observe the same decohesion (sphere matrix) occurring all over the material thickness. Such a process results in material internal cavitation. The material becomes more and more compressible. Those bulk cavities grow which generates local micrometric fibril instabilities associated to the debonding front between the matrix and the spheres (figure 3.9). These instabilities are the consequence of the high stretch close to the local debonding front and the incompressibility of the matrix constituting the cavity walls. Those mechanisms contribute to the overall energy dissipation. Then, as the material is more and more loaded (high adherence cases), walls between cavities become thinner and thinner which develops a strongly oriented fibrillar structure through all the material bulk. At some point, this fibrillating process mostly controls energy dissipation. The adherence is then directly related to the extension of those fibrils. If the interfacial adhesion of the PSA substrate is large enough, cohesion fracture of the adhesive material may cause debonding.

To explain quantitatively the dissipative processes, we built a phenomenological model inspired by recent literature from the SIMM lab [78, 77, 13]. We called it Equivalent Fibril Model or EFM. EFM describes bulk fibrillation as the uniaxial extension of a single equivalent fibril throughout all the debonding region thickness. Dissipated energy is then the energy expended in the stretch of this virtual fibril up to the critical stretch of debonding. For foam PSA, the EFM described well the debonding process for high adherence. This result supports the description of the debonding region of foam PSA as being loaded in uniaxial tension for high adherence regime. In the EFM application domain, a quantitative explanation of the dissipation process was found in the non-linear rheological behavior of the material. Based on this understanding, we eventually proposed a method to transpose peel adherence results to probe tack adherence results.

To go further, we then explored the relationship between the shape of the debonding region and the adhesive performance. We developed a protocol to study the evolution of the debonding region morphology. This method is based on the description of the debonding region through five parameters. Three of them were already used in recent literature for office PSA where the debonding region generally consists of a set of straight stretched fibrils [78, 77] : the radius of curvature of the backing, the maximal fibril extension, the debonding region length. Two more parameters are introduced here in order to capture the peculiar behavior of foam PSA, which develop a more singular crack front behavior in the lower adherence regime (figure 3.7): the suction length and the interfacial debonding angle. Results highlighted a transition regime occurring for a defined adherence energy (here $\approx 2000 \text{J.m}^{-2}$ for our backing choice). This transition was explained theoretically by a change in compressibility in the bulk material. According to our conclusions on the dissipative process detailed above, this transition regime corresponds to the point where the fibrillating process mostly controls energy dissipation in the tape. This transition matches with the beginning of the EFM validity domain. Through in-situ measurements, we can now detect this behavior change. Extending our study to weak adherence energies, we identified another transition for a lower adherence (here $\approx 1000 \text{J.m}^{-2}$ for our backing choice). This other particular regime corresponds to the transition where bulk mechanisms are dominated by the local PSA substrate interfacial dissipative region.

In terms of fracture mechanics, we proposed to see foam PSA debonding for low adherence energies as a singularity based problem. All the dissipative mechanisms remain limited to a small region close to the interfacial debonding front between PSA and substrate. This vision remains the more pertinent until a first transition (estimated at 1000J.m^{-2} for the chosen backing). Then, when adherence increases, bulk mechanisms are little by little activated through the whole thickness, which forms a bulk dissipation region. When the bulk dissipation is large enough, we observe a second transition regime (estimated at 2000J.m^{-2} for the chosen backing). The large strain model of the figure 1.12 can then be applied, and more specifically the viscoelastic foundation approach as in the classic thin PSA. After the second transition, the bulk effect takes over the singularity, but the latter remains. This makes foam PSA a very interesting model material for understanding the debonding of soft and dissipative materials. It goes from a singular fracture approach to a large strain viscoelastic foundation model by simply triggering peeling velocity or substrate surface chemistry.

Eventually, we studied the effects of the debonding process on both the tape and the substrate by focusing on the performance of the adhesives after repositioning. When repositioned onto glass substrates, foam PSA lose $\approx 40\%$ of adherence due to substrate contamination and $\approx 60\%$ due to bulk damage. Contamination is made of polymer residuals coming from the tape. Cleaning substrate with isopropanol removes the contaminants. Damage

comes from a pseudo Mullin's effect related to the debonding of the microspheres from the matrix in the bulk of the tape. Heating the sample before repositioning induces healing and eliminates most damage effects.

Although the initial purpose of those spheres is mainly economic, they account for a relevant part of the overall tape energy dissipation. They force the material to dissipate energy. This is the first time that such effect is elucidated in a PSA.

Even if the foam PSA have a particular structure (syntactic foam), latest advances in the modeling of the debonding region of thin office PSA can be extended in the high adherence regime (after the second transition). We made this extension thanks to the EFM construction. We quantitatively described energy dissipation in this regime by using the rheological approach of Chopin et al. [13].

However, this project also suffered from some limitations. The biggest one concerns our single type of sample. The generalization of the results to other systems with the same structure would have been relevant. This limitation was due to contract terms with the industrial partner. Samples without microspheres or with a different volume ratio would have been a panacea to decouple mechanisms.

Another limitation comes from the differences observed in the Transposition peel tack Model (TM). Although we found a quantitative method to transpose results in adherence, maximal fibril extensions follow opposite trends. This point still remains puzzling for us. It is one of the main orientations to guide future research on this topic.

Relevant future works should also focus on the transition to a more predictive approach to adherence. Going further in fracture mechanics, the idea would be to apply theoretical models according to the two identified debonding regimes (singularity and large strain viscoelastic foundation). More precisely, in the two regimes, the missing ingredient to complete the modeling is the physics of debonding at the smaller scales around the crack front. To a certain extent, this would lay the foundations for FEM calculations regarding debonding process. Thus, the main underlying objective is to build a robust model taking into account dissipative processes at all scales.

Appendix A

Classic use of adhesives in automotive

External applications

Internal applications

Appendix B

Influence of the high adhesive thickness on the stiffness of a peel sample

A peel sample is made with the adhesive and the backing. Carrying out a peel test can be assimilated to bend this multilayer beam in large strain. According to beam theory, bending moment of such a structure can be written as follow:

$$EI = \frac{b}{3}(E_{adhesive}h_{adhesive}^3 + E_{backing}h_{backing}^3) \tag{B.1}$$

$$EI = E_{backing}h_{backing}^3\frac{b}{3}(1 + \frac{E_{adhesive}}{E_{backing}}(\frac{h_{adhesive}}{h_{backing}})^3) \tag{B.2}$$

In our case, we have $E_{adhesive}$ = 350kPa, $E_{backing}$ = 70Gpa, $h_{adhesive}$ = 1.2mm and $h_{backing}$ = 127μm. Calculations give:

$$\frac{E_{adhesive}}{E_{backing}}(\frac{h_{adhesive}}{h_{backing}})^3 \approx 10^{-2} \tag{B.3}$$

Because it is very soft compared to the aluminum backing, the large thickness of foam PSA do not affect peel sample bending. It is only driven by the bending of the backing.

Bibliography

[1] Adhesive bonding. In M.J. Troughton, editor, *Handbook of Plastics Joining (Second Edition)*, pages 145 – 173. William Andrew Publishing, Boston, second edition edition, 2009.

[2] A.W. Adamson. *Physical Chemistry of Surfaces*. Wiley-Interscience, New-York, 1990.

[3] D.S. Ambwani and T. Jr. Fort. *Pendant drop technique for measuring liquid boundary tensions*. Plenum Press, New-York, 1979.

[4] E.H. Andrews and A.J. Kinloch. Mechanics of adhesive failure i. *Proc. R. Soc.*, 332:385–99, 1973.

[5] E.H. Andrews and A.J. Kinloch. Mechanics of adhesive failure ii. *Proc. R. Soc.*, 332:401–14, 1973.

[6] A. Aruniit, J. Kers, J. Majak, A. Krumme, and K. Tall. Influence of hollow glass microspheres on the mechanical and physical properties and cost of particle reinforced polymer composites. *Proceedings of the Estonian Academy of Sciences*, 61, 01 2012.

[7] H.T. Banks, S. Hu, and Z.R. Kenz. A brief review of elasticity and viscoelasticity for solids. *Advances in Applied Mathematics and Mechanics*, 3(1):1–51, 2011.

[8] C. Barrios. Anatomy of the deformation of pressure sensitive adhesives from rigid substrates. *PSTC Tech 40 papers*, 1, 2018.

[9] E. Bartholomew. Acrylic pressure-sensitive adhesives. *ASI Adhesives & Sealant Industry mag*, 09 2011.

[10] I. Benedek and M.M. Feldstein. *Technology of Pressure-Sensitive Adhesives and Products*. CRC Press, Taylor and Frnacis Group, 2009.

[11] A. Carré. *J. Coating technol.*, 54:31–35, 1982.

[12] A. Chiche and C. Creton. Cavitation in a soft adhesive. 03 2004.

[13] J. Chopin, R. Villey, D. Yarusso, E. Barthel, C. Creton, and M. Ciccotti. Nonlinear viscoelastic modeling of adhesive failure for polyacrylate pressure-sensitive adhesives. *Macromolecules*, 51(21):8605–8610, 2018.

[14] D. Choqueuse. *Experimental study and analysis of the mechanical behaviour of syntactic foams used in deep sea*. Thesis, 2012.

[15] J. Cognard. *Science et technologie du collage*. Presses polytechniques et universitaires romandes, 2000.

[16] W. F. Cooper and W. H. Nuttall. The theory of wetting, and the determination of the wetting power of dipping and spraying fluids containing a soap basis. *The Journal of Agricultural Science*, 7(2):219–239, 1915.

[17] C. Creton. Pressure-Sensitive Adhesives: An Introductory Course. *Materials Research Society Bulletin*, 28(06):434–439, 2003.

[18] C. Creton and M. Ciccotti. Fracture and adhesion of soft materials: a review. *Reports on Progress in Physics*, 79:046601, 2016.

[19] C. Creton and P. Fabre. Tack. In A.V. Pocius and Manoj Chaudhury, editors, *Adhesion Science Science and Engineering, Vol I : The Mechanics of Adhesion*, volume II, chapter 14, pages 535–576. Elsevier, 2002.

[20] C. Creton and L. Leibler. How does tack depend on time of contact and contact pressure? *Polymer Physics*, 34:545–554, 02 1996.

[21] C.A. Dahlquist. *Pressure-Sensitive adhesives. In Treatise on Adhesion and Adhesives*. Patrick, R.L. and Dekker, New York, vol. 2, p 219 edition, 1969.

[22] P. G. de Gennes. FRACTURE OF A WEAKLY CROSSLINKED ADHESIVE. *Compes-Rendus de l'Académie des Sciences Série II*, 307(19):1949–1953, December 1988.

[23] M. Defrancisis and Y. Liu. Characterization of pressure sensitive adhesives by rheology. *PSTC Conference*, PSTC 39 2016.

[24] W. Demarteau and J.M. Loutz. Rheology of acrylic dispersions for pressure sensitive adhesives. *Progress in Organic Coatings*, 27(1):33 – 44, 1996.

[25] C. Derail, A. Allal, G. Marin, and Ph. Tordjeman. Relationship between viscoelastic and peeling properties of model adhesives. part 1. cohesive fracture. *The Journal of Adhesion*, 61(1-4):123–157, 1997.

[26] J. Diani, B. Fayolle, and P. Gilormini. A review on the mullins effect. *European Polymer Journal*, pages 601–612, 2009.

[27] R.S. Drago, G.C. Vogel, and T. E. Needham. Four-parameter equation for predicting enthalpies of adduct formation. *Journal of the American Chemical Society*, 93(23):6014–6026, 1971.

[28] A.M. Dupré and P. Dupré. *Théorie mécanique de la chaleur*. Gauthier-Villars, 1869.

[29] J.G. Eberhart. *Trans. Met. Soc.*, 236:1362–1363, 1966.

[30] P. Elziere, C. Dalle-Ferrier, E. Barthel, C. Creton, and M. Ciccotti. Large strain viscoelastic dissipation during interfacial rupture in laminated glass. *Soft Matter*, 13, 01 2017.

[31] L. Flandin, A. Hiltner, and E. Baer. Interrelationships between electrical and mechanical properties of a carbon black-filled ethylene–octene elastomer. *Polymer*, 42(2):827 – 838, 2001.

[32] F. M. Fowkes. *Donor-Acceptor Interactions at Interfaces*, pages 43–52. Springer US, Boston, MA, 1980.

[33] F.M. Fowkes. *Treatise on adhesion and adhesives*. Marcel Dekker, 1967.

[34] K.N.G. Fuller and D. Tabor. The effect of surface roughness on the adhesion of elastic solids. *Proceedings of the Royal Society of London. Series A. Mathematical and Physical Sciences*, 345, 09 1975.

[35] C. Gay. Some fundamentals of adhesion in synthetic adhesives. In *11th International Congress on Corrosion and Fouling*, volume 19 (suppl.), pages 53–57, San Diego, United States, July 2002.

[36] C. Gay and L. Leibler. Theory of Tackiness. *Physical Review E*, 82(5):936–939, 1999.

[37] A. N. Gent and R. P. Petrich. Adhesion of Viscoelastic Materials to Rigid Substrates. *Proceedings of the Royal Society A: Mathematical, Physical and Engineering Sciences*, 310(1502):433–448, May 1969.

[38] A.N. Gent and J. Schultz. Effect of wetting liquids on the strength of adhesion of viscoelastic materials. *J. Adhes.*, 3:281–294, 1972.

[39] N. J. Glassmaker, C.Y. Hui, T. Yamaguchi, and C. Creton. Detachment of stretched viscoelastic fibrils. *The European Physical Journal E*, 25(3):253–266, Mar 2008.

[40] J.A. Greenwood, J.B.P. Williamson, and F.P. Bowden. Contact of nominally flat surfaces. *Proceedings of the Royal Society of London. Series A. Mathematical and Physical Sciences*, 295, 12 1966.

[41] A. Griffith. A 221:163–98, 1920.

[42] Renault Group. Groupe renault facts & figures 2018. 03 2018.

[43] N. Gupta, Kishore, E. Woldesenbet, and S. Sankaran. Studies on compressive failure features in syntactic foam material. *Journal of Materials Science*, 36(18):4485–4491, Sep 2001.

[44] V. Gutmann. The donor-acceptor approach to molecular interactions. *SERBIULA (sistema Librum 2.0)*, 01 1979.

[45] F.L. Harding and D.R. Rossington. Wetting of ceramic oxides by molten metals under ultrahigh vacuum. *J. Am. Ceram. Soc.*, 53:87–90, 1970.

[46] M. Horgnies. Adhésion et adhérence entre les peintures automobiles et des adhésifs sensibles à la pression : influence du nettoyage sur la physico-chimie et la tenue mécanique des interfaces. *PhD Thesis*, 2004.

[47] C.Y. Hui, Y.Y. Lin, and J.M. Baney. The mechanics of tack: viscoelastic contact on a rough surface. *J. Polym. Sci. B*, 38:1485–95, 2000.

[48] J. Jasper. The surface tension of pure liquid compounds. *Journal of Physical and Chemical Reference Data*, 1, 10 1972.

[49] K. L. Johnson. *Rough surfaces*, page 397–423. Cambridge University Press, 1985.

[50] D K. J. Owens and R.C.J. Wendt. Owens, d. k. wendt, r. c. estimation of the surface free energy of polymers. j. appl. polym. sci. 13, 1741-1747. *Journal of Applied Polymer Science*, 13:1741 – 1747, 08 1969.

[51] D H Kaelble. Theory and Analysis of Peel Adhesion : and Mechanics Mechanisms. *Transactions of the society of rheology*, 3:161–180, 1959.

[52] D H Kaelble. Theory and Analysis of Peel Adhesion : Bond Stresses and Distributions. *Transactions of the society of rheology*, 4:45–73, 1960.

[53] D. H. Kaelble. Peel Adhesion : Micro-Fracture Mechanics of Interfacial Unbonding of Polymers. *Transactions of the society of rheology*, 9(2):135–163, 1965.

[54] D H Kaelble. Peel Adhesion : Influence of Surface Energies and Adhesive Rheology. *Journal of Adhesion*, 1:102–123, 1969.

[55] D H Kaelble. Rheology of Adhesion. *Journal of Macromolecular Science, Part C : Polymer Reviews*, 6(1):85–112, 1971.

[56] D.H. Kaelble. Theory and analysis of peel adhesion: rate-temperature dependence of viscoelastic interlayers. *Journal of colloid science*, 19:413–424, 1964.

[57] K. Kendall. Molecular adhesion and its applications - the sticky universe. 1, 2001.

[58] K. Kendall and A.D. Roberts. Van der waals forces influencing adhesion of cells. *Philosophical transactions of the Royal Society of London. Series B, Biological sciences*, 370, 02 2015.

[59] A. Kinloch. *Adhesion And Adhesives: Science And Technology*. 01 1987.

[60] A. Kowalski and Z. Czech. The effects of substrate surface properties on tack performance of acrylic pressure-sensitive adhesives (psas). *International Journal of Adhesion and Adhesives*, 60, 03 2015.

[61] A. Kowalski, Z. Czech, and L. Byczyński. How does the surface free energy influence the tack of acrylic pressure-sensitive adhesives (psas)? *Journal of Coatings Technology and Research*, 10(6):879–885, Nov 2013.

[62] H. Lakrout, P. Sergot, and C. Creton. Direct Observation of Cavitation and Fibrillation in a Probe Tack Experiment on Model Acrylic Pressure-Sensitive-Adhesives. *The Journal of Adhesion*, 69(3-4):307–359, March 1999.

[63] G. Lefebvre, R. Wunenburger, and T. Valier-Brasier. Ultrasonic rheology of visco-elastic materials using shear and longitudinal waves. *Applied Physics Letters*, 112:241906, 06 2018.

[64] B. Lestriez, H. Lakrout, A. Chiche, A. Roos, and C. Creton. Probe tack tests as a characterization tool in pressure-sensitive-adhesives. In *Proceedings of the PSTC Technical Seminar TECH XXIV, Orlando, FL, USA*, pages 2–4, 2001.

[65] D. Maugis and M. Barquins. Fracture mechanics and the adherence of viscoelastic bodies. 11(14):1989–2023, oct 1978.

[66] F. Mazzeo. Characterization of pressure sensitive adhesives by rheology. *TA Instruments Report RH082*, 01 2002.

[67] J.C. Melrose. Advances in chemistry series. *Am.Chem. Soc.*, page 43, 1964.

[68] J.G. Minonzio, M. Talmant, and P. Laugier. Guided wave phase velocity measurement using multi-emitter and multi-receiver arrays in the axial transmission configuration. *The Journal of the Acoustical Society of America*, 127(5):2913–2919, 2010.

[69] J.G. Minonzio, M. Talmant, and P. Laugier. Measurement of guided mode wave vectors by analysis of the transfer matrix obtained with multi-emitters and multi-receivers in contact. *Journal of Physics: Conference Series*, 269:012003, 02 2011.

[70] S. Mora, E. Ando, J.M. Fromental, and Y. Pomeau. The shape of hanging elastic cylinders. *soft matter physics*, 01 2019.

[71] C.W. Paul. *Pressure-Sensitive Adhesives (PSAs)*, pages 341–372. Springer Berlin Heidelberg, Berlin, Heidelberg, 2011.

[72] B. Persson, O. Albohr, C. Creton, and V. Peveri. Contact area between a viscoelastic solid and a hard, randomly rough, substrate. *The Journal of chemical physics*, 120:8779–93, 06 2004.

[73] B. N. J. Persson. Adhesion between elastic bodies with randomly rough surfaces. *Phys. Rev. Lett.*, 89:245502, Nov 2002.

[74] A. Pizzi and K.L. Mittal. *Handbook of adhesive technology*. CRC press, 2017.

[75] J.M. Ruckebusch. Microsphères creuses de verre pour mousses syntactiques. *Techniques de l'ingénieur Matériaux composites : présentation et renforts*, 2016.

[76] J. Tse and A.W. Adamson. Adsorption and contact angle studies: Iii. organic substances on polished polyethylene. *J. Coll. Int. Sci.*, 72:144–153, 1979.

[77] R. Villey, P.P. Cortet, C. Creton, and M. Ciccotti. In-situ measurement of the large strain response of the fibrillar debonding region during the steady peeling of pressure sensitive adhesives. *International Journal of Fracture*, 204(2):175–190, 2016.

[78] R. Villey, C. Creton, P.P. Cortet, M.J. Dalbe, T. Jet, B. Saintyves, S. Santucci, L. Vanel, D.J. Yarusso, and M. Ciccotti. Rate dependent elastic hysteresis during the peeling of pressure sensitive adhesives. *Soft Matter*, 11(17):3480–3491, 2015.

[79] R.E. Webber, K. Shull, A. Roos, and C. Creton. Effects of geometric confinement on the adhesive debonding of soft elastic solids. *Physical review. E, Statistical, nonlinear, and soft matter physics*, 68:021805, 09 2003.

[80] Cox W.P. and Merz E.H. Correlation of dynamic and steady flow viscosities. *Journal of Polymer Science*, 28(118):619–622, 1958.

[81] Z. Xu, G. Anyasodor, and Y Qin. Painting of aluminium panels – state of the art and development issues. *MATEC Web of Conferences*, 21:05012, 01 2015.

[82] D.J. Yarusso. Quantifying the relationship between peel and rheology for pressure sensitive adhesives. *Journal of Adhesion*, 70(3):299–320, 1999.

[83] D.J. Yarusso. *Effect of rheology on PSA performance*, volume 1, pages 499–533. 12 2002.

[84] T. Young. Iii. an essay on the cohesion of fluids. *Phil. Trans. R. Soc.*, 95, 1805.

[85] M.J. Zajaczkowski. Acrylate-polyether based pressure sensitive adhesives. *Pressure Sensitive Tape Council Tech 30 Global Conference VI*, page 2, 05 2007.

[86] W.A. Zisman. Relation of the equilibrium contact angle to liquid and solid constitution. *Adv. Chem. Ser.*, 43:1–51, 1964.

Mécanismes dissipatifs lors du décollement d'adhésifs sensibles à la pression haute performance (foam PSA) dans l'automobile.

Les adhésifs de type foam PSA sont de plus en plus utilisés dans l'automobile. Principalement, cette hausse de l'utilisation est motivée par deux facteurs : économique et stratégique. Le premier concerne la volonté des constructeurs à délivrer des voitures uniques pour chaque client. Pour ce faire, ils utilisent le procédé dit de « customisation ». Cela consiste à ajouter un ensemble de détails, essentiellement décoratifs, choisis par le client qui rendent l'esthétique du véhicule quasi-exclusive. Dans ce dessein, un élément proposé par les constructeurs est l'ajout de pièces non structurelles telles que des baguettes de carrosserie. Afin d'assembler ces pièces sur la voiture, deux technologies d'assemblage sont principalement employées. La première consiste à utiliser des solutions dites « positives » comme des vis. Cette technique datant des premières heures de la construction industrielle est extrêmement couteuse en temps de production et donc, financièrement. Pour y remédier, ces dernières années ont vu l'éclosion d'une nouvelle technique : l'assemblage par adhésifs. Cette technique est une réelle révolution pour le monde de la production de masse dans le sens où elle permet en une seule opération d'assembler des pièces mécaniques. Dans une moindre mesure, il apparaît également comme une solution d'allègement sachant que la masse d'un adhésif est significativement plus faible qu'un assemblage vissé. L'objectif majeure de la thèse est donc de comprendre comment ces adhésifs appelés foam PSA fonctionnent et comment les impératifs de la production de masse (température ambiante d'une ligne de production, projections de poussières et d'huile…) affectent les performances d'assemblage.

La compréhension du décollement d'un adhésif type foam PSA est d'autant plus intéressant pour les constructeurs automobiles car cela fournit les premières bases dans la construction d'un modèle prédictif de la rupture d'un joint adhésif. Pour l'industriel partenaire du doctorat, cette étude est pertinente pour deux aspects plus pragmatiques : la protection de l'image de marque et le renforcement de la sécurité des véhicules autonomes ou semi-autonomes. Protection de l'image car les logos de la marque sont adhésivés sur la carrosserie des véhicules. Tout décollement d'un emblème ou du nom de la marque serait catastrophique pour la qualité perçue et donc résulterait en une diminution de l'attractivité des voitures pour de potentiels acquéreurs. Renforcement de la sécurité car nombre de capteurs permettant aux véhicules autonomes de se repérer dans l'espace sont eux-mêmes portés par des supports capteurs collés à l'aide de foam PSA. Un décollement d'une ou plusieurs de ces pièces engendrerait une perte ou une mauvaise information pour une voiture sans pilote ce qui pourrait déclencher un accident. L'intérêt du constructeur automobile dans ce programme doctoral est donc réel.

D'un point de vue scientifique, un tel travail de thèse est également extrêmement pertinent. Un état de l'art exhaustif a été réalisé en se concentrant sur la création du contact adhésif et sur la phase de décollement. Pour le premier cas, on a vu que la rhéologie du matériau est prépondérante dans la bonne formation du contact pour les PSA classiques, non moussés et de faibles épaisseurs (qqs dizaines de micromètres). Une bonne rhéologie au sens « adhésif », c'est-à-dire très visqueuse (= dissipative) pour les conditions de température/fréquence d'accostage, permet l'établissement d'adhésion moléculaire à l'interface entre l'adhésif et le substrat. Il est à noter que jamais une telle étude n'a été étendue aux foam PSA commerciaux, pourtant largement plus épais et de composition inconnue. Cela a constitué le point de départ de la recherche du doctorat résumé ici. Au niveau de la phase de

décollement, l'étude bibliographique a montré que la performance d'un PSA est directement liée à sa capacité à dissiper l'énergie qui lui est apportée par l'action de le décoller. En effet, des mécanismes dissipatifs prennent place dans le volume de l'adhésif ce qui dissipe une partie de l'énergie qui pourrait rompre l'adhésion moléculaire à l'interface entre l'adhésif et le substrat. Ainsi plus ces mécanismes sont nombreux et efficaces pour dissiper de l'énergie plus la résistance de l'assemblage adhésivé est augmentée. Ce point est de tout premier intérêt pour les foam PSA qui sont extrêmement épais et donc ont potentiellement un plus grand volume susceptible de dissiper de l'énergie. Cette étude des mécanismes dissipatifs se déclenchant pendant la phase de décollement est le cœur du travail de recherche réalisé durant ce doctorat sur les foam PSA. Avant cette thèse, aucune information concernant ce type de matériaux n'avait été communiquée à la communauté scientifique, tant au niveau de l'initiation du décollement qu'à sa propagation. Seuls des modèles phénoménologiques concernant la description du comportement des PSA classiques ont été relevés.

Forts de la pertinence industrielle et scientifique d'une telle recherche et en se basant sur les limites de l'état de l'art actuel, la problématique de la thèse de doctorat résumé ici est logiquement : *Mécanismes dissipatifs lors du décollement d'adhésifs sensibles à la pression haute performance (foam PSA) dans l'automobile.*

Comme il a été dit précédemment, les foam PSA n'ont jamais été étudiés dans le cadre d'un travail tel qu'un doctorat. La thèse résumée ici s'est, dans son second chapitre, attachée d'abord, à caractériser ce type de matériau puis, à étudier son comportement adhésif et enfin, à développer une méthodologie pour surmonter le problème majeur de répétabilité de ce type de tests.

Dans un premier temps, la caractérisation s'est basée sur des observations multi-échelles (optiques, électroniques à balayage et à rayons X). C'est analyses ont révélé une structure très particulière de l'adhésif. Il s'agit en effet d'une architecture dite de mousse syntactique. Une mousse syntactique diffère des mousses classiques dans le sens où elle présente une forte incompressibilité due à la présence de cavités artificielles. Dans le cas d'une mousse classique où les porosités sont le résultat d'un processus émulsif, ici les cavités sont en réalité des charges micrométriques ayant la forme de sphères de verre creuses. La proportion volumique de ces charges est de 37% (vol). Leur présence tend à perdre l'idée de continuum du matériau qui apparaît désormais comme un composite. La matrice étant faite selon les formulations chimiques des PSA classiques et les charges étant assimilées aux sphères creuses. La distribution des sphères dans le matériau est homogène. Aucune anisotropie n'a été remarquée. Aucun n'ensimage de la surface des sphères n'a également été noté. Les sphères présentent une épaisseur de coque de 2 mm et sont remplies d'un gaz neutre pour le polymère. Il est enfin pertinent de souligner la présence de nano charges dans la matrice polymère. Ces charges sont constituées d'agrégats de noirs de carbone et de particules de dioxyde de titane. La proportion globale volumique de ces éléments n'excède pas 5% (vol). D'un point de vue du comportement mécanique des échantillons, ces nano charges sont trop peu nombreuses pour avoir un quelconque effet. Elles sont uniquement ajoutées à des fins marketing pour colorer les échantillons et respecter l'identité de chaque fournisseur ainsi que s'adapter aux exigences esthétiques des utilisations sur véhicule. Une approximation raisonnable est de considérer la structure de mousse syntactique comme étant incompressible.

Dans un second temps, la caractérisation du matériau d'intérêt s'est basée sur une approche rhéologique. Des tests en petites déformations de cisaillement (balayage en fréquence sur une large plage de températures) ont montré que les adhésifs type foam PSA ont un comportement proche de celui des PSA classiques. Ces conclusions illustrent la faible influence en régime de petites déformations des microsphères de verre sur le comportement global des échantillons. De plus, il est à noter que les adhésifs foam PSA suivent les critères établis empiriquement par Dahlquist. Ces critères, qui se basent sur la rhéologie d'un matériau pour définir sa capacité d'adhésion à un substrat, sont une donnée importante à prendre en compte pour le partenaire industriel de la thèse dans la mesure où ils sont facilement et industriellement vérifiables par un test rhéologique de cisaillement en petites déformations. Cela permet une approche discriminante des références commerciales utilisées pour déceler des potentiels défauts d'accostage. Se basant sur le principe de Cox-Merz, ce travail de thèse a permis de mettre en lumière une manière simple de privilégier une application manuelle ou robotisée.

Pour finir, le travail de caractérisation s'est attaché à l'étude du comportement du foam PSA en sollicitation de traction uniaxiale. Dans cette configuration de chargement, un comportement hyper(visco)élastique a été mis en avant. C'est-à-dire que l'on observe une grande déformation à rupture supérieure à 1000% et une très grande sensibilité au taux de déformation ce qui illustre l'important pouvoir dissipatif du matériau. Un endommagement de type adoucissement a finalement été mis en lumière à la suite de tests cycliques.

Pour entrer plus en profondeur dans la problématique de thèse, une stratégie d'étude du décollement a été conçue. Celle-ci se focalise sur l'initiation du décollement avec le test du poinçon plat (flat ended probe tack test) et sur la propagation du décollement en régime permanent avec le test du pelage à 90°. Ces deux tests sont largement utilisés par la communauté scientifique depuis le début des recherches sur les adhésifs de type PSA. Leur extrapolation aux foam PSA est relativement simple et ce chapitre 2 de la thèse fournit les connaissances suffisantes à leur prise en main. La seule réelle difficulté recèle dans l'obtention de résultats véritablement répétables. Obtenir cette répétabilité est un obstacle à la réalisation de tests fiables et quantitatifs tels que voulus dans l'industrie. Ce point dur a été résolu dans la dernière partie du chapitre 2 où un protocole basé sur la préparation de la surface des substrats des tests est proposé.

La mise en place de ces tests constitue le fondement du chapitre 3. Dans ce chapitre l'objectif est d'identifier qualitativement puis quantitativement les mécanismes dissipatifs ayant lieu dans l'adhésif lors de la phase de décollement. Les résultats sont présentés en considérant d'abord l'initiation de la rupture puis la phase de propagation du décollement. A la différence des PSA classiques où l'on observe un phénomène de cavitation apparaissant à l'interface entre l'adhésif et le substrat, dans le cas des foam PSA on observe de la cavitation apparaissant proche de l'interface mais pas à l'interface. En réalité, la cavitation des foam PSA est engendrée par le décollement des sphères de verre de la matrice qui sont proches de l'interface mais à l'intérieur du PSA. Cette décohésion interne est due à une augmentation locale de la pression hydrostatique dans le matériau liée à la sollicitation de décollement de l'adhésif. En aucun cas à ce stade, il n'y a apparition d'une fissure interfaciale entre l'adhésif et le substrat. Pour aller plus loin dans l'étude de cette phase particulière, une étude en pelage à 90° a été réalisée.

Lors de tests de pelage à 90°, une modification de forme de l'adhésif dépendant du niveau d'adhérence a été observée. Plus précisément, on observe que le matériau a tendance à se déformer en volume différemment selon que la résistance du joint adhésif est plus au moins importante. Ceci suppose que le volume de l'adhésif joue un rôle dans la dissipation d'énergie. On a notamment remarqué que plus l'adhérence est élevée plus la déformation est importante. On observe une localisation de la déformation dans le volume du foam PSA dans une région proche de l'interface là où se produit la cavitation détaillée ci-dessus. Puis, lorsque l'adhérence augmente, une nouvelle zone de déformation se développe au milieu de l'échantillon. Ces deux localisations se rejoignent alors lorsque l'adhérence augmente encore. Ainsi de suite jusqu'à une rupture cohésive du matériau. Une analyse au microscope électronique à balayage (test insitu de traction uniaxiale) a permis de révéler que ces zones de localisation correspondent à des zones où les microsphères de verre se décollent de la matrice et engendrent l'occurrence et la croissance de cavités d'air. Ces cavités, tout en grossissant, s'orientent dans une direction privilégiée qui est guidée par le pelage lui-même. Au fur et à mesure que l'adhérence augmente, le nombre et la taille de ces cavités augmentent jusqu'à orienter macroscopiquement le matériau. Les parois entre ces cavités nouvellement créées deviennent de plus en plus fines jusqu'à devenir des fibrilles. Le foam PSA s'apparente alors à un ensemble fibrillé prompte à dissiper une grande quantité d'énergie (sachant que la matrice de l'adhésif est très viscoélastique). Pendant ces tests, on observe que le développement de ces mécanismes est sensible à la vitesse du décollement et au niveau d'adhésion à l'interface entre l'adhésif et le substrat.

A l'échelle micrométrique, le décollement des sphères de la matrice génèrent des instabilités qui donnent naissance à des microfibrilles. Ces microfibrilles sont susceptibles de dissiper une faible quantité d'énergie mais qui devient non négligeable compte-tenu de l'importante proportion de sphères dans le volume de l'adhésif. Une observation a également permis de mettre en évidence l'occurrence d'un autre phénomène qui est la rupture des sphères de verre elles-mêmes. En effet, l'importante déformation de l'adhésif lors du décollement dans les cas fortement adhérents semble exercer des chargements significatifs sur les sphères qui cassent. Cette casse constitue un endommagement irréversible de l'adhésif. Cependant, si une telle situation doit se produire, cette dernière n'apparaît que pour des niveaux de déformations supérieurs à la plupart des cas problématiques en usage industriel. En revanche, une situation est quant à elle largement rencontrée. Il s'agit d'un pseudo effet Mullins résultant de la présence de ces microsphères de verre. Ce phénomène a été mis en évidence durant ces travaux de doctorat en réalisant des tests de traction cyclique. Lors d'un cycle pour un niveau de déformation suffisant (env. 50%), la majorité des sphères est décollée de la matrice. Lorsque le chargement revient à zéro, les interfgaces sphères/matrice se recréent. Or, cette recréation d'interface est imparfaite et le niveau d'adhésion interfaciale local entre les sphères de verre et la matrice est plus faible que précédemment. Ainsi, lors de la traction suivante, les sphères se décollent plus facilement et l'on observe que la contrainte à fournir pour atteindre le même niveau de déformation est plus faible que pour le premier cycle. Pour pallier à cet effet, le travail de thèse a permis de montrer la pertinence d'un chauffage à 80°C pendant 2 heures entre deux cycles (pour l'industriel un chauffage à l'aide d'un sèche-cheveux durant quelques secondes devrait avoir le même effet). Ce type d'endommagement est, quant à lui, recouvrable thermiquement.

Ayant qualitativement identifié et caractérisé les principaux mécanismes dissipatifs ayant lieu lors du décollement des foam PSA, l'accent a ensuite été mis sur l'aspect quantitatif. Pour ce faire, un premier modèle phénoménologique a été proposé, il s'agit du : *Equivalent Fibril Model* (modèle de fibrille équivalente). Celui-ci s'appuie sur les travaux les plus récents

concernant la description des mécanismes dissipatifs dans les PSA classiques. La majeure différence avec les foam PSA tient dans le fait que les PSA classiques présentent une structurent clairement fibrillée lors de leur décollement. Les fibrilles se créent spontanément sur toute l'épaisseur du matériau. Celles-ci sont clairement indépendantes les unes des autres. L'idée du *Equivalent Fibril Model* est d'appliquer un schéma de pensée aux foam PSA en considérant qu'ils sont eux-aussi fibrillés dans toute leur épaisseur et que la direction de ces fibrilles est déterminée par l'orientation macroscopique du volume de l'adhésif pendant le décollement. Ainsi, on considère que la plupart de l'énergie dissipée pendant le décollement est dissipée par l'extension uniaxiale de cette fibrille équivalente lors de sa déformation durant la phase de décollement. La quantité d'énergie dissipée dépend donc du taux de déformation de cette fibrille équivalente et de sa déformation maximale lors du détachement de son extrémité du substrat. Il a alors été montré que ce modèle marche à partir d'une certaine valeur d'adhérence propre à un couple adhésif/substrat (dans notre cas, ce seuil est à environ 2000 J/m²).

Dans un second temps, une description de l'*Equivalent Fibril Model* a été faite en utilisant une approche rhéologique non linéaire. Le fondement de cette approche est de réaliser un réétalonnage d'un coefficient de recalage rhéologique en grandes déformations en utilisant les coefficients de transposition temps-température obtenus en régime linéaire de petites déformations. Cette description rhéologique marche extrêmement bien et permet de réaliser un seul test de traction uniaxiale du matériau et d'extrapoler les résultats à des taux de déformations non atteignables avec des équipements standards. Ce résultat illustre la pertinence d'aborder les problèmes d'adhérence par la rhéologie en régime non linéaire.

Enfin, le dernier modèle présenté dans ce chapitre concerne la transposition des résultats d'un test à l'autre. Plus particulièrement, il s'agit de transposer les résultats d'un test de pelage à 90° à un test de poinçon plat, et vice versa. Ce modèle appelé *Transposition Model* (modèle de transposition) se base sur le fait que la dissipation d'énergie est pilotée par le taux de déformation des fibrilles équivalentes. Ainsi, le modèle stipule qu'en égalisant les taux de déformation de ces fibrilles équivalentes dans les deux tests, on dissipe des quantités d'énergie semblables. L'énergie dissipée étant directement liée à l'adhérence d'un PSA, les deux tests devraient avoir les mêmes résultats. Les travaux résumés ici montrent la pertinence de ce modèle. Ce dernier fournit donc un outil précieux pour l'industriel afin de réduire le nombre des tests de référencement d'un nouvel adhésif. Il est toutefois à noter que ces outils ne sont valables qu'à partir d'un certain seuil (ici 2000 J/m²). La présence de ce seuil est explicitée dans le chapitre suivant qui s'attarde à comprendre le lien existant entre la taille de la zone dissipative et la performance d'un joint adhésif.

Les premières observations d'une relation entre forme de la zone dissipative et adhérence d'un foam PSA ont été faites lors du chapitre 3. Ces dernières ont témoigné d'une augmentation de la taille de cette zone lorsque le niveau d'adhérence augmente. Sachant que les mécanismes identifiés précédemment (décollements des sphères, fibrillation, instabilités…) se développent dans cette région, il est raisonnable du supposer qu'une plus grande déformation de la zone dissipative engendre l'activation de plus de mécanismes et donc, est directement liée à une plus grande quantité d'énergie dissipée.

Afin d'analyser la forme de la zone dissipative de manière quantitative, le premier point dur a été de mettre en place des paramètres géométriques prenant en compte la variation de taille. Cinq paramètres sont proposés dans la thèse résumée ici. Chacun de ces paramètres

revêt un intérêt particulier. Le premier est issu de la littérature. Il s'agit du rayon de courbure du backing (l'endos qui est placé sur l'adhésif lorsque celui-ci est pelé à 90°). Cela permet de comprendre l'influence des mécanismes internes à l'adhésif sur la valeur d'adhérence mesurée pendant un test. En effet, il est très important de garder à l'esprit que la valeur de l'adhérence mesurée, quelle qu'elle soit, dépend du choix du backing. Le second paramètre a été introduit spécifiquement dans ce travail de thèse pour tenir compte de phénomènes dus à la grande épaisseur du foam PSA. Il s'agit de la longueur de succion. Cette longueur décrit l'impact de l'incompressibilité sur la déformation de l'adhésif. Plus l'adhésif est incompressible, plus cette longueur est grande. Le troisième paramètre concerne l'angle fait par l'adhésif avec le substrat lors du décollement. Cet angle n'avait été utilisé qu'une seule fois dans la littérature mais pour des PSA classiques présentant une structure complètement fibrillée. Ce paramètre permet de voir si l'angle au niveau du décollement est le même que l'orientation du volume de l'adhésif comme il est supposé dans l'*Equivalent Fibril Model*. Le quatrième paramètre utilisé est appelé *Debonding Region Length* (longueur de la zone dissipative). Cette longueur est largement utilisée dans une approche descriptive du comportement d'un adhésif en sollicitation de pelage. L'évolution de cette dernière est extrêmement pertinente pour, à l'instar du rayon de courbure du backing, visualiser l'influence des mécanismes de la zone dissipative sur le comportement global de l'adhésif. Enfin, le dernier paramètre est la déformation maximale des fibrilles équivalentes utilisée dans le chapitre 3.

L'évolution de ces cinq paramètres a permis de très clairement mettre en lumière un niveau seuil d'adhérence de transition de comportement du foam PSA. Ce seuil arrive (pour notre choix de backing) à environ 2000 J/m². Cette valeur est tout sauf anodine. Elle correspond en effet au début du domaine de validité de l'*Equivalent Fibril Model*. Ceci signifie qu'à partir de ce seuil, la zone dissipative du foam PSA peut être vue comme une structure fibrillée où les fibrilles sont soumises à une sollicitation de traction uniaxiale dirigée par l'orientation du matériau. La présence de ce seuil a également été prouvée théoriquement. Elle correspond à la transition où les mécanismes internes au foam PSA deviennent aussi influents sur la courbure du backing que la sollicitation de pelage elle-même. D'un point de vue physique, avant ce seuil, le foam PSA est encore en cours de fibrillation, les cavités issues des décollements des microsphères de verre au sein de la matrice de l'adhésif ne sont pas encore assez grande pour qu'un modèle de type *Equivalent Fibril Model* s'applique. En termes simples, l'adhésif se déconfine jusqu'à un certain seuil où le mécanisme principal de dissipation d'énergie est l'extension uniaxiale de fibrilles équivalentes viscoélastiques. Cette compréhension physique a été vérifiée par simulation en éléments finis.

Pour aller plus loin, une approche expérimentale se basant sur une modification chimique de la surface des substrats a ensuite été utilisée. Ce procédé permettait d'englober des cas de très faible adhérence jusqu'aux cas extrêmes de rupture adhésive (très forte adhérence). Les résultats ont montré l'existence d'un second seuil de transition présent à environ 1000 J/m² (pour notre choix de backing). Physiquement, ce seuil correspond au moment où le volume de l'adhésif commence à contribuer autant que la zone locale proche de l'interface à la dissipation globale du foam PSA. Autrement dit, la dissipation d'énergie est, dans les cas de faible adhérence, principalement pilotée par des mécanismes singuliers dans une zone petite proche de l'interface entre l'adhésif et le substrat. Puis, au fur et à mesure que l'adhérence augmente, cela correspond à l'activation de plus en plus de mécanismes volumiques. Passé 1000 J/m², les mécanismes volumiques commencent à dominer les mécanismes locaux (même si ces derniers continuent à dissiper tout de même de l'énergie). Jusqu'à 2000 J/m², les mécanismes volumiques continuent à se développer en déconfinement le matériau qui adopte

de plus en plus un comportement appréhendable par une structure fibrillée. Où les fibrilles sont soumises à une traction uniaxiale. Le taux de déformation de ces fibrilles pilote alors la dissipation d'énergie et donc la résistance mécanique du joint adhésivé.

Afin de se rapprocher des situations industrielles, la fin du chapitre 4 présente le cas du repositionnement d'un foam PSA rencontré en usine. Lors de la phase de collage de pièces adhésivées, il arrive que la pièce soit « mal collée », c'est-à-dire mal alignée. Un défaut d'alignement peut se révéler inesthétique dans le cas d'un logo ou de baguettes décoratives par exemple. Il faut donc décoller la pièce et la recoller. Or, dans cette opération les travaux de doctorat ont montré que la résistance du joint adhésivé après le second collage est divisée par 3. Cette diminution est due à environ 40% à une contamination du substrat par l'adhésif lui-même et à environ 60% par un endommagement de l'adhésif (cf. effet Mullins dans le chapitre 3). Une telle perte d'adhérence est inacceptable pour l'industriel. De ce fait, un protocole a été proposé réduire drastiquement cette perte de performance après un recollage. Ce protocole détaillé dans le chapitre 4 est complètement adapté aux exigences d'un environnement industriel. En ce qui concerne le travail réalisé sur la forme de la zone dissipative en fonction de l'adhérence, on observe que l'évolution de nos cinq paramètres géométriques suit parfaitement nos courbes maîtresses définis précédemment que ce soit lorsque l'adhésif s'endommage ou lorsque le substrat se contamine. Ceci renforce la véracité de l'existence des courbes maitresses pour chaque adhésif type foam PSA.

La thèse se termine par un chapitre de conclusions et perspectives qui reprend l'ensemble des connaissances et grands résultats à connaître au terme de ce travail de recherche de doctorat. Les foam PSA sont maintenant caractérisés, on connaît leur structure et leurs principales caractéristiques comportementales. A la suite de cette thèse, une approche pour aborder les problèmes d'adhésion avec des protocoles expérimentaux solides est donnée. Basé sur celle-ci, ce mémoire fournit les clés de compréhension du fonctionnent dissipatif des foam PSA. Ceux-ci sont ensuite modélisés de manière descriptive par deux modèles. Enfin, une étude morphologique donne des outils puissants et industrialisables pour pousser développer une démarche systématique afin d'avancer vers la prédiction de performance. Tout du moins, ce travail définit les bases de la prescription en matière d'assemblage collé par foam PSA.

RÉSUMÉ

Cette thèse a porté sur l'étude des mécanismes dissipatifs se développant dans les adhésifs sensibles à la pression haute performance (appelés foam PSA). Ces adhésifs sont à la base des nouvelles techniques d'assemblage dans le secteur automobile. Leur bon fonctionnement dépend de leur capacité à dissiper de l'énergie lorsqu'ils sont soumis à de fortes déformations. Ces fortes déformations sont permises grâce à leur caractère mou. La littérature sur les problématiques d'adhésion ou, plus récemment, sur la mécanique de la fracture des matériaux mous a jeté les fondements de l'étude de ce genre de matériau. Néanmoins, les précédents travaux se sont toujours concentrés sur l'étude de matériaux fins et non chargés. Dans la thèse ici présentée, l'accent est mis sur un type d'adhésifs au moins 10 fois plus épais et chargé à l'aide de sphères de verre creuses de diamètres allant de 10 à 100µm. C'est en particulier cette structure qui confère au foam PSA de nouveaux types de mécanismes dissipatifs. Ces derniers permettent d'atteindre des niveaux d'adhérence rarement atteints avec des adhésifs conventionnels. D'une manière générale, ces mécanismes dissipatifs apparaissent à trois niveaux pendant le décollement. Pour les faibles adhérences, l'ensemble de la dissipation se fait par un décollement des microsphères de la matrice en volume dans un espace proche de l'interface entre l'adhésif et le substrat. Ces décollements engendrent un phénomène de fibrillation qui reste confiné dans une région de taille restreinte proche de l'interface. Ensuite, lorsque l'adhérence augmente, tout le volume de l'adhésif se déforme. Cette déformation entraine le décollement des sphères avec la matrice en volume. Ces décohésions volumiques génèrent des cavités (phénomène de cavitation) qui peu à peu déconfine l'adhésif. Ce dernier perd alors son caractère de continuum. Durant la croissance de de ces cavités en volume, on observe à l'échelle micrométrique l'occurrence d'instabilités permettant de minimiser l'énergie de déformation. Une fois le matériau déconfiné, l'adhésif s'oriente suivant une direction privilégiée. Cette orientation se fait en adoptant une structure fibrillaire à l'échelle millimétrique. Un modèle semble bien expliquer ce procédé où chacune de ces fibrilles est soumise à un chargement de type traction uniaxiale. Ainsi, la dissipation d'énergie est conduite par la rhéologie non-linéaire de ces fibrilles en extension. Le paramètre pertinent à prendre en considération dans le pilotage de cette dissipation est alors le taux de déformation. Ce lien sous-entendu entre forme de la zone dissipative et niveau d'adhérence a enfin été expliqué quantitativement.

MOTS CLÉS

Adhésion – Foam PSA – Viscoélasticité – Mécanique de la fracture – Automobile

ABSTRACT

Dissipative mechanisms developing in high performance pressure sensitive adhesives (called PSA foam) are extensively studied. New assembly techniques in the automotive domain are based on those materials. Their proper functioning depends on their ability to dissipate energy when they undergo high deformations. Such a large deformations behavior comes from their soft character. The literature on adhesion problems or, more recently, on the fracture mechanics of soft materials has laid the foundations for the study of this type of material. Nevertheless, previous works always focused on the study of thin and unfilled polymers. In this thesis, one emphasizes foam adhesives. They are at least 10 times thicker and filled with hollow glass spheres with diameters ranging from 10 to 100µm. In particular, this structure gives foam PSA, new types of dissipative mechanisms. The latter make it possible to reach adherence levels rarely achieved with conventional adhesives. These dissipative mechanisms appear at three levels during debonding. For low adhesions, the entire dissipation comes from debondings between the microspheres and the matrix in a volume close to the interface between the adhesive and the substrate. These detachments generate a fibrillation phenomenon that remains confined to a small area near the interface. Then, as the adhesion increases, the entire volume of the adhesive deforms. This deformation causes the spheres to detach from the matrix in volume. These volume decohesions generate cavities (cavitation phenomenon) which gradually deconfines the adhesive. The latter then loses its continuum. During the growth of these cavities in volume, instabilities occur at the micrometric scale to minimize the strain energy. Once the material has been deconfined, the adhesive moves in a preferential direction. This orientation is allowed by adopting a millimeter-scale fibrillar structure. A model explains this process well where each of these fibrils is assumed to be loaded in uniaxial tension. Thus, the extensional non-linear rheology of these equivalent fibrils drives the energy dissipation process. The relevant parameter is then the strain rate of the equivalent fibrils. Eventually, we explained quantitatively the link existing between the shape of the debonding region and the adherence level.

KEYWORDS

Adhesion – Foam PSA – Viscoelasticity – Fracture mechanics - Automotive